

Tambora 1815:

Impacts of a volcanic eruption on climate and crop yields in Switzerland

Master Thesis

Presented by

Simon Flückiger

2015

Faculty of Science

University of Bern

Supervisor:

Prof. Dr. Stefan Brönnimann

Institute of Geography of University of Bern and Oeschger Centre for Climate
Change Research, University of Bern

Co-Supervisor:

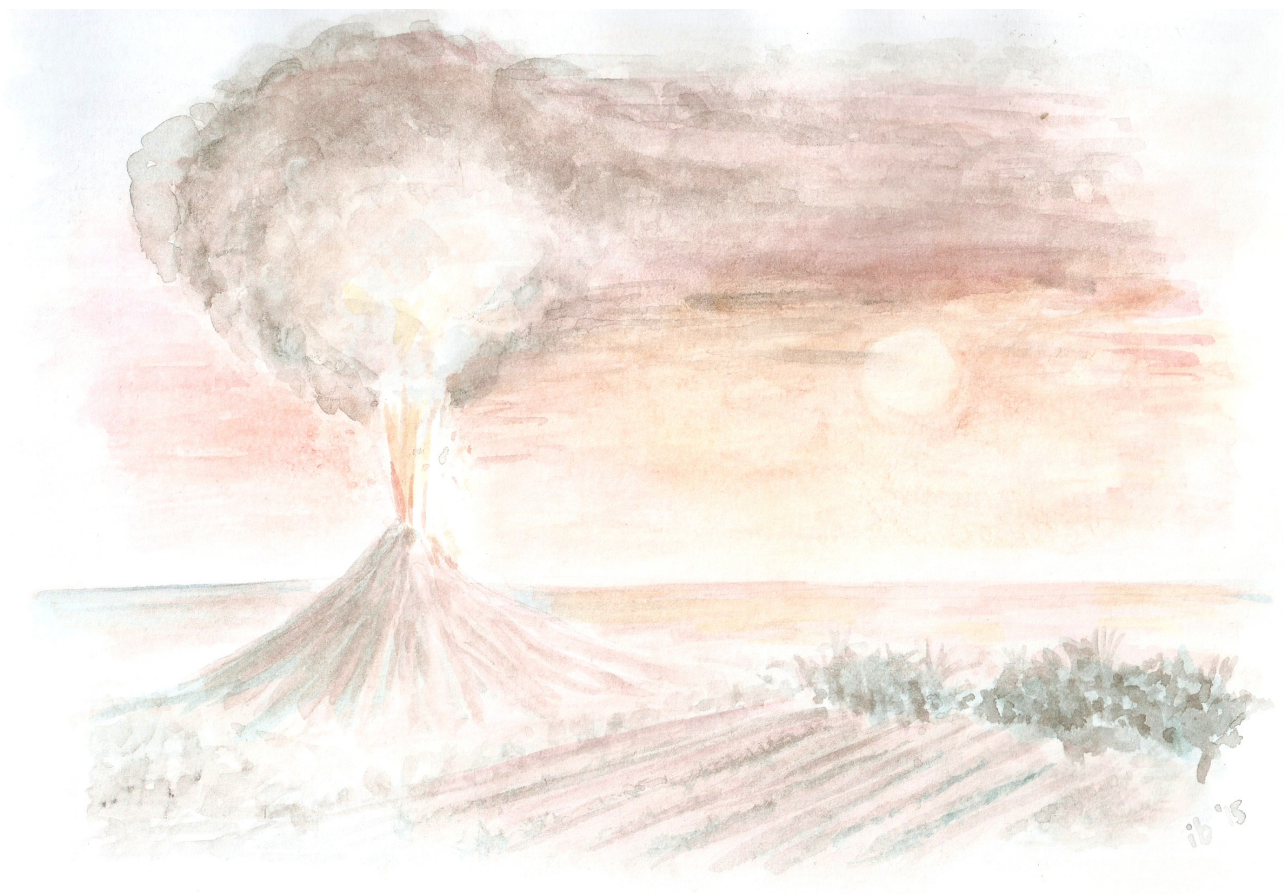
Prof. Dr. Jürg Fuhrer

Research Station Agroscope Reckenholz-Tänikon ART and Oeschger Centre for
Climate Change Research, University of Bern

Advisor:

Annelie Holzkämper

Agroscope, Institute for Sustainability Sciences ISS, Zurich-Reckenholz



Abstract

The eruption of Tambora in April 1815 had changed climate conditions almost all over the northern hemisphere, especially in North America and Europe, causing the *Year without summer* in 1816. These adverse climate conditions led to low crop yields and late harvest dates. Famine and malnutrition in Switzerland led to increased mortality, especially in eastern parts of Switzerland. Therefore, this master thesis focuses on evaluating possible consequences of a recurrence of a Tambora-like eruption today and under present climate conditions. Given this scenario, the thesis aims to identify magnitude and spatial distribution of changes in climate and crop yields in Switzerland. A further aim of this thesis is to investigate whether there is a gradient in crop yields along a West-East transect that might have amplified differences in mortality between Western and Eastern Switzerland. Potential crop yields are assessed with CropSyst, a generic crop model that estimates potential crop yields based on daily climate data. Climate data input into CropSyst is constituted by days resampled within the 1982-2009 period. A weather type classification is derived based on time series of daily minimum and maximum temperatures, pressure, precipitation sums and wind directions recorded at three weather stations for 1800-1820 and 1982-2009. Each day within the 1981-2009 period is subsequently attributed to the corresponding weather class, within which the closest analogue with respect to the Euclidean distance is chosen. For the days selected in this way, values of temperature and precipitation were taken from a high-resolution gridded data set while solar radiation was obtained by interpolating station data to constitute the climate in 1816/17 today. The reconstructed climate is evaluated in comparing it with the climate of a shorter reference period (2000-2009), for which climate warming is less significant. The comparison shows a significant decrease in minimum and maximum temperatures with respect to a shorter reference period, mostly pronounced in summer 1816 and spring 1817. The highest precipitation surplus is simulated for summer 1816. The most distinguished West-East gradient is found for solar irradiance. CropSyst estimates severe losses in yields of barley, potato and maize in 1816 and 1817. Furthermore, crop model output shows a West-East gradient in crop yields primarily triggered by differences in intercepted radiation.

Acknowledgment

First of all, I would like to express my gratitude to Prof. Dr. Stefan Brönimann who inspired me with his interest and fascination for the topic and gave me the opportunity to present this thesis at the International Conference on Volcanoes, Climate and Society¹. This thesis would not have been possible without his vigour and knowledge. He was always available with advice and support whilst leaving me free to develop my own ideas.

Furthermore, I would like to thank Prof. Dr. Jürg Fuhrer for his advise on the crop modelling and the interesting meetings. I am also deeply thankful to Annelie Holzkämper for assisting me in conceiving CropSyst and her valuable advise on my thesis. Further thanks go to Renate Auchmann for advising me on R and sharing her expertise on weather type classification.

Last but not least I would thank my family for their moral and financial support throughout all my studies. A special thank goes to my parents Sandra and Christian for reviewing language and orthography of this thesis and to Isabelle Bachmann, who drew the magnificent aquarelle on the front page of this thesis.

¹ *Bicentary of the great Tambora eruption*, April 2015. Hosted by the Oeschger Centre for Climate Change Research at the University of Bern.

Contents

1	Introduction	1
1.1	Background	1
1.1.1	Impacts on climate in Europe.....	1
1.1.2	Impacts on society and economy in Switzerland	4
1.2	Objectives	6
2	Data	8
2.1	Station data	8
2.1.1	Ref_hist	8
2.1.2	Ref_today	9
2.2	Raster data	10
2.3	Topography	11
3	Methods	12
3.1	Climate simulation	12
3.1.1	Data interpolation.....	12
3.1.2	Weather type classification	14
3.1.3	Resampling of days	15
3.2	Crop modelling.....	17
3.2.1	Sowing time	17
3.2.2	Rooting.....	17
3.2.3	Phenology.....	17
3.2.4	Biomass accumulation	18
3.2.5	Crop yield.....	19
3.3	Model setup	20
3.3.1	Weather data	20
3.3.2	Soil	20
3.3.3	Crop Management.....	20
3.3.4	Environment.....	20

4	Results	21
4.1	Weather type classification	21
4.1.1	Winter (<i>DJF</i>)	22
4.1.2	Spring (<i>MAM</i>)	23
4.1.3	Summer (<i>JJA</i>)	23
4.1.4	Fall (<i>SON</i>)	25
4.2	Climate simulation	26
4.2.1	Climate in 1816/17 and 1816/17_today at the stations G, D & Hpb	26
4.2.2	Climate of 1816/17_today in Switzerland	35
4.3	Crop modelling.....	44
4.3.1	Barley	46
4.3.2	Potato	49
4.3.3	Maize.....	53
4.3.4	Soil moisture	55
4.3.5	Phenology.....	59
5	Discussion	60
5.1	Climate simulation	60
5.2	Method evaluation.....	61
5.3	Crop modelling.....	63
5.3.1	Direct impacts: Weather conditions	63
5.3.2	Indirect impacts: Phenology.....	65
5.3.3	Comparison with crop data from 1816/17	66
6	Conclusion	68
	Appendix	70
	References	75

List of figures

1.1.1	Frequency of temperature anomalies	2
1.1.2	Temperature anomalies in Europe 1816.....	3
1.1.3	Development of crop prices 1815-1818.....	5
2.1.1	Distribution of the weather stations	10
2.3.1	Topography	11
3.1.1	Interpolation of wind data	13
3.1.2	Flow chart of the climate simulation process.....	16
4.1.1	Frequency distribution of weather classes: winter	22
4.1.2	Frequency distribution of weather classes: spring	23
4.1.3	Frequency distribution of weather classes: summer	24
4.1.4	Frequency distribution of weather classes for Geneva and Hohenpeissenberg: summer	24
4.1.5	Frequency distribution of weather classes: fall.....	25
4.2.1	Differences in z-scores of temperature between 1816/17 and 1816/17_today ...	27
4.2.2	Temperature development in 1816/17 and 1816/17_today at Geneva.....	30
4.2.3	Temperature development in 1816/17 and 1816/17_today at Delsberg	31
4.2.4	Temperature development in 1816/17 and 1816/17_today at Hohenpeissenberg	32
4.2.5	Precipitation anomalies in 1816/17 and for 1816/17_today at Geneva	33
4.2.6	Regions for analysis	35
4.2.7	Average seasonal anomalies in minimum temperature.....	36
4.2.8	West-East transection: Minimum temperature	37
4.2.9	Average seasonal anomalies in maximum temperature	39
4.2.10	West-East transection: Maximum temperature	40
4.2.11	Average seasonal anomalies in precipitation	41
4.2.12	West-East transection: Precipitation	42
4.2.13	Average seasonal anomalies in solar irradiance	44
4.2.14	West-East transection: Solar irradiance	44

4.3.1	Climate warming component for spring and summer.....	45
4.3.2	Percentage change in potential yield 1816/17_today: Barley	46
4.3.3	West-East transection for potential yield: Barley	47
4.3.4	Percentage change in potential yield 1816 and 1816_today: Barley	48
4.3.5	Change in intercepted radiation: Barley.....	49
4.3.6	Percentage change in potential yield 1816/17_today: Potato	50
4.3.7	West-East transection for potential yield: Potato.....	50
4.3.8	Percentage change in potential yield 1816 and 1816_today: Potato.....	51
4.3.9	Change in intercepted radiation: Potato	52
4.3.10	Percentage change in potential yield 1816/17_today: Maize.....	53
4.3.11	West-East transection for potential yield: Maize	54
4.3.12	Change in intercepted radiation: Maize	55
4.3.13	Average anomalies in water depth 1816/17_today: Swiss Plateau.....	56
4.3.14	West-East transection: Number of days with saturated soils	57
4.3.15	West-East transection: SDI	58

List of tables

2.1	Nomenclature of time periods.....	8
4.1	Thresholds for the weather type classification.....	21
4.2	Seasonal anomalies at the stations G, D, Hpb: Mean temperature	28
4.3-1	Potential crop yields for different climate scenarios: Barley	48
4.3-2	Potential crop yields for different climate scenarios: Potato	52
4.3-2	Potential crop yields for different climate scenarios: Maize.....	54
4.3-4	CS and NCS for corn	58
4.3-5	Schedule of Phenology for the different climate scenarios.....	59

1 Introduction

1.1 Background

Volcanic eruptions can have great ecological and socioeconomic impacts. They affect both, short-term weather conditions and agricultural output on a local as well as on a large scale.

One of the most severe volcanic eruptions in the past centuries was the one of Tambora (IDN) on 10th of April 1815, which led to the “Year without summer” in 1816 in Europe [Robock, 2000]. Historians [Skeen, 1981; Pfister, 1999, Bodenmann et al., 2011] as well as climate scientists [Briffa and Jones, 1998; Kington, 1992; Shindell et al., 2004, Auchmann et al., 2012 & 2015] and economists [Puma et al., 2015] extensively studied this event. The following sections give a short summary of the state of research investigating climatic and socio-economic impacts of the Tambora eruption in 1815.

1.1.1 Impacts on climate in Europe

The global decrease in temperature is estimated to be approximately 0.5 °C. Nevertheless, the “Year without summer” was not a global, but a regional event [Auchmann et al., 2012], as the eruption changed the climate mainly in Western Europe and North America [Trigo et al.; 2009] between 1815 and 1818.

A considerably large fraction of cooling can be explained by a decrease of solar irradiance due to volcanic particles and increased cloudiness. The force of severe volcanic eruptions propels sulphur-dioxide (SO₂), ashes and other volcanic particles into the stratosphere. The Tambora eruption is estimated to have released 4 times the amount of energy the Krakatau eruption in 1883 did. About 160 km³, equivalent to over 140 Billion tons of pyroclastic material were ejected leaving a caldera with a diameter of 6-7 km and a depth of roughly 600m [Oppenheimer, 2003].

However, it was not the ash that caused the long lasting global effects, but the large amount of ejected SO₂. It is a highly toxic and water-soluble gas forming sulphur aerosols in reaction with H₂O. The vast majority of natural sulphur aerosols are of volcanic origin, especially per-

ceptible in the years following big eruptions [Bates et al., 1992]. Whereas the rain normally washes ashes out during the consecutive few weeks [Stothers, 1984], sulphur aerosols may be transported within the stratospheric circulation over large distances. By this, the aerosols get globally distributed and may have impacts on climatic conditions in the consecutive months and years in regions remote from the eruption location [Chenoweth, 2001; Stendel et al., 2005; McGee et al., 1997].

The processes of how sulphur aerosols lead to cooling and increased cloudiness are yet not fully understood [MR Rampino, 1984]. Aerosols reflect sunlight and additionally emit long wave radiation (heat) into space, and as a consequence act reverse to greenhouse gases. Furthermore, they induce cloud formation by coagulating to condensation cores. As the size of droplets decreases with the number of cloud condensation nuclei, which is equivalent to an increasing total droplet-surface, more sunlight is reflected which amplifies the cooling effect. This phenomenon is pronounced in regions with a high cloudiness [Auchmann et al., 2012]. However, some of the shift in cloud cover and thus in temperature and precipitation can be attributed to a change in prevailing weather types [Auchmann et al., 2012].

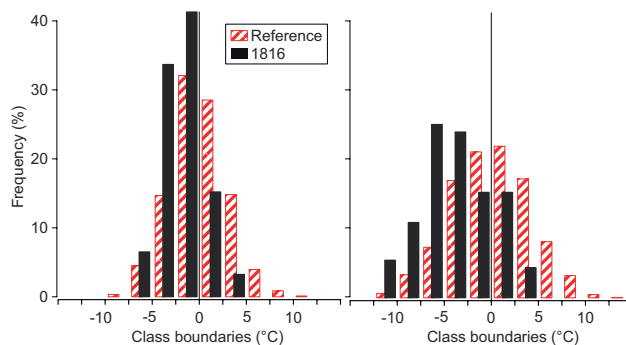


Figure 1.1.1: Frequency of occurrence of temperature anomalies at 2pm (right panel) and at sunrise (left panel) in the summer months June, July and August for 1816 (black) and a contemporary reference period (red).

[From: Auchmann et al., 2012]

Also worth to mention is the difference comparing temperature anomalies at sunrise and at 2pm. As shown in *figure 1.1.1*, the decrease in temperature was exceptionally large during the summer months. Temperature at sunrise, which coincides approximately with the daily minimum temperature, decreased on average by 1.8°C , whereas the anomaly in daily maximum temperature (at 2pm) was much larger (about -3.8°C). This difference can be explained to a great extent by cloud patterns. Clouds are expected to have a cooling effect at daytime and an isolation effect during night. Considering cloud change only, this would lead to higher minimum and lower maximum temperatures [Auchmann et al., 2012].

Figure 1.1.2 shows anomalies in temperature 1816 for Europe. Large deviations from average temperatures were observed in summer in Central Europe with a core over northern France (lower left panel). In winter and spring, mainly northern Europe suffered from colder conditions. The South and East of Europe had been affected only to a small extent by the Tambora eruption.

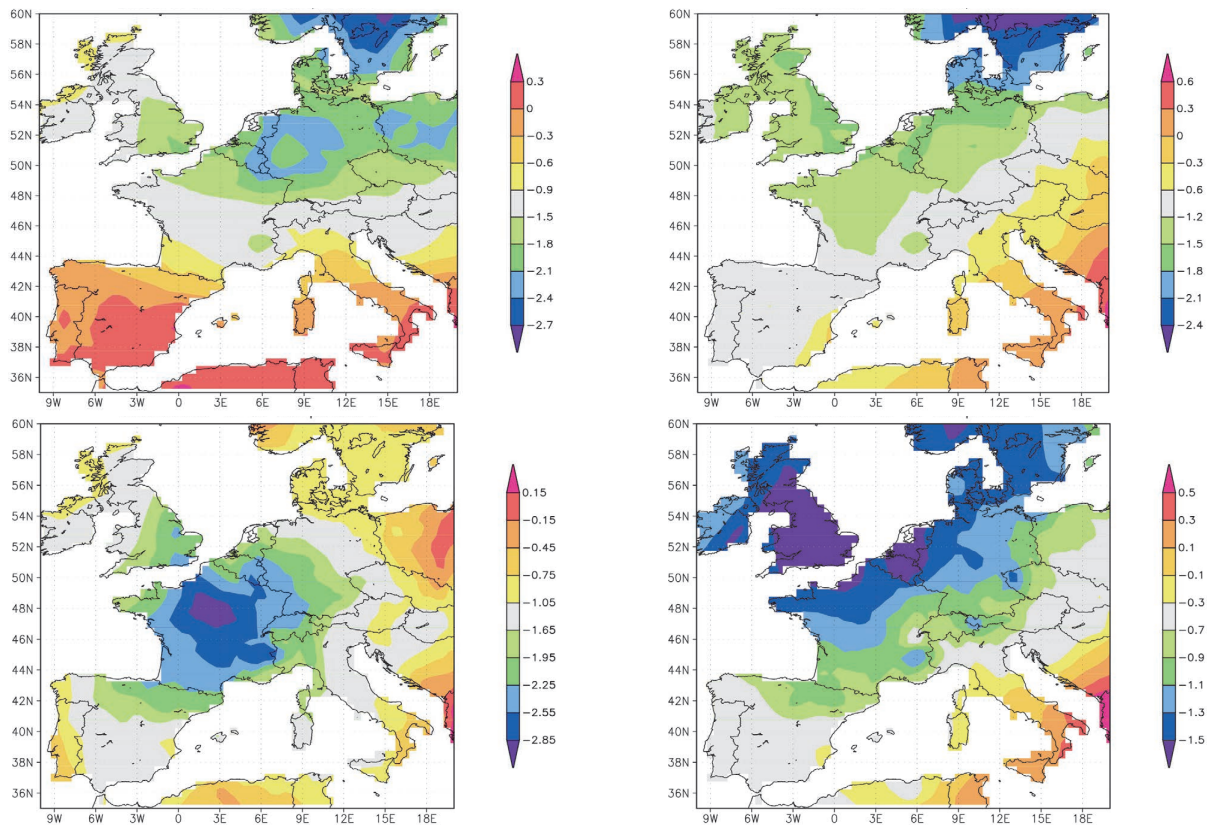


Figure 1.1.2: Temperature anomalies in Europe 1816 compared to a contemporary reference period in winter (upper left), spring (upper right), summer (lower left) and fall (lower right). Note the different scaling for each plot.

[Taken from: Krämer 2015; Source: Luterbacher et al. 2004]

Not only lower solar radiation and temperatures but also a significant increase in precipitation are associated to higher cloud coverage particularly in the summer months. However, there is no evidence for higher frequency of extreme rainfall events in 1816 at Geneva. Furthermore, no significant change in intensity distribution could be found, although the total amount of precipitation was approximately 80% higher in summer 1816 compared to a reference period for 1816 [Auchmann et al., 2012]. Additionally, due to cooling effects, snowfall events had been recorded during summer even for lower altitudes [Krämer, 2015]. Generally, the weather during summer 1816 is characterised as wet and cold, but not by extreme weather events.

Repercussions of changes in weather conditions did not only appear in 1816. Large amount of snowfall during the winters 1815/16 and 1816/17 in combination with the low temperatures in summer 1816 had significantly decreased the amount of thaw, which led to a threefold increased snow cover in early spring 1817. A rainfall event of moderate intensity in June 1817 in combination with increasing temperatures then resulted in a massive snow melting causing severe floodings [Pfister, 1999; Krämer, 2015].

1.1.2 Impacts on society and economy in Switzerland

The change in climate also entailed severe social-economic impacts in Europe such as food shortage, higher incidence of humidity-related diseases and as a consequence increased food prices and mortality. But changing weather conditions was not the only factor responsible for the socio-economic crises in Europe over the consecutive years. In the early 19th century, crop prices had been of decisive importance for a vast majority in Central Europe and fluctuations could be life-threatening [Pfister, 1998; Schürmann, 1974]. As of 1815, Europe was emaciated as a consequence of the Coalition Wars (1792-1815) and the economic conditions were still highly fragile. After the eruption of Tambora 1815, shortages in food supply and the consequential increase in crop prices caused a economical recession. Furthermore, international trade decreased significantly triggered by national shortages in staple food [Krämer, 2015]. This relation is among others discussed in Puma et al. (2015), suggesting that weather disturbances like those characterising the 1815-1818 period also affect international trade networks and may triggering global systemic disruptions. By the national recession together with a collapse of international trade volume, the already precarious situation in Switzerland had further aggravated finally evolving to a humanitarian crisis [Krämer, 2015].

In the early 19th century, the most important strategy to cope with shortages in a staple was to substitute it. Thus, the demand for substitute goods to wheat and corn such as oat, fruits, turnip and potatoes had rapidly increased [Reith, 2011]. As a consequence, many farmers butchered their livestock as its fodder had become too expensive to maintain profitable. Due to the butchering of horses, one of the most important means of transportation suddenly became scarce, which motivated Karls Drais to focus on a valid replacement. As such, he invented the velocipede, a running machine and the first prototype of the bicycle [Lessing, 2003].

Interestingly, crop prices in 1817 differ significantly between western and eastern parts of Switzerland as it is shown in *figure 1.1.3*. The curve of crop price at Bern has a double peak just before the harvest season in late spring reaching an inflation of 317% and 344% respec-

tively. This trend is also characteristic for the price development in other Swiss cities especially in Eastern Switzerland [Krämer, 2015]. However, this sharp increase in crop prices was not observed at Geneva and Lausanne where inflation did not exceed 270%. Historical sources also reported differences in mortality between the western and eastern part of Switzerland [Krämer, 2015]. This disparity between West and East is remarkable, considering that Switzerland is a small country with similar preconditions for each city.

The gradient could be explained by differences in social-economical habits such as food storage utilities, trade interconnections, political decisions in disaster management or the level of social equality. Such differences have been intensively discussed in Krämer 2015. Further explanation might be given by a gradient in climate anomalies between eastern and western parts of Switzerland causing differences in crop yields. Pfister suggests that 95% of variance in yearly crop yields can be explained by different weather conditions (the other 5% by soil-depletion) [Pfister, 1984] and differences in crop yields could be observed indeed. Crop yield losses of two third of mean harvest have been recorded for Luzern [Bossard-Borner, 1998], whereas only one third got lost in the canton of Vaud [Michaud, 1976].

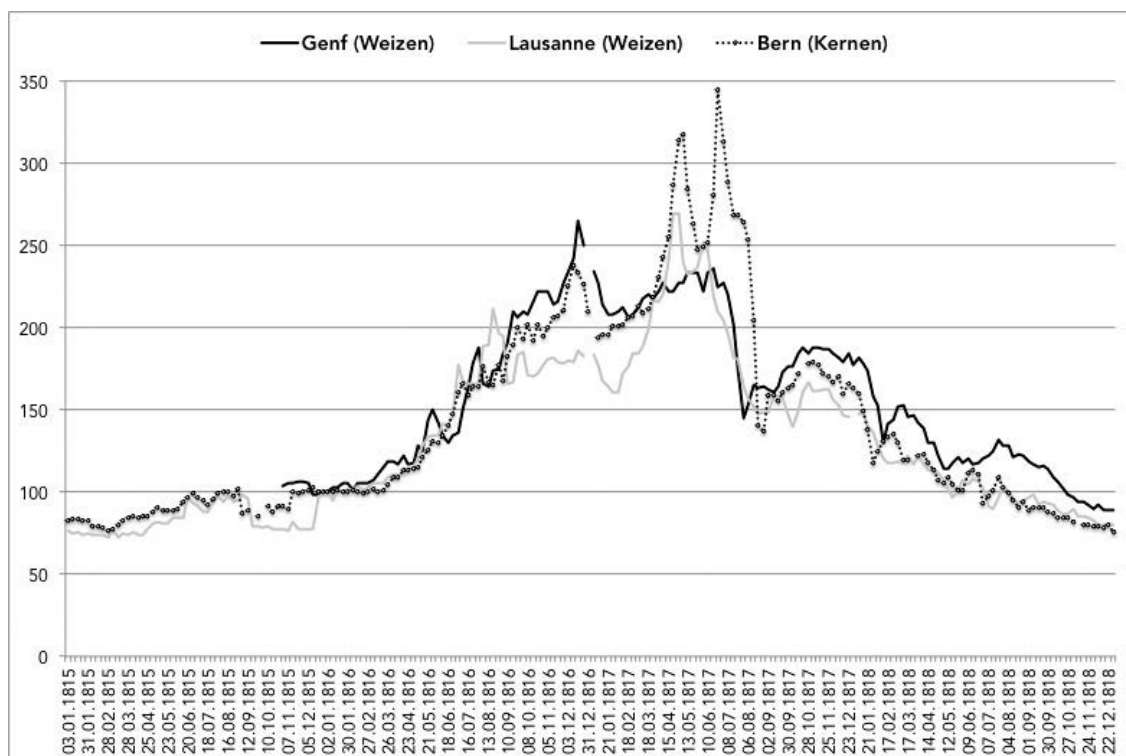


Figure 1.1.3: Development of crop prices (wheat for Geneva and Lausanne, corn for Bern) between March 1815 and December 1818. Index value 100 is set at the first price notation in 1816.

[From: Krämer, 2015]

1.2 Objectives

The overall aim of this study is to analyse how a volcanic eruption may affect climate and agricultural output and in more detail, the impacts on yield productivity in Switzerland triggered by a reoccurrence of the eruption of Tambora today. This requires first a simulation of climatic conditions, which output variables subsequently serve as input to a crop model. As only a few station time series exist for 1816/17, the analysis of this study includes further a broad downscaling of climate variables and crop yields for the Swiss Plateau. From the underlying scenario and the overall aim, two main research questions arise. First, anomalies in climatic conditions between the years 1816 and 1817 simulated for today (1816/17_today) and the past few years are to be described and compared with the anomalies between 1816/17 and a reference period for 1816/17. Therefore, a method to extrapolate station data from 1816/17 to raster data for today as well as an algorithm defining the climate scenario today has to be framed to answer the first research question:

- *How would the climate in Switzerland change on small scale if the eruption of Tambora 1815 reoccurred today?*

Secondly, anomalies in crop yields between the 1816/17_today scenario and the past few years will be analysed. Additionally, yields in 1816 will be reconstructed and subsequently compared to a historical reference period (ref_hist) as well as to yields assessed for the 1816_today scenario in order to analyse the effect of climate warming on crop productivity.

- *Based on the climate simulation, how would crop yields in the Swiss Plateau evolve under the scenario of 1816_today and might had been evolved in 1816?*

One further aim is to investigate whether an West-East gradient within climate variables and hence in crop yields in 1816/17 exists for Switzerland:

- *Does the simulation show a West-East gradient in climate and crop yields in Switzerland for 1816/17?*

This thesis is structured as follows: In chapter 2, the data used for the climate simulation are presented. Chapter 3 describes the methodical approach applied for the downscaling of cli-

mate variables and presents the crop model used to estimate potential crop yields. The results of the climate simulation and the output of the crop model are shown in chapter 4 and discussed in chapter 5. To conclude, the thesis ends with a short summary of the main empirical findings and an outlook on further research that might be of interest (chapter 6).

2 Data

Data of six climate parameters are used in this thesis. Daily maximum and minimum temperature [T_{max} , T_{min}], precipitation sums [$Prec$] and irradiance [I] serve as input variables into a generic crop model that is described in chapter 3.2. Furthermore, surface pressure [p] and wind direction [wd] are used for the weather type classification (chapter 3.2).

Table 2.1 gives an overview over the different time periods used in this study and shows the nomenclature applied to define each period. Whenever we refer to the actual years 1816 or 1817, 1816 or 1817 is used (1816/17 if we refer to both years) and we use 1816/17_today if we refer to 1816/17 simulated for the scenario of a reoccurrence of the Tambora eruption today. The reference period for 1816/17 is called `ref_hist`. The definition of its timeframe is given in the next section (chapter 2.1.1). The reference period used for the day

Table 2.1: Nomenclature of the time periods used in this study. If we refer to both years, 1816 and 1817, 1816/17 and 1816/17_today are used respectively.

Time period	Nomenclature	
Actual 1816	1816	
Actual 1817	1817	1816/17
1816 simulated for today	1816_today	
1817 simulated for today	1817_today	1816/17_today
Reference for 1816/17	ref_hist	
Reference for 1816/17_today	ref_today	
Short Reference (2000-2009)	ref_2000	

resampling process (chapter 3.1.4) is labelled as `ref_today` and includes the years 1982-2009. Anomalies in climate and crop yield for 1816/17_today are computed on comparison with a shorter reference period (2000-2009), called `ref_2000` (chapter 4.2.1).

2.1 Station data

Data from two different time periods are needed to simulate climatic conditions. One period includes years between 1800 and 1820, the second time period is `ref_today`.

2.1.1 Ref_hist

For the 1800-1820 time period, daily climate data recorded at the weather observation stations in Geneva (G, 420mamsl), Delsberg (D, 439mamsl) and Hohenpeissenberg (Hpb, GER,

977mamsl) is available. The temperature time series of Geneva and Hohenpeissenberg include sub-daily records, measured at local sunrise and 2pm (Geneva) and 7.30am and 2.30pm (Hohenpeissenberg) respectively. Only daily mean temperature is accessible for Delsberg. Additionally, daily pressure levels measured at 2pm at all three stations and daily precipitation sums at Geneva are available. Furthermore, discrete wind direction data measured at noon is available for Geneva and Hohenpeissenberg.

Time series of Geneva and Delsberg are retrieved from the Swiss National Basic Climatological Network (Swiss NBCN). Swiss NBCN has been defined by MeteoSwiss in 2007 [Begert et al., 2007] and consists of 29 climate stations and 46 precipitation stations. The time series have been digitalised and homogenised in course of the DigiHom project under the lead of Stefan Brönimann [Fülleman et al., 2011]. However, most time series do not start before 1864 when MeteoSwiss became operational at 88 weather stations. Thus, records for the years 1800 to 1820 are only available for Basel (1755 – 2010), recorded at the weather station near Delsberg, and Geneva (1753 – 2010).

As Geneva and Delsberg lie both in the western part of Switzerland, data from a third station in the East is needed to cover the Swiss Plateau sufficiently. The only station that came into question was Hohenpeissenberg (GER), situated in the East of lake Bodensee (*figure 2.1.1*). Other Stations like Frankfurt, Mannheim or Milan would have been too distant. Hohenpeissenberg is globally the oldest weather station and is affiliated with the German Meteorological Service (Deutscher Wetterdienst). The time series starts in 1781 and ends 2009; a detailed data description of temperature homogenisation is given in Winkler 2009 [P. Winkler, 2009].

For the definition of `ref_hist`, all volcanically perturbed years have been removed from the 1800-1820 period according to Auchmann et al., 2012. These are the years 1815 to 1817 being perturbed by the eruption of Tambora and the years 1809 to 1811, perturbed by an unknown eruption in 1809 [Cole-Dai et al., 2009].

2.1.2 Ref_today

Gridded data of solar irradiance does not start before 2004, hence the time series would have been too short for the purpose of this study. Furthermore, no raster data for pressure exists. Thus, station records of daily pressure levels and solar irradiance from 31 stations of the automatic measurement network of MeteoSwiss (SwissMetNet) located in or around the Swiss Plateau will be used. The stations are listed in the Appendix (*table A*) and the geographical

distribution is shown in *figure 2.1.1*. Detailed information for each station is available on the homepage of MeteoSwiss (www.meteoschweiz.admin.ch).

Most records start in 1981 and end in 2009 (Hohenpeissenberg) or 2010 as of the date this study started. To ensure a homogeneous cover over the whole time period, only measurements from 1982 to 2009 have been used in this study. For Hohenpeissenberg, the time series described above (section 2.1.1) are used, as this station is not captured by the raster data of MeteoSwiss.

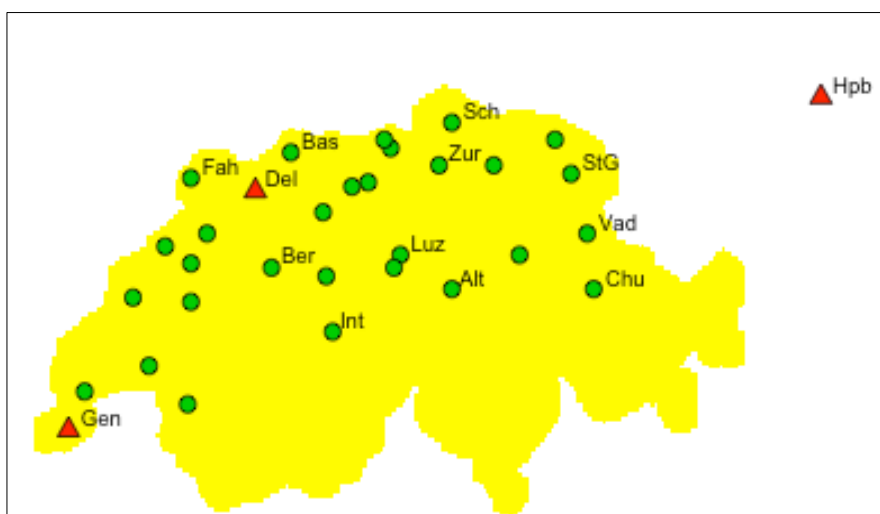


Figure 2.1.1: Distribution of the 32 weather stations of SwissMetNet. The red triangles mark the three stations, whose time series for the early 19th century are used in this study.

2.2 Raster data

For `ref_today`, daily raster data interpolated to the `ch02.lonlat` grid is available for mean, minimum and maximum temperature (in degree Celsius) as well as for precipitation (in mm/day). The grid `ch02.lonlat` has a resolution of 1.25 minutes in longitude (approx. 2.3km) and latitude (approx. 1.6km). This raster dataset had been achieved by interpolation between 90 homogenous long-term hourly time series, recorded at stations of the operational station network SwissMetNet of MeteoSwiss [Stöckli, 2013]. It is rectangular constituted as a two-dimensional 241 x 103 matrix with grid cells lying outside the Swiss border being flagged as “NA”. The geographic coordinate system used as reference for the grid edge-points is the World Geodetic System 1984 (WGS-84).

Data accuracy of temperature appears high as standard errors of more than 1 degree Celsius may occur (1.7 °C over the Alps in winter). Furthermore, influences on local temperature due

to small-scale topography and land cover (agriculture, lakes etc.) are not modelled, resulting in a too smooth spatial variation [Frei, 2013]. However, this is not of great significance for the purpose of this study since rather differences than absolute values are analysed (chapter 3.1).

The model of precipitation shows a systematic measurement error correlating significantly with rainfall intensity (negative correlation), wind speed (positive correlation) and altitude (positive correlation: from 4% in summer at low altitudes to over 40% in winter above 1500 mMSL) [Neff, 1977; Yang et al., 1999; Sevruk, 1985]

2.3 Topography

CropSyst requires altitude data in addition to climate variables. The digital height model DHM25 is used in this study. DHM25 has a grid cell-width of 200m and is provided by swiss-topo. It uses the Swiss coordinate system CH1903+ and is online available in a xyz-format. [http://www.toposhop.admin.ch/de/shop/products/height/dhm25200_1]. The model is mainly based on altitude information of the Landeskarte 1:25 000 (LK25).

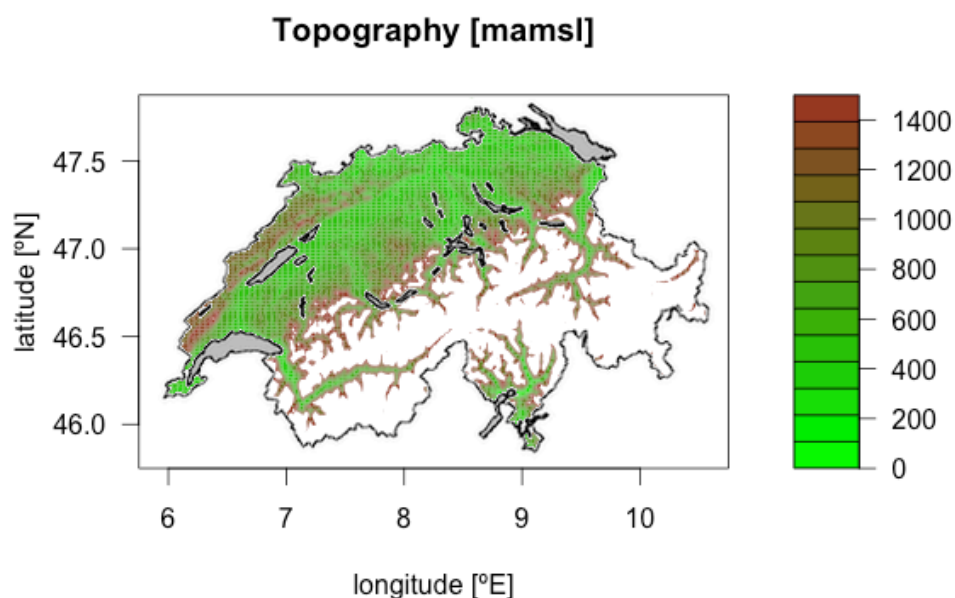


Figure 2.3.1: Grid data of altitude (in meters above mean sea level [mamsl]) from the DHM25 model extrapolated to the ch02.lonlat grid for grid cells with altitude <1500mamsl.

As climate data of a lower resolution is used in this thesis (ch02.lonlat, see chapter 2.2), the altitude attributed to one grid cell of the MeteoSwiss raster dataset is the median over all grid cells of the DHM25 within the respective 1.25 x 1.25 degrees minutes. The outcome of this transformation is presented in *figure 2.3.1*.

3 Methods

Crop yields are basically derived in two steps. In the first part, values of climate parameters are simulated for the different climate scenarios. Therefore, climatic conditions as they had prevailed in 1816 and 1817 (1816/17) need to be reconstructed and subsequently combined with the climatic framework of today (1816/17_today). This climate data (daily minimum and maximum temperature, precipitation sums and solar irradiance) will then be used as an input into a crop model in a second step in order to generate agricultural output data.

3.1 Climate simulation

The climate is partly simulated on the basis of an approach already applied in Auchmann et al. (2012). The main idea is to establish a classification of weather types. Therefore, weather classes separated by pressure, pressure tendency (p_{tend}) and wind direction are created and each day is subsequently allocated to its fitting weather class. All the calculations are done in R, a programming language and software environment developed for statistical purposes [Fox et al., 2005].

3.1.1 Data interpolation

Initially, two different approaches have been taken into consideration to select the analogue days. One possibility was to classify each day in 1816/17 separately for the three stations G, D and Hpb. Even though this approach would give a much higher specification, it was not suitable for the purpose of this study. Theoretically, this classification gives 19^3 possible weather constellations, for which the pool of analogues for each constellation was clearly too small. Thus, only 19 weather types are derived representing the entire Swiss Plateau by using, for each day, the mean of the variables of the three stations. This is straightforward for pressure and pressure tendency but somewhat more difficult for wind direction because of its circular nature.

Wind direction

As wind is a nonlinear, direction-dependent variable, no mean can be directly derived. A bilinear interpolation is applied on the rotational data instead. In the following, a short explanation of the procedure is given.

The wind directions in Geneva [X] and Hohenpeissenberg [Y] (no wind data is available for Delsberg) are stored in a two-column matrix and subsequently arranged in order of “size” for each day (shown in *figure 3.1.1*). Wind data from Geneva is scaled clockwise from 1-8, 1 representing northerly wind and 8 north-westerly wind. At Hohenpeissenberg, the data had originally been scaled from 4 to 32. Thus, we transformed the data from Hohenpeissenberg into the scale applied at Geneva. In a next step, 8 is added to each value i in the first column (now containing the smaller daily value of the two) that is smaller than its corresponding value i in the second column minus 4. In doing this, the daily pairs of values that geometrically, but not numerically, lie in the same semicircle (e.g. N =1 and W = 6) are transferred, so that its values also numerically lie within the same semicircle.

$$(1) \begin{Bmatrix} x_1 & y_1 \\ x_2 & y_2 \\ x_3 & y_3 \end{Bmatrix} \rightarrow \begin{Bmatrix} z_1 & y_1 \\ x_2 & y_2 \\ y_3 & x_3 \end{Bmatrix} \text{ with } y_i \geq x_i + 4, \text{ hence } y_1 \rightarrow z_1 = x_1 + 8, \text{ and } x_3 > y_3$$

$$(2) \begin{Bmatrix} z_1 & y_1 \\ x_2 & y_2 \\ y_3 & x_3 \end{Bmatrix} \rightarrow \left(\begin{Bmatrix} z_1 \\ x_2 \\ y_3 \end{Bmatrix} + \begin{Bmatrix} y_1 \\ y_2 \\ x_3 \end{Bmatrix} \right) * 0.5 = \begin{Bmatrix} b_1 \\ a_2 \\ a_3 \end{Bmatrix} \rightarrow \begin{Bmatrix} a_1 \\ a_2 \\ a_3 \end{Bmatrix} \text{ with } a_i = b_i - 8$$

Figure 3.1.1: Example to illustrate the interpolation of wind data. x is the wd at Geneva, y at Hohenpeissenberg. For reasons of clarity and comprehensibility, the process is only shown for three days (x_1, x_2, x_3 and y_1, y_2, y_3 respectively).

Having processed the wind data that way, the bilinear interpolation can now be conducted resulting in one daily average. From the means i that yet are still greater than one full circle (=8), 8 has to be subtracted again to get the final value. Non-integer numbers are round according to long-term wind situation considering the last and previous 5 days.

Solar irradiance of ref. today

As mentioned in section 2.2, there is only station and no raster data of a long enough time series available for solar irradiance. Therefore, a gridded dataset needs to be generated for that variable. This is done by a weighted interpolation applying a k-nearest neighbours algorithm.

First, the coordinate system used by MeteoSwiss is transferred such that the south-western edge point sets the origin (0;0). For each grid cell in the MeteoSwiss raster, the distance of its mid-point to the origin is then calculated and the station coordinates are subsequently defined. The value for solar irradiance of each grid cell mid-point i is then derived simply by taking

the mean over the three stations with the shortest Euclidean distance to grid i (3-nearest neighbours).

3.1.2 Weather type classification

In a first step, the time series of climate variables from the three stations G, D and Hpb are interpolated for the two time periods 1800-1820 and ref_today in order to get one daily value for each variable representative for the Swiss Plateau. For pressure, absolute as well as tendency values are used. Pressure tendency is calculated as the difference between pressure levels at day i and day $i-1$. The interpolated values of pressure and pressure tendency then have to be normalised by removing the annual cycle and a subsequent standardisation. This is necessary as pressure shows large annual variation. The mean and the standard deviation (sd) are computed as the first two harmonics based on the daily data at the respective day-of-the-year in the corresponding time period (1800-1820 or 1982-2009). This process is among others discussed in Aslan et al. (1997) and Justino et al. (2010). The first two harmonics describe an oscillation over a certain time period. In this case, the first harmonic describes an oscillation with a wavelength of 365 days, the second an oscillation with wavelength of 365/2 days:

$$(3) \quad \text{First harmonics:} \quad A_1 = \sin\left(\frac{2\pi i}{T}\right); \quad B_1 = \cos\left(\frac{2\pi i}{T}\right)$$

$$(4) \quad \text{Second harmonics:} \quad A_2 = \sin\left(\frac{4\pi i}{T}\right); \quad B_2 = \cos\left(\frac{4\pi i}{T}\right)$$

T stands for the entire time period, in this case 365 days. The harmonics are computed for each day-of-the-year, represented by i . The annual cycle component acc of the mean and the standard deviation is then generated using a least squares fitting algorithm:

$$(5) \quad \text{acc at day } i: \text{acc}_i = \beta_0 + \beta_1 * a_1 + \beta_2 * a_2 + \beta_3 * b_1 + \beta_4 * b_2$$

In this equation, all β are coefficients obtained from a least square estimate for the mean and the standard deviation on the four harmonical cycles. The corresponding values of the harmonics at day i are represented by lower case letters (a, b).

The corrected mean ($\langle v \rangle$) and standard deviation σ_v of pressure and pressure tendency are then obtained by subtracting the annual cycle. Finally, z-scores z of pressure and pressure tendency are computed on these adjusted mean and standard deviation. As from two different time periods, the variables have to be normalised with respect to the corresponding time period (ref_hist and ref_today, respectively). Following this, weather types will be classified by

thresholds of pressure, pressure tendency and wind direction to define weather classes. Thresholds set by Auchmann et al. (2012) are applied in this study.

$$(6) \quad \text{Z-score of variable } v: z_v = \frac{v - \langle v \rangle}{\sigma_v}; \text{ with } v \in \{p; p_{tend}\}$$

Each day in ref_hist and ref_today as well as in 1816/17 will then be allocated to the most appropriate weather class with regard to pressure, pressure tendency and wind direction. This results in a specific frequency distribution of the weather types for the three time periods. According to results in Auchmann et al. (2012), this pattern is expected to be significantly different for summer 1816 compared to the two reference periods.

3.1.3 Resampling of days

Once the distribution is done, for each day in 1816/17 its most appropriate representative within ref_today is selected. This selection is based on z-scores of temperature and precipitation acquired from the station time series for Geneva, Delsberg and Hohenpeissenberg (chapter 2.1). The main objective of the resampling process described in this section is to indirectly obtain values of solar irradiance (I). For the time period 1800-1820, only discrete or descriptive data of cloud coverage exists that cannot be transferred into radiation information. However, values of solar irradiance are needed for the crop modelling (see chapter 3.2).

In order to compute the Euclidean distances, z-scores of temperature and precipitation have to be computed for each day in 1816/17 and ref_today. Temperature data (daily minimum and maximum temperature at G and Hpb and daily mean temperature at D) is standardised in the same way as pressure data (see above). However, temperature in ref_today shows a time dependent trend that has to be removed first. The trend is computed with a regression of temperature on time with fitted values representing the trend and the residuals the detrended time series.

Once the z-scores are computed, the Euclidean distances can be derived. For each day i in the two years 1816/17, within all days in ref_today distributed to the same weather class, the one day is selected that has the smallest Euclidean distance to day i with respect to normalised precipitation and temperature. Days that might be considered are narrowed down by a time window of ± 30 calendar days around day i to account for seasonal patterns. Since the standard deviation also shows an annual cycle, every selected day x has to be divided by its yearday-specific standard deviation σ_x and subsequently multiplied by the standard deviation σ_i at

yearday i . In a last step, the cell-specific component of the annual cycle of ref_today at day i is added to the chosen day for each grid cell of the raster data. Minimum and maximum temperature, precipitation and solar irradiance of those days selected in that way constitute the climate in $1816/17_today$. *Figure 3.1.2* gives an overview over this process.

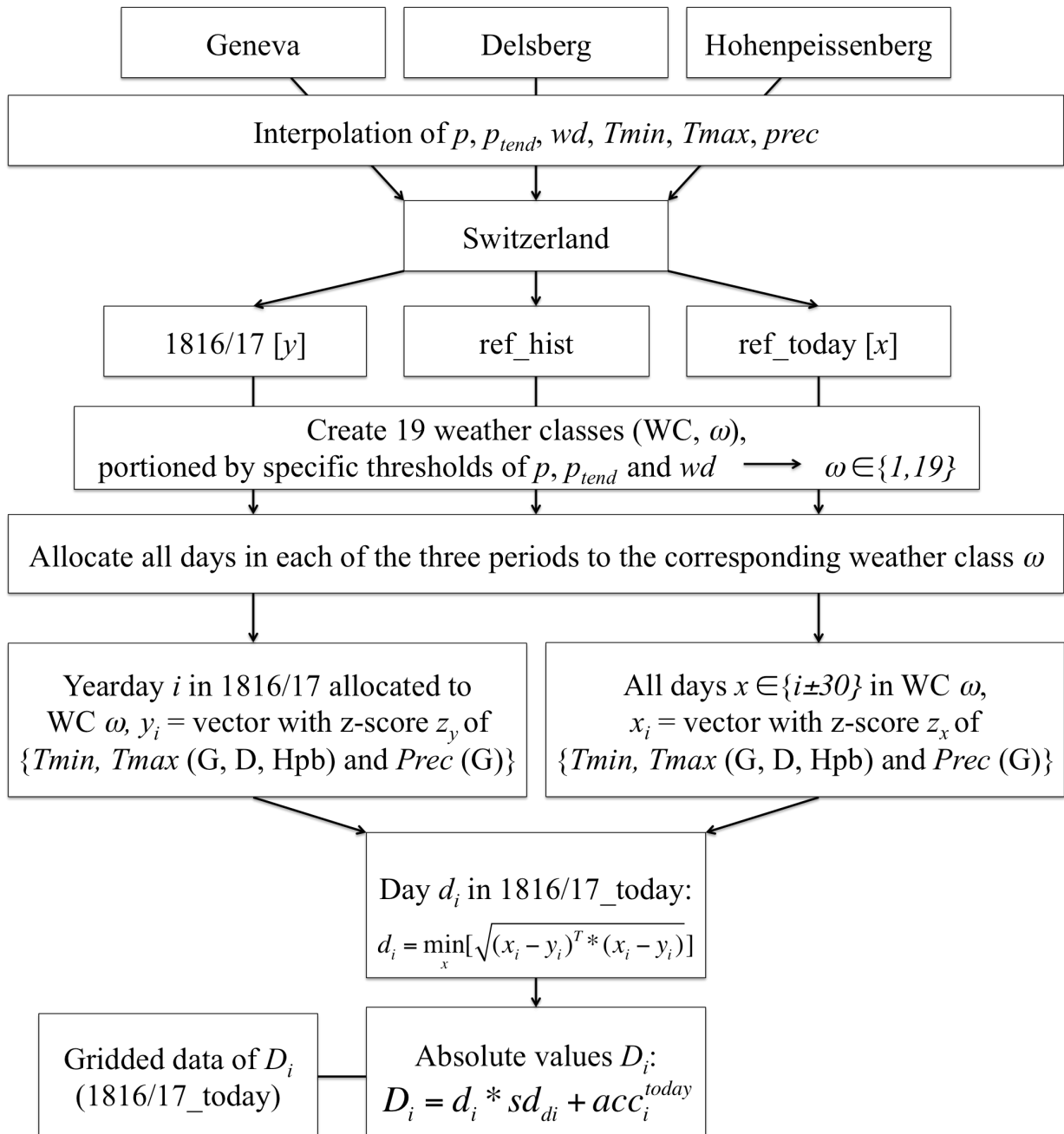


Figure 3.1.2: Flow chart for the simulation of climate data. acc_i^{today} is the annual cycle component of the annual cycle for ref_today at day i .

3.2 Crop modelling

The simulation of crop yields is conducted with CropSyst. CropSyst is a daily time step cropping system simulation model specifically designed for crop management assessments with regard to crop productivity. The framework of CropSyst is explained in detail in Stöckle et al. (2003) and in the online user manual. That user manual is available on: <https://nishat2013.files.wordpress.com/2013/11/cropping-system-manual-book.pdf>. The model is designed for simulating crop growth in a single land block fragment. Potential above ground crop growth is measured in terms of total potential above ground biomass accumulation B . In the following, the most important equations constituting the model as they are described in the users manual (chapter 3.2) and the setup of the initial conditions (chapter 3.3) are presented.

3.2.1 Sowing time

CropSyst allows the user to choose between a fixed (crop growth begins at a fixed date) and a computed planting mode. In this study, the computed planting mode is used in order to capture temperature effects. In that mode, the date of sowing is defined by a five-day average air temperature $[(T_{max} + T_{min})/2]$, which has to be above a crop specific required planting temperature T_{req} , and a specified water content [m^3 water / m^3 soil] in the second soil layer, that must not be below the required water content.

3.2.2 Rooting

Root growth is determined by root depth and root density. Root depth is calculated on the leaf area index per unit soil area (LAI), which is determined as a function of accumulated above ground biomass B :

$$(7) \quad \text{Leaf area index } LAI [m^2 m^{-2}] = \frac{SLA * B}{1 + p * B}$$

SLA is the specific leaf area (m^2/kg) and p a coefficient controlling the fraction of biomass that is attributed to leaves. It is zero if all biomass is allocated to the leaves. Root density is determined as a linear function of root depth.

3.2.3 Phenology

Each stage of crop development is determined by accumulated thermal time measured in growing degree days (GDD). Thermal time accumulates over the entire growing season, starting with the sowing date until harvest. Thermal time at day i , GDD_i , is computed as the dif-

ference between daily average temperature T and a crop-specific daily base temperature $T_{GDDbase}$. The accumulated thermal time since planting, $CGDD_i$, is calculated as the sum of the accumulated thermal time at the day before $CGDD_{i-1}$ and today's thermal time. For $T < T_{GDDbase}$, GDD_i is zero. The maximal GDD_i is reached for a certain threshold temperature $T \geq T_{cutoff}$.

Vernalization

Vernalization is the induction of flowering by a previous cold period. This phenomenon is observed especially for winter crops, which need to be exposed to temperatures between 0-12°C for 10-60 days after germination to promote to the flowering stage [Stöckle et al., 2013]. CropSyst calculates vernalization on a vernalization factor f_{ver} with values between 0 and 1. This factor is zero for crops insensitive to vernalization.

Photoperiod

Some crops (long-day plants, e.g. winter barley) start to accumulate physiological time towards flowering when the day length exceeds a crop-specific minimum and some (e.g. maize or potato) when the day length becomes shorter than a maximum threshold. Other crops are insensitive to day length. In CropSyst, the influence of photoperiod on phenological development is computed by a simple linear approximation.

3.2.4 Biomass accumulation

In a first step, above ground biomass accumulation B is computed under unstressed circumstances, defining the potential biomass growth given a certain set of parameters. Above ground biomass production is dependent on three factors: intercepted radiation iR (radiation dependent, $B_{R,Tlim}$), transpiration Tr (water dependent, B_{Tr}) and nitrogen uptake N (nitrogen dependent). For the simulations in this study, nitrogen uptake was not considered. The total above ground biomass accumulation B is eventually derived as the minimum of $B_{R,Tlim}$ and B_{Tr} .

Radiation dependent production

Radiation dependent daily biomass production B_R is temperature limited. Thus, B_R is corrected by a temperature limitation factor T_{lim} to get the actual radiation dependent growth:

$$(8) \quad \text{Total radiation dependent biomass production [kg/m}^2 \text{ day}^{-1}] B_{R,Tlim} = B_R * T_{lim}$$

where T_{lim} is 1 for T exceeding a crop specific optimal growth temperature T_{opt} and zero for $T \leq T_{GDDbase}$. Otherwise, it is calculated as a fraction of $T - T_{GDDbase}$ with respect to the range T_{opt}

– $T_{GDD_{base}}$. Following Monteith, B_R can be computed either on photosynthetically active radiation (PAR) or on total radiation (TR) [Monteith, 1977]. In this study, the second method is applied with B_R computed as:

$$(9) \quad \text{Radiation dependent biomass production [kg/m}^2 \text{ day}^{-1}] B_R = RUE_{max} * iR$$

RUE_{max} (kg MJ⁻¹) is a crop dependent maximum radiation use efficiency parameter. iR is calculated as fraction of total daily solar irradiance I above the crop. The fraction of incident I intercepted by the green canopy (FCC) is calculated as follows:

$$(10) \quad FCC = 1 - e^{(\min(-1.4Kc, 0.9) * GAI * clumping)},$$

$$(11) \quad clumping = (0.75 + 0.25(1 - e^{(-0.25GAI)}))$$

Kc is the evapotranspiration (ET) crop coefficient. It is either equal to the ET crop coefficient input parameter Kc' or calculated as $1 + LAI(Kc' - 1)/3$ for $Kc' > 1$ and $LAI < 3$. GAI is the green area index that is determined by the leaf area expansion-related biomass accumulation ($LAERB$). It has generally the same value as the LAI during period of active growth of green area. However, the leaf area index decreases after flowering.

Water dependent production

Daily biomass production depending on crop transpiration (B_{Tr}) is calculated on the assumption of a conservative relationship suggested in Tanner and Sinclair, 1983:

$$(12) \quad \text{Potential crop transpiration biomass production (kg/m}^2 \text{ day}^{-1}) B_{Tr} = \frac{K_{B_{Tr}} T_p}{VDP}$$

VDP is the daytime mean atmospheric water vapour pressure deficit (in kPa), T_p the actual potential crop transpiration (kg/m² day⁻¹) and $K_{B_{Tr}}$ a biomass transpiration coefficient, the values of which can be taken from Tanner and Sinclair (1983). The Tanner-Sinclair relationship becomes unstable for low VDP (humid conditions), thus only radiation dependent biomass accumulation is calculated in such cases.

3.2.5 Crop yield

Crop harvest takes place after a specific number of days after maturity. Potential yields are computed as the total accumulated biomass production B , from sowing until harvest date, multiplied with a harvest index HI . The HI defines the proportion of above ground biomass

that is usable as yield and is adjusted by the average water stress index, giving account to sensitivity towards water stress during flowering and grain filling.

3.3 Model setup

3.3.1 Weather data

For weather data, the climate variables (T_{max} , T_{min} , $precipitation$ and I) of each climate scenario simulated in the first part of the thesis are used. Therefore, grid values of the four variables are stored in a first textfile (.dat) and the grid's geolocation information (altitude, longitude and latitude) in a second textfile (.st). A UED import wizard provided by CropSyst is used to transform the location files into an UED format, which can then be loaded into CropSyst. The model requires time series with length of a minimum of 3 years. Thus, the time series for the yield simulation of the 1816/17_today scenario is constituted by twice the 1816_today and once the 1817_today weather. For 1816_today, the simulation output for the second year is chosen as growing season for winter crop lies within two calendar years.

3.3.2 Soil

All crop simulations are conducted using the soil Teanikon_NABO.sil. This soil is classified as weakly clay loam (Lt2) by AG Boden, constituted by 25-35% clay, 15-45% sand and 30-50% silt [AG Boden, Bodenkundliche Kartieranleitung, Hannover 1994]. Daily cascade is chosen for the infiltration submodel and the soil is subdivided into 7 layers and 22 sublayers. Average pore volumes for clay loam soils are between 39.5% and 44% [AG Boden, 1994]

3.3.3 Crop Management

All parameters have been set to allow optimal growth conditions. Irrigation starts automatically, if soil water availability falls below a certain threshold and no fixed irrigation events are set. Early sow (for spring crops) or late sow (for winter crops) is allowed if more biomass can be accumulated. As sowing date depends on weather conditions, it varies between each grid cell and no single date is fixed. An illustrative example is given in chapter 4.3.5.

3.3.4 Environment

Freezing is set to be only temperature dependent. The potential evapotranspiration (ET) model is selected automatically by CropSyst depending on the variables available. For the set of climate variables used as model input in this study, the Priestley-Taylor equation is used with a Priestley-Taylor constant PT_C of 1.26.

4 Results

4.1 Weather type classification

The outcome of the weather type classification based on thresholds derived by Auchmann et al. (2012) is presented in this first part of the results. A detailed overview over the characteristics of each weather class is given in *table 4.1*.

Table 4.1: Thresholds of the weather type classification. The second column indicates thresholds for pressure and the third column for pressure tendency. The fourth column indicates which wind directions are associated with the respective weather class.

<i>Weather class</i>	p	P_{tend}	wd
Front	$p \leq 2.5$ or $p > 0.75$	$-2.5 < Dp/dt > 2.5$	-
High pressure, northerly wind		-	NW, N
High pressure, easterly wind			NE, E
High pressure, southerly wind			SE, S
High pressure, westerly wind			SW, W
Low pressure, northerly wind	$-2.5 < p \leq 1$	-	NW, N
Low pressure, easterly wind			NE, E
Low pressure, southerly wind			SE, S
Low pressure, westerly wind			SW, W
Rising pressure, northerly wind	$-1 < p \leq 0.75$	$Dp/dt > 0.2$	NW, N
Rising pressure, easterly wind			NE, E
Rising pressure, westerly wind			SW, W
Stationary pressure, northerly wind		$-0.2 < Dp/dt \leq 0.2$	NW, N
Stationary pressure, easterly wind			NE, E
Stationary pressure, westerly wind			SW, W
Falling pressure, northerly wind		$Dp/dt \leq -0.2$	NW, N
Falling pressure, easterly wind			NE, E
Falling pressure, westerly wind			SW, W
Medium pressure, southerly wind		-	SE, S

Days with very low or very fast rising or falling pressure are often associated with cold fronts. Thus, those cases are merged to 1 class with thresholds of -2.5 sd for pressure and ± 2.5 sd for pressure tendency. The other days are classified as high, medium or low pressure cases, separated by thresholds of $+0.75$ sd and -1 sd, respectively. High pressure and low-pressure areas are further distinguished by wind direction (N, E, S, W), which sums up to 8 classes. The initial 8 wind classes (N, NE, E, SE, S, SW, W, NW) are merged by combining each cardinal direction (N, E, S, W) with its clockwise prior intermediate direction (NW, NE, SE, SW). A majority of days show medium pressure values, which makes it necessary to divide these cases not only by wind direction but also by pressure tendency in order to get a more accurate

specification. Three tendency classes (falling, stationary and raising pressure) are specified using thresholds of ± 0.2 sd. This division is negligible for days with medium pressure and southerly wind as only a few such cases appear. The other cases of medium pressure are differentiated with respect to wind directions from N, E and W. This results in 10 classes for medium pressure systems and a total of 19 weather classes.

In the following, the outcome of the weather type classification is described in more detail for each season in 1816/17. The histograms show the frequency of each weather class for the meteorological seasons in 1816 and 1817 (red). Additionally, in the same histogram the frequency of the weather classes is shown for ref_today (black) and ref_hist (black patterned). Implications of differences and possible underlying causes are further discussed in chapter 5.

4.1.1 Winter (DJF)

The frequency distribution of weather classes in winter 1816 does not significantly differ from the distribution in ref_hist or ref_today (figure 4.1.1, left plot). However, the distribution pattern in winter 1817 shows some stronger pronounced deviations (right plot).

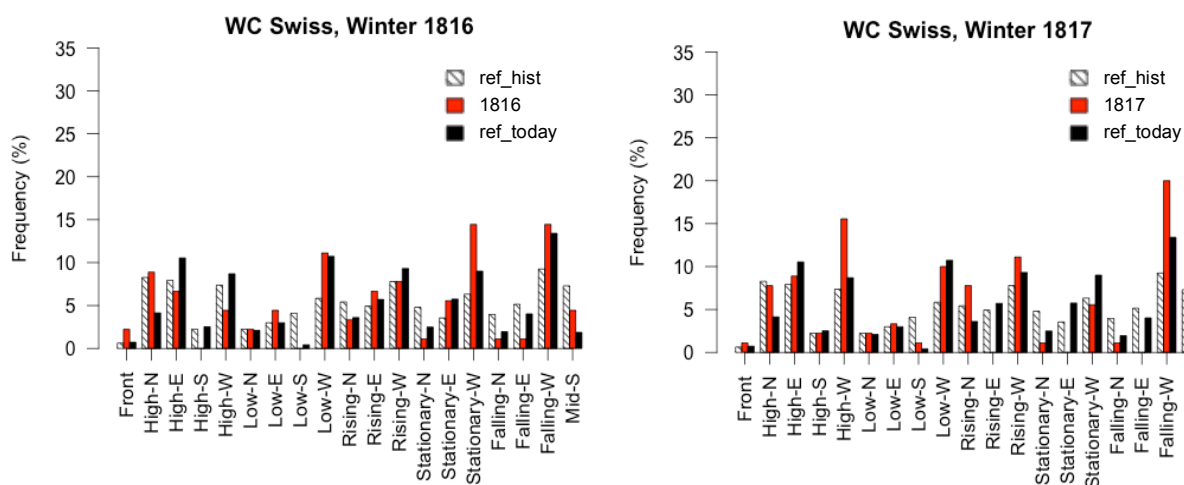


Figure 4.1.1: Histograms showing the relative frequency distribution [%] of weather classes (WC) for winter 1816 (left panel) and 1817 (right panel), represented by red bars, in ref_hist (black patterned) and ref_today (black).

Weather classes with westerly winds appear more frequently. Conversely, not one day characterised by prevailing easterly wind and medium pressure has been classified in winter 1817. Furthermore, there are differences in the distribution pattern between ref_hist and ref_today. Apparently, west wind situations have occurred more frequently since 1982, whereas less northern and southern winds have prevailed.

4.1.2 Spring (MAM)

Figure 4.1.2 shows the outcome of the weather classification for spring 1816 (left plot) and 1817 (right plot). Rather contrary to expectations, the frequency distribution of neither spring 1816 nor spring 1817 is strongly different from the reference periods.

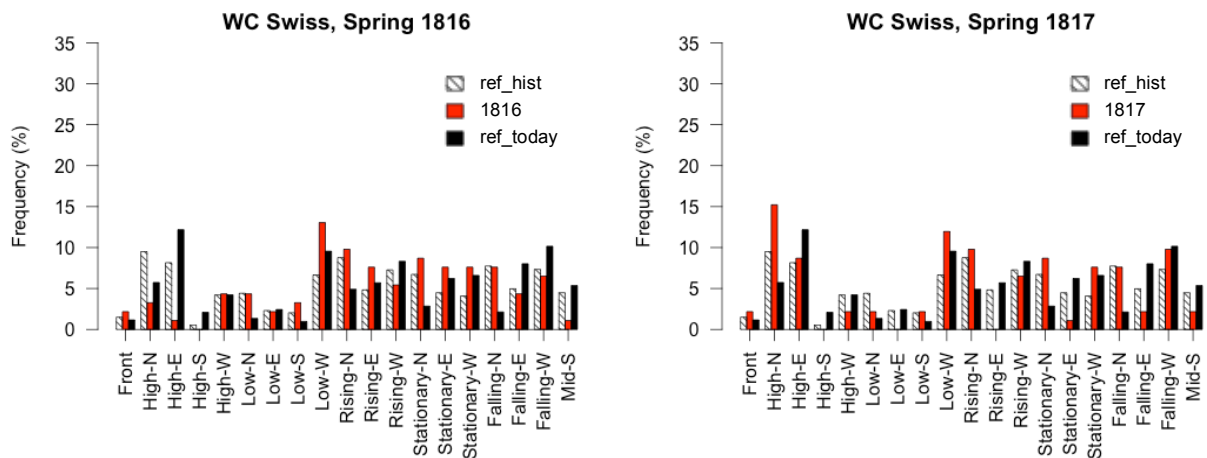


Figure 4.1.2: Histograms showing the relative frequency distribution [%] of weather classes (WC) in spring 1816 (left panel) and 1817 (right panel), represented by red bars, in *ref_hist* (black patterned) and in *ref_today* (black).

Nonetheless, there is a significant decrease in frequency of high-pressure systems in spring 1816 while more cases with medium pressure are observed. The frequency of low-pressure situations remains rather unchanged except for a slight increase in cases with westerly winds. Furthermore, there is a significant increase in frequency of days with northerly wind under medium pressure systems in 1816 compared to *ref_today*.

The same increase can also be observed in spring 1817. However, there is no decline in frequency of days with high-pressure systems as it is found for spring 1816. Instead, only a few medium-pressure cases with easterly wind appear in 1817. Distribution patterns of both years further show a remarkable decline in frequency of days with southerly winds.

4.1.3 Summer (JJA)

The frequency distribution shows the most distinctive shifts in weather types for both years in summer, which is well illustrated by the respective histograms (figure 4.1.3). In addition, the frequency distribution of weather types classified only for Geneva is presented separately in figure 4.1.4 (left panel) in order to compare it with the distribution pattern of the classification applied for Hohenpeissenberg (right panel).

In summer 1816, there are significantly more low-pressure situations, accompanied by a significant decline in frequency of high-pressure systems. Low-pressure systems with westerly winds occurred 5 times as often as in ref_hist and with northerly winds up to 12 times more

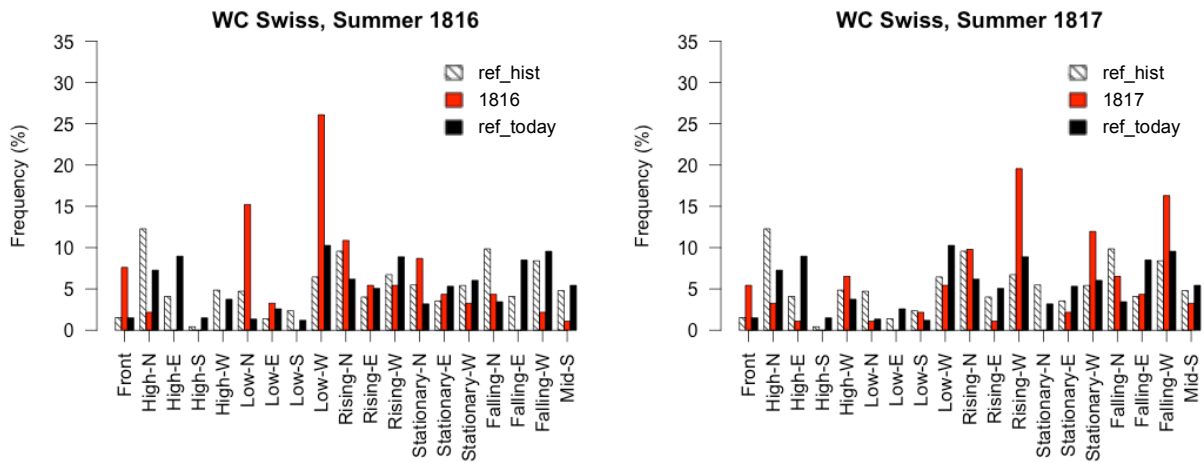


Figure 4.1.3: Histograms showing the relative frequency distribution [%] of weather classes (WC) in summer 1816 (left panel) and 1817 (right panel), represented by red bars, in ref_hist (black patterned) and ref_today (black).

frequent than in ref_today. Fronts did occur almost five times more frequently than in the reference periods. Meanwhile, the frequency of cases with medium, but falling pressure is clearly below average. Similar to the situation in spring 1816 and 1817, days with southerly winds were scarce in summer 1816 compared to both reference periods.

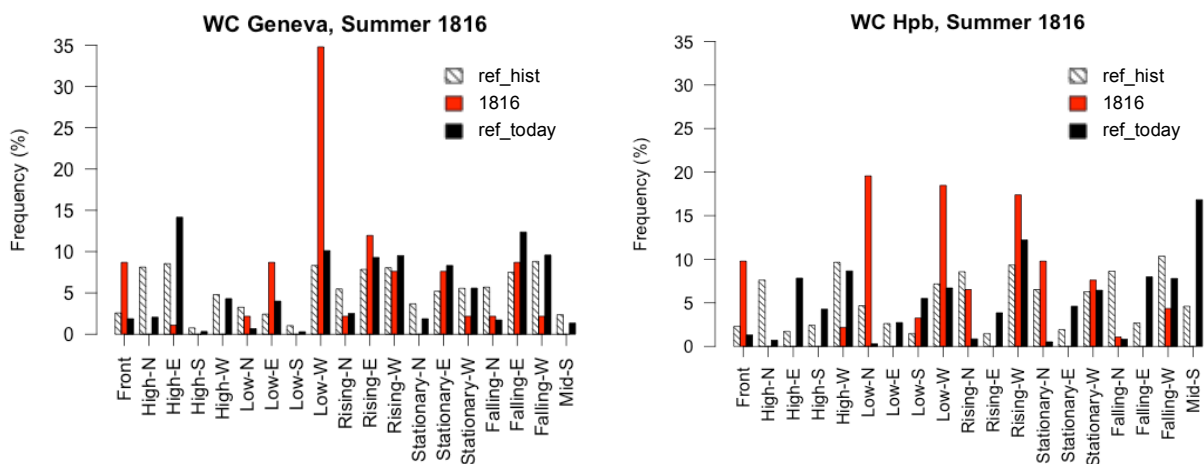


Figure 4.1.4: Histograms showing the relative frequency distribution [%] of weather classes (WC) in summer 1816, represented by red bars, in ref_hist (black patterned) and ref_today (black) for Geneva (left panel) and Hohenpeissenberg (right panel).

The distribution pattern looks different for summer 1817 (figure 4.1.3, right panel). There are no peaks in low-pressure cases with westerly and northerly winds. Instead, days with western wind and medium-pressure appear more often in all three pressure tendency subclasses. Over-

all, fewer cases with northerly winds and stationary medium- or high-pressure are observed. Also, more fronts appear, but not as many as in summer 1816 and the decrease in frequency of southerly winds is less strong.

The outcome of the weather type classification separately applied for Geneva and Hohenpeissenberg shows an even stronger pronounced distribution pattern. At both stations, low-pressure systems prevailed on approximately 45% of days in summer 1816 and more than 20% of cases show a medium but rising pressure. However, the frequency distribution varies within the same pressure-subclass with regard to wind directions: At Hohenpeissenberg, northerly and westerly winds occurred each at about 50% of low-pressure situations, whereas at Geneva there are much more cases with westerly winds. An additional difference between the two stations can be found in the frequency of cases with medium-pressure and southerly winds, which appeared 7.5 times more often at Hohenpeissenberg (15%) than at Geneva (2%).

4.1.4 Fall (SON)

The classification does not reveal any decisive shifts in prevailing weather types for fall 1816 (*figure 4.1.5*, left panel). The only distinction to mention is the higher frequency of cases with medium and rising pressure accompanied by westerly winds and the lower occurrence of high-pressure situations.

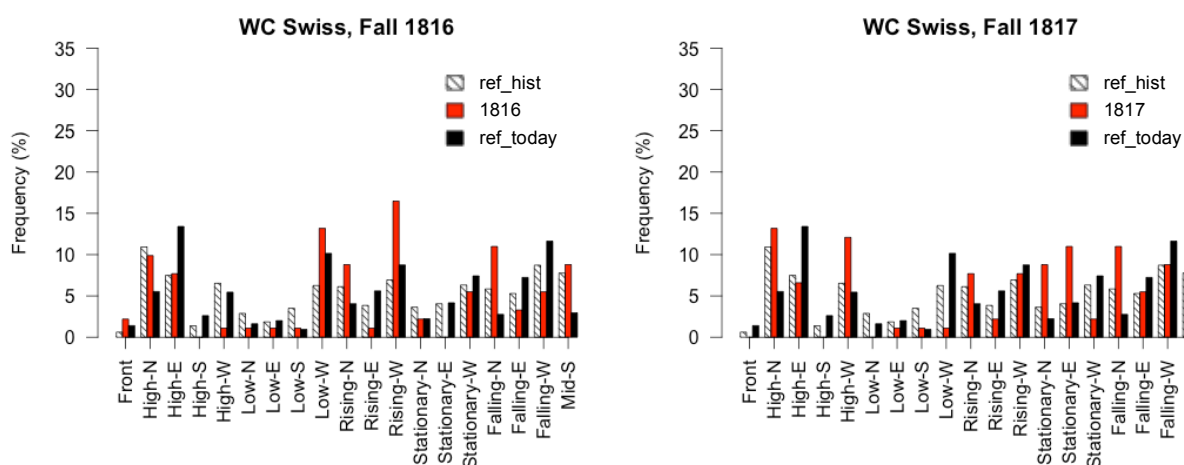


Figure 4.1.5: Histograms showing the relative frequency distribution [%] of weather classes (WC) in fall 1816 (left panel) and 1817 (right panel), represented by red bars, in ref_hist (black patterned) and ref_today (black).

The pattern of fall 1817 looks somewhat different (*figure 4.1.5*, right panel). Cases with low-pressure systems are almost completely missing (only 4% against circa 15% in both reference periods) and no cases with southerly winds are classified. On the contrary, high-pressure sys-

tems appeared in over 30% of the cases and hence noticeably more frequent than in the reference periods. The same applies for medium and stationary pressure situations with winds from the North or the East.

4.2 Climate simulation

In this section, the outcome of the climate simulation obtained by the day resampling process (chapter 3.1.4) is presented. First, z-scores of temperature in 1816/17 and in 1816/17_today are compared and anomalies in daily average temperature and precipitation between 1816/17_today and the ref_2000 average are described separately for the three stations Geneva, Delsberg and Hohenpeissenberg. Afterwards, the result of the downscaling to the ch02.lonlat grid is presented together with the development along a West-East transection through the Swiss Plateau.

4.2.1 Climate in 1816/17 and 1816/17_today at the stations G, D & Hpb

The 1800-1820 period shows no trend in temperatures at neither of the three stations. But there is a positive trend within ref_today that is removed in the way described in chapter 3.1.4. The trend is of significant magnitude (approximately 1.2°C) for time series of all three stations. However, there is no significant trend within ref_2000, which is consistent with findings of the IPCC Report 2014 [IPCC, 2014]. Thus, anomalies in the climate variables of the 1816/17_today scenarios are always based on comparisons with the ref_2000 average.

A first basis for evaluating the methodical approach is given by comparing daily variances in 1816/17 and in 1816/17_today. Daily variances are measured in z-scores of temperature and precipitation, computed as described in chapter 3.1.4. This comparison of z-scores serves the purpose of quantifying anomalies between resampled (1816/17_today) and actual days (1816/17) without a bias due to differences in trend or seasonality.

4.2.1.1 Temperature

In this section, z-scores and absolute values of temperature time series of the 1816/17_today scenario are analysed and compared with the time series of 1816/17.

Z-scores

The average difference over this two-year time period is close to zero, though there is deviation found by seasonal comparison. All seasons in 1816/17_today are too cold (negative z-scores of daily mean temperature). The average z-score for 1816 (z_{1816}) is -0.41 and -0.36 for

1816_today (z'_{1816}) equalling 87% of z_{1816} . The largest anomalies in 1816 and 1816_today are both found for summer with a z_{1816} of -0.83 and z'_{1816} of -0.74 or 89% of z_{1816} . Z-scores in spring and fall do also differ significantly from zero for 1816 (-0.3 and -0.36, respectively) and 1816_today (-0.26 or 88% of z_{1816} and -0.34 or 95%, respectively), as does further z_{1816} in winter (-0.14). The p-value of a student's t-test for winter z'_{1816} (-0.08 or 60% of z_{1816}) suggests significance only on the 95% (p-value = 0.0043) but not on the 99% confidence level (p-value = 0.058).

Average z-scores for 1817 (z_{1817}) and 1817_today (z'_{1817}) also indicate a year colder than the average (-0.14 each), although clearly not as distinctive as for 1816. The z-scores z'_{1817} computed for winter (+0.24) and spring (-0.5) reach 85% of z_{1817} (+0.28 for winter and -0.58 for spring). Anomalies in fall and summer are computed somewhat too high (-0.14 and -0.16, equalling to 107% and 114% of z_{1816} , respectively).

Figure 4.2.1 shows the deviations of the variance in daily mean temperature obtained by the day resampling (1816/17_today) from the variance for 1816/17. Selected days in 1816/17_today with a higher z-score than the respective day in 1816/17 are represented by red bars, days with a lower z-score by blue bars. Overall, the resampling simulates approximately 92% of the variance in temperature in 1816/17.

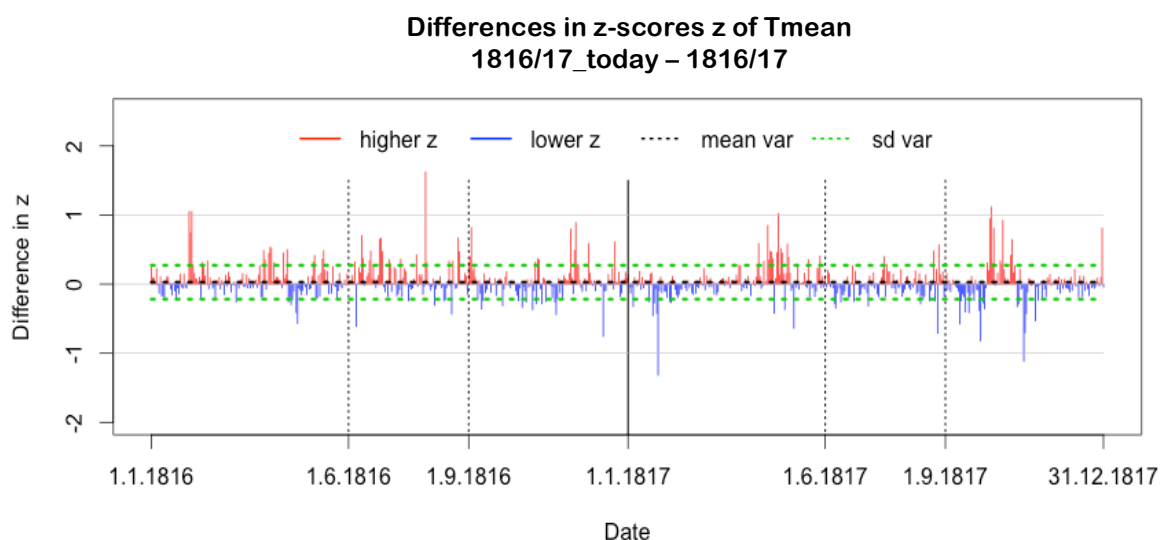


Figure 4.2.1: Comparison of z-scores of daily mean temperature between 1816/17 and 1816/17_today. Red bars represent cases with a higher z-score in simulated temperature (1816/17_today), blue bars cases with a lower z-score. The black dotted line shows the mean difference in z-scores and the green dotted lines the standard deviation of the difference.

Absolute temperature

The *figures 4.2.2 to 4.2.4* show mean temperature time series at Geneva, Delsberg and Hohenpeissenberg for 1816 and 1817. Time series of daily temperature are shown in plot A, respectively, together with the ref_hist average (red dotted line) and the ref_hist standard deviation (blue bolt lines). The time series of simulated temperatures (1816/17_today) are presented in plot B. Mean temperature and the standard deviation are calculated on the ref_2000 average. Plot C serves the purpose of a graphical evaluation of the simulation performance: the anomalies in temperature of the scenarios 1816_today and 1817_today can be compared with the anomalies of the actual years 1816 and 1817. A short summary of the findings for each station will be given in the following.

The time series of temperature in 1816/17 at Geneva and Delsberg look quite similar with respect to day-to-day variance (*figures 4.2.2 & 4.2.3*, plot A). The average standard deviation of temperature is 3.5 for Geneva and 3.7 for Delsberg. The time series for Hohenpeissenberg in 1816/17 (*figure 4.2.4*, plot A) shows more variance and the mean standard deviation of ref_hist is higher (4.6). Variance of temperature within ref_2000 is lower for Geneva and Delsberg (3.1 each), though the deviations show a seasonal pattern with an on average lower variance from late fall to early spring and a higher variance in summer. The variance in temperature at Hohenpeissenberg is generally higher than in ref_hist (4.8) with no seasonal pattern in deviations.

Table 4.2: Seasonal average temperature anomalies in 1816 at the three stations G, D, Hpb. In each case, the first column shows the observed anomalies in 1816 and the second the simulated anomalies for 1816_today. The third column contains p-value of weather the difference in anomalies between 1816 and 1816_today is significant (y) or not (n).

Season	Geneva			Delsberg			Hpb		
	1816	1816_today	p	1816	1816_today	p	1816	1816_today	p
Winter	-0.3	-0.3	n	-0.2	-0.3	n	-1.8	-1.8	n
Spring	-0.7	-1.6	y	-1.5	-1.9	y	-2.1	-2.7	y
Summer	-2.9	-3.1	n	-3	-3.2	y	-2.9	-3.6	y
Fall	-0.6	-1	y	-1.8	-1.6	n	-1.4	-1.8	y

1816 and 1817 were too cold at all three stations, though with significantly stronger negative anomalies in 1816. The average annual temperature 1816 at Hohenpeissenberg was 2.1°C lower than the ref_hist average, 1.2°C lower at Geneva and 1.7°C lower at Delsberg. *Table 4.2* presents the mean seasonal temperature anomalies in 1816 and 1816_today. Temperature anomalies are negative for all seasons in both, the actual year 1816 and the 1816_today scenario. However, the temperature for 1816_today shows stronger negative anomalies with the

largest deviation from the observed anomalies (1816) in spring. The mild climate in winter 1816/17 (+1.7°C at Geneva and Delsberg and +1.3°C at Hohenpeissenberg) is captured well on average by the simulation, although with large variability in day-to-day variance especially for Delsberg (plot C in *figures 4.2.2-4.2.4*). The mild winter 1816/17 had been followed by a cold spring 1817 with negative anomalies in average temperature clearly exceeding the ones in spring 1816 (-1.4°C at Geneva, -2.5°C at Delsberg and -2.7°C at Hohenpeissenberg). The simulations show colder conditions for Delsberg (-2.8°C) and Geneva (-2.4°C) and a slightly higher average temperature at Hohenpeissenberg (-2.5°C). Average temperature in summer 1817 followed approximately the ref_hist average (-0.2 at Geneva, -0.7°C at Delsberg, +0.2°C at Hohenpeissenberg) and was even slightly above the average in fall 1817. Temperature anomalies in summer and fall of 1817_today deviate between -0.2°C and -0.6°C from the observed values except for the simulated summer at Hohenpeissenberg, for which simulations show a cooling of 1.7°C. Those disparities decrease if the median instead of the mean is computed. This indicates outliers and a higher variance, also to be seen in *figures 4.2.2-4.2.4*, plot C.

The strong cooling in summer 1816 and spring 1817 does also reflect in a smaller number of days with temperatures over the seasonal average of the respective reference. In summer 1816, more than 80% of days experienced a temperature below average. Even though a somewhat too strong cooling has been simulated for summer 1816_today, temperatures at all three stations exceed the ref_2000 average on more days than in 1816. For spring 1817, this pattern is most pronounced for Hohenpeissenberg where temperatures above average occurred only on 22 days (24% of days). At Geneva and Delsberg, the average had been exceeded at 30 (33%) and 37 (40%) days respectively. Furthermore, there wasn't a day in April 1817 that experienced temperatures above average at any of the three stations. In contrast, 73% of days in winter 1816/17 show a temperature above average at Geneva and Delsberg and 60% at Hohenpeissenberg.

Differences in temperature anomalies between 1816_today and 1816 are generally higher than between 1817_today and 1817. This variability is most distinct in the simulation for Hohenpeissenberg. The variance of the difference in temperature anomalies over both years differs for the three stations G, D and Hpb with the lowest standard deviation at Geneva (2°C), the highest at Hohenpeissenberg (2.9°C) and 2.4°C at Delsberg. Absolute temperatures are simulated too low on average, which intuitively contradicts the higher z-scores.

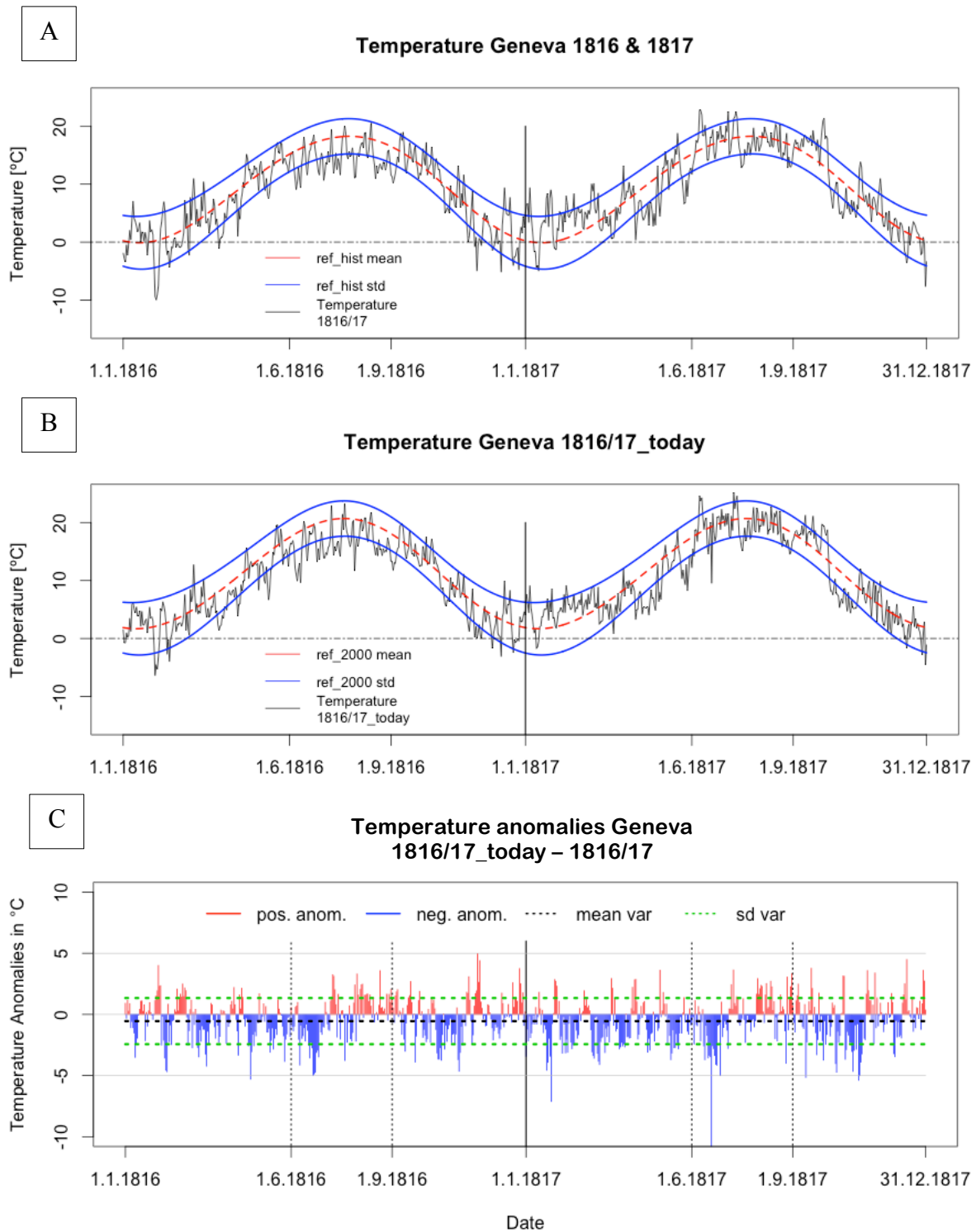


Figure 4.2.2: Plot A shows the time series of daily mean temperature at Geneva in 1816/17 (black line) and the mean of `ref_hist` (red dotted line). The blue lines denote ± 1 sd from the `ref_hist` average. The same is presented for 1816/17_today and `ref_today` in plot B. The deviation of anomalies estimated for 1816/17_today from the observed anomalies in 1816/17 is illustrated in plot C. By the resampling selected days with a larger temperature anomaly are represented by red bars, days with a smaller anomaly by blue bars. The green dotted lines denote ± 1 sd from the mean variance (black line).

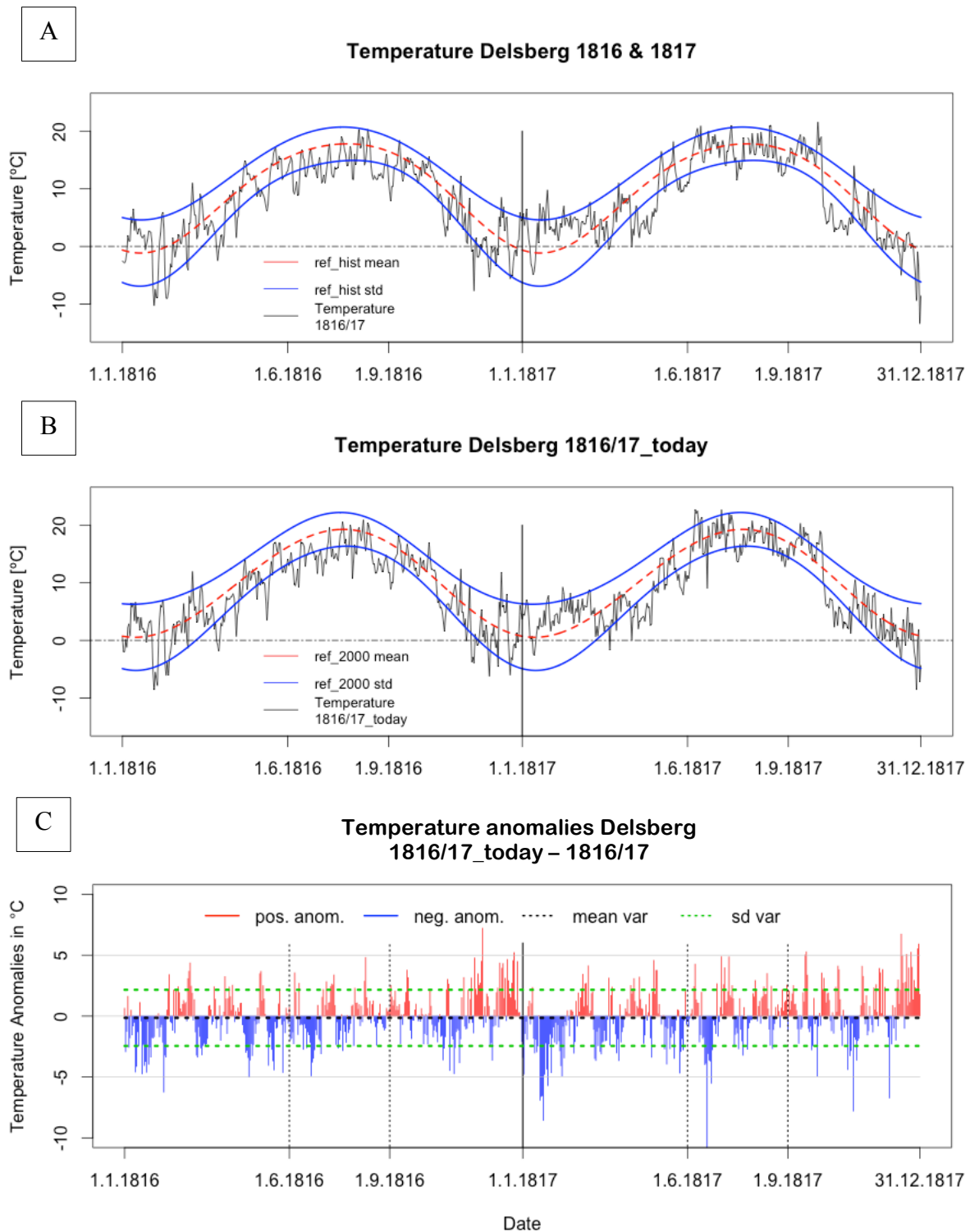


Figure 4.2.3: Plot A shows the time series of daily mean temperature at Delsberg in 1816/17 (black line) and the mean of *ref_hist* (red dotted line). The blue lines denote ± 1 sd from the *ref_hist* average. The same is presented for 1816/17_today and *ref_today* in plot B. The deviation of anomalies estimated for 1816/17_today from the observed anomalies in 1816/17 is illustrated in plot C. By the resampling selected days with a larger temperature anomaly are represented by red bars, days with a smaller anomaly by blue bars. The green dotted lines denote ± 1 sd from the mean variance (black line).

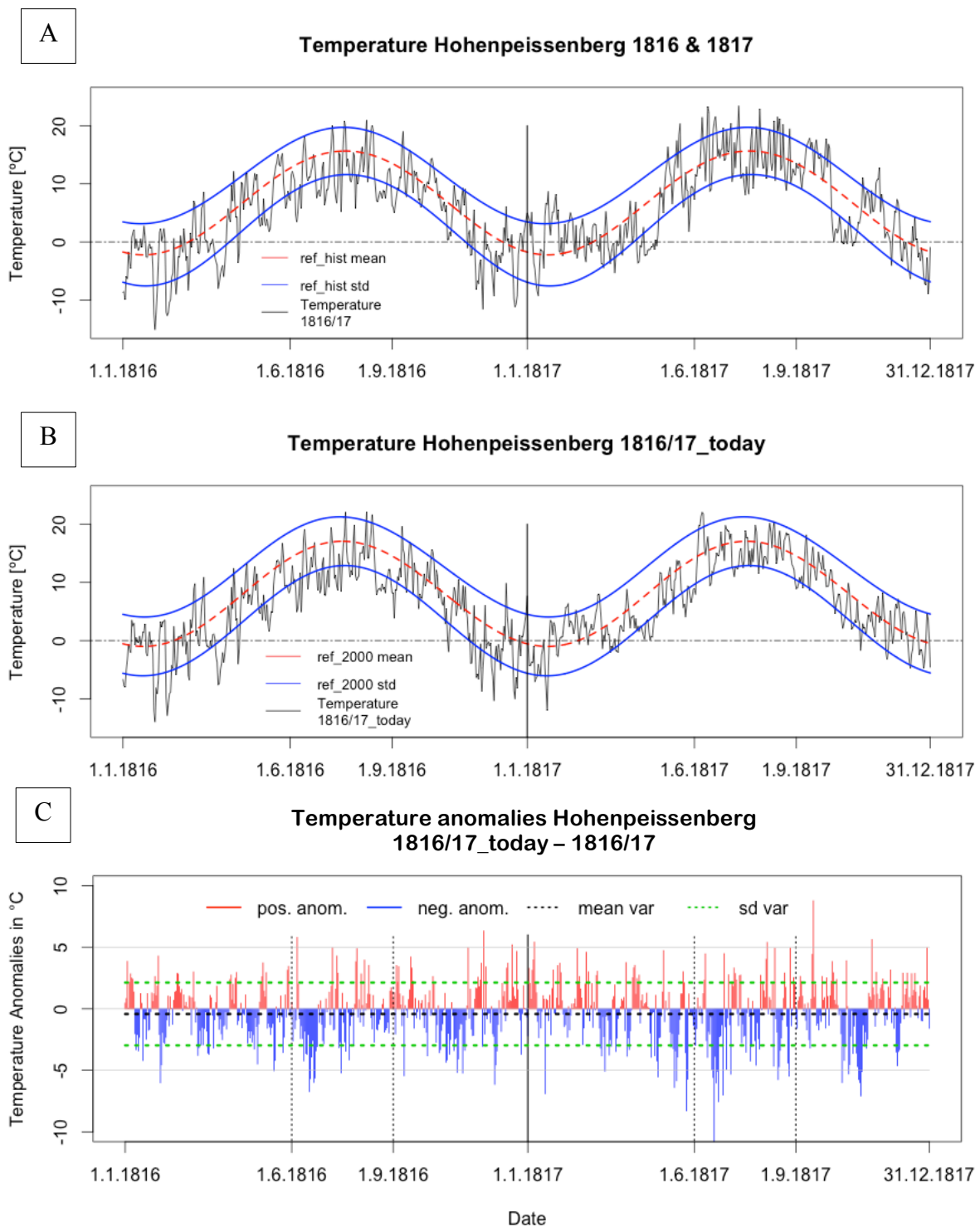
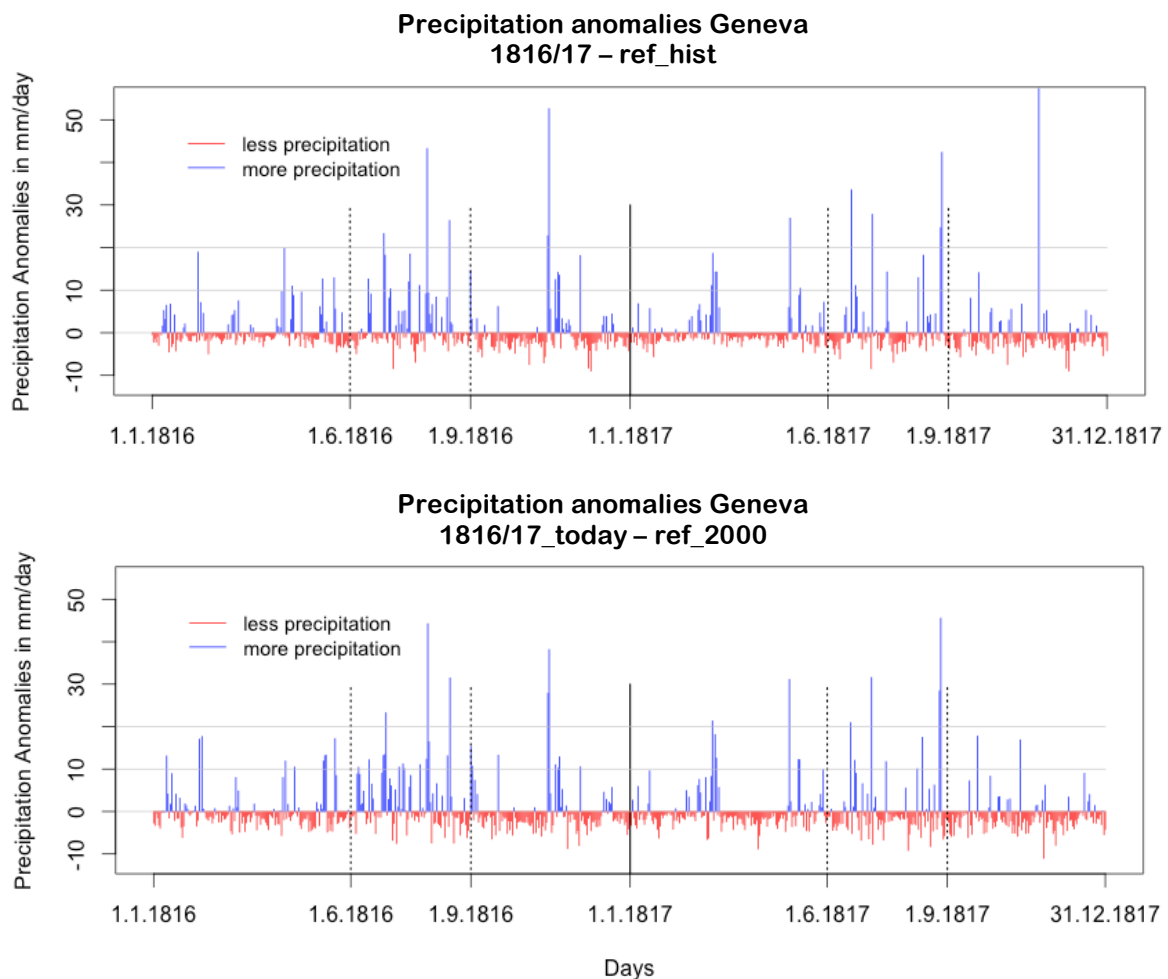


Figure 4.2.4: Plot A shows the time series of daily mean temperature at Hohenpeissenberg in 1816/17 (black line) and the mean of ref_hist (red dotted line). The blue lines denote ± 1 sd from the ref_hist average. The same is presented for 1816/17_today and ref_today in plot B. The deviation of anomalies estimated for 1816/17_today from the observed anomalies in 1816/17 is illustrated in plot C. By the resampling selected days with a larger temperature anomaly are represented by red bars, days with a smaller anomaly by blue bars. The green dotted lines denote ± 1 sd from the mean variance (black line).

4.2.1.2 Precipitation

Anomalies in daily precipitation sums at Geneva are presented in *figure 4.2.5* for 1816/17 with respect to *ref_hist* (upper panel) and for 1816/17_today with respect to *ref_2000* (lower panel). Blue bars represent days with precipitation above the average of the respective reference period and red bars days with less precipitation.



*Figure 4.2.5: Anomalies in precipitation at Geneva for 1816/17 (upper panel) and 1816/17_today (lower panel). Days with more precipitation than in the respective reference period (*ref_hist* and *ref_2000* respectively) are coloured blue and days with less precipitation red.*

The year 1816 was too wet compared to the *ref_hist* average, especially in summer. It rained almost on every second summer day (45) and thus on double as many days as in the reference summer (23) and the precipitation sum exceeded the ones of an average summer by 80%. In July, only 11 days with no rainfall occurred and more than 360% of precipitation of an average July in *ref_hist* had been recorded. On the contrary, rainfall intensity did not change (8mm per day with precipitation > 0.1mm). The precipitation sum in spring 1816 was 20% above the average, though most rain fell in May. Fall 1816 and 1817 experienced both aver-

age rainfalls, although precipitation intensity was 1mm lower in fall 1816 and 1.2mm higher in fall 1817 than the ref_hist mean. Summer 1817 was again too wet with a precipitation sum more than 40% above average. Contrary to the situation in summer 1816, the number of days with precipitation > 0.1mm did not change, but the rainfall intensity was significantly increased (9.6mm). Apart from a few outliers, there were no significant changes in precipitation pattern in spring and fall 1817. Winter 1816/17 was too dry with only 70% of average winter precipitation.

The simulation of summer 1816 (1816_today) shows similar results for rainfall-intensity and percentage increase in precipitation sum relative to the ref_2000 average (+75%). Although, more days with precipitation > 0.1mm are selected by the simulation (58 instead of 45) than in summer 1816 (+30%), which holds for all four seasons in 1816/17_today. This leads to considerably higher simulated precipitation sums for summer of 1816_today (+120mm or 34%) and spring of 1817_today (+35mm or 20%). However, the absolute deviation from the respective reference summer (in number of days) is the same for the simulated and the actual summer 1816 (+20 more rainy days) as also more rainy days occur on average in the ref_2000 than in the ref_hist. This again applies to all seasons.

The percentage anomaly of seasonal precipitation sums simulated for 1816/17_today are similar to the anomalies in 1816/17. Only precipitation of spring 1816_today (-47) and 1817_today (-30) and summer 1816_today (-31) shows deviations of more than 10 percentage points from the observed values in 1816/17. Nevertheless, there are some outliers with respect to deviations in daily precipitation anomalies, with one outstanding case: An extreme precipitation event occurred on the 9th of November (60mm), only two days within ref_hist experienced heavier rainfall. At the selected day for 1817_today however, precipitation was only little above average.

There are noticeably differences between the two reference periods with respect to variance in absolute precipitation sums and in rainy days. Both variances are higher in ref_hist than in the ref_today, even though the latter period is almost double as long. Precipitation intensity in ref_today varies between 4.2mm and 8mm on average, whereas minimum and maximum intensities are 4.1 and 11 respectively in ref_hist. On the other hand, more rainy days occur in the ref_today, which on average leads to higher annual precipitation sums (930mm versus 755mm).

4.2.2 Climate of 1816/17_today in Switzerland

In this section, the climate constituted by the days selected in the resampling process is presented for the ch02.lonlat grid. As winter and fall show less significant anomalies and are of minor importance for crop growth, the focus lies on the analysis of the situation in spring and summer. Thereby, five regions will be distinguished (*figure 4.2.6*): The lowlands of the Swiss Plateau (<700mamsl), the Alps (region 4, grids with altitude >1500mamsl) and southern Switzerland (region 5, Ticino and Valais, <700mamsl). For analysis of the gradient, the Swiss Plateau is divided into West (region 1), Central (region 2) and East (region 3). Simulation assesses climate anomalies for the Pre-Alps (region 6, 700mamsl< and >1500mamsl) quite similar as for the Alps. Thus, these two regions are merged together to region 4 for this section.

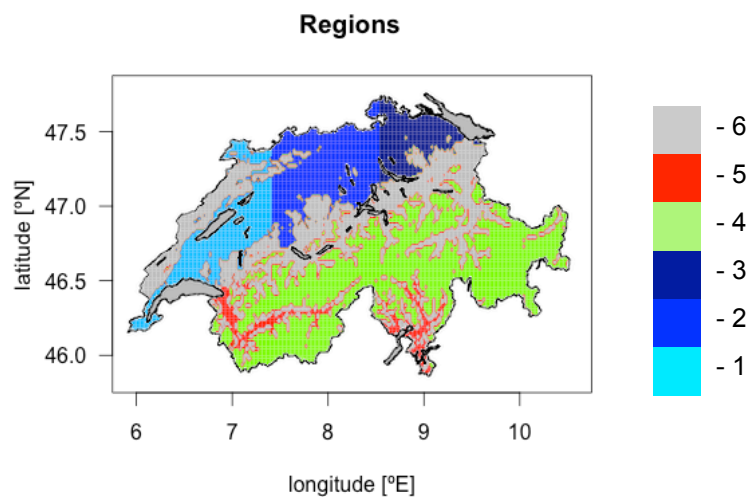


Figure 4.2.6: Regions for analysis: Swiss Plateau is divided in 3 regions “West” (light blue - 1), “Central” (blue - 2) and “East” (dark blue - 3). The Alps are shown in green (4), southern Switzerland in red (5). Grey coloured (region 6) are the pre-Alps and the Jura.

The spatial distributions of average anomalies estimated for summer and spring of 1816/17_today are separately illustrated for each of the four variables Tmin, Tmax, Prec and I (*figures 4.2.7, 4.2.9, 4.2.11 & 4.2.13*). Mean seasonal anomalies for spring (plot A) and summer (plot B) of the 1816_today scenario are shown in the two left panels and the ones for 1817_today in the panels on the right (plots C&D) respectively. An additional figure (*figures 4.2.8, 4.1.10, 4.2.12 & 4.2.14*) shows the behaviour of the seasonal anomalies in the variable under consideration along a West-East transect through the Swiss Plateau. It serves the purpose of answering the third research question of this study, whether there is a West-East gradient in climate and crop yields for Switzerland in 1816/17. Anomalies are measured in abso-

lute values ($^{\circ}\text{C}$, mm/day , MJ/m^2) and each computed as the difference between the simulations for 1816_today and 1817_today and the ref_2000 average.

4.2.2.1 Minimum temperature

Figure 4.2.7 presents average anomalies in daily minimum temperature. A positive correlation can be found for magnitude of negative anomalies and altitude above sea level, with an average correlation coefficient of 0.5. The correlation is slightly more pronounced for spring than for summer. This relation and especially the contrast between the low Swiss Plateau and the mountainous regions Alps and Jura are also apparent from the spatial plots.

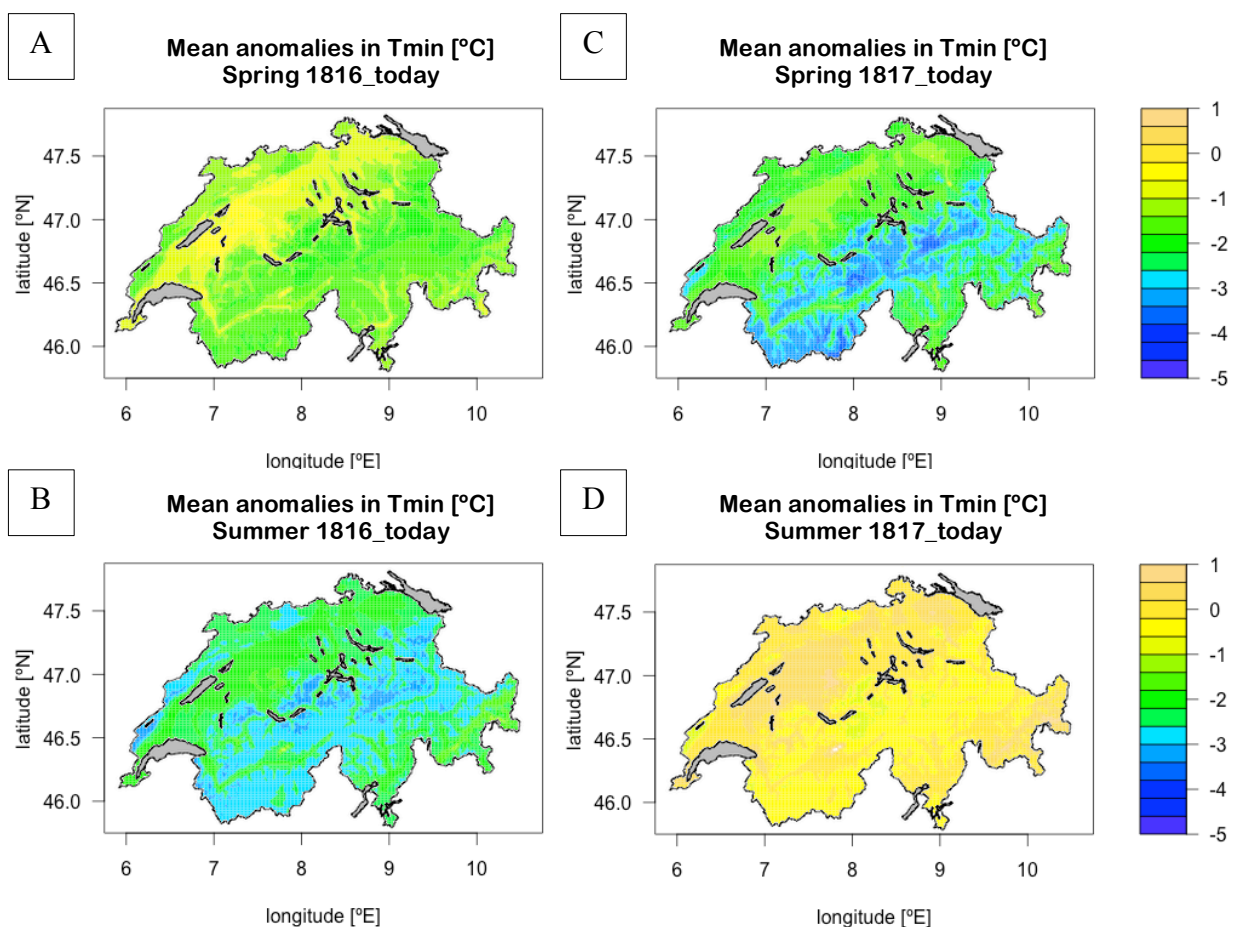


Figure 4.2.7: Average seasonal anomalies in daily minimum temperatures [in $^{\circ}\text{C}$] between the simulated years 1816/17_today and the ref_2000 average. The upper plots show the seasonal means of temperature anomalies for spring 1816_today (A) and 1817_today (C), the lower plots the anomalies in summer 1816_today (B) and 1817_today (D), respectively.

Spring 1816 today

In the Alps, minimum temperature decreases by 1.6°C on average with a maximum anomaly of -2.27°C and a minimum of -0.1°C . The variance in minimum temperature is smallest on the southern side of the Alps, varying between -1.85°C and -0.55°C with an average decrease of

1.2°C. Changes in minimum temperature are smallest in the lowlands of the Swiss plateau (-0.9°C), though with a higher variance than in southern Swiss (between -0.3°C and -1.9°C).

Summer 1816_today

The most distinctive anomalies for the Swiss Plateau (-2.2°C) and Southern Swiss (-2.3°C) in the 1816_today scenario occur in summer with deviations varying between -1.6°C and -3.2°C. The average anomaly in the Alps is -2.6°C, though there is large variance between grids with maximum anomalies (-3.4°C) similar to those in the Swiss Plateau and Southern Switzerland (-3.2°C) but considerably smaller minimum anomaly (-0.7°C)

Spring 1817_today

The largest deviations from the ref_2000 average are found in the Central Swiss Alps and Southern Valais (maximum anomaly -3.8°C each), interestingly not for summer of the 1816_today scenario but in spring of 1817_today. The smallest anomaly in this region is -0.9°C, the same as in southern Switzerland where the maximum anomaly is -3.4°C. Anomalies vary between -1°C and -2.9°C in the Swiss Plateau and the variance is significantly lower than in the other two regions. Average decrease in minimum temperature is 1.6°C for the Swiss Plateau, which is somewhat less than on the south side of the Alps (-1.8°C).

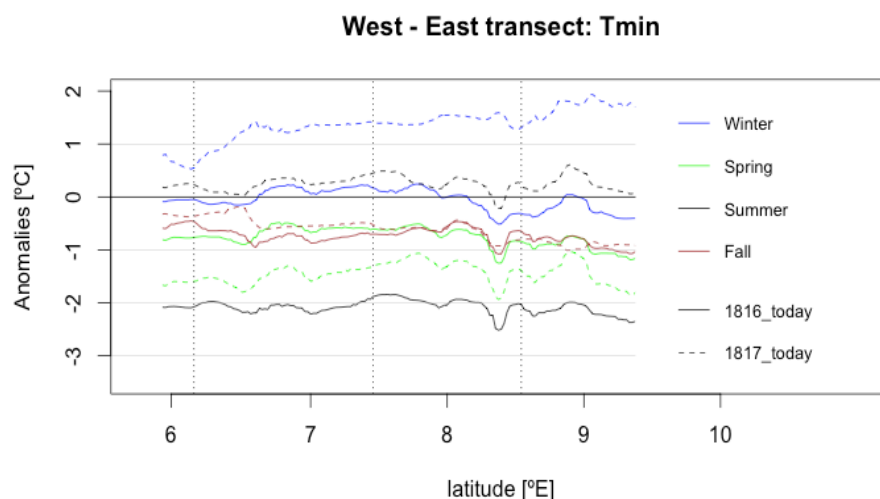


Figure 4.2.8: West-East transect through the Swiss plateau. Bold lines represent mean seasonal anomalies in minimum temperature [°C] from ref_2000 average for 1816_today and dotted lines for 1817_today. Blue lines show anomalies for winter, green for spring, black for summer and brown lines for fall.

Summer 1817_today

Summer in the 1817_today scenario shows temperatures slightly too warm in the Swiss Plateau (+0.1°C) and too cool in Southern Switzerland (-0.1°C) and the alpine region (-0.2°C).

However, mean anomalies are not significant on a 95%-confidence interval for all three regions with a p-value of 0.11 for the Swiss Plateau and the South and 0.011 for the Alps. Although the maximum and minimum anomalies are significantly different from average anomalies of summers in ref_2000, there is only a small variance in anomalies for all regions.

Transection

Figure 4.2.8 presents the behaviour of average anomalies in minimum temperature along the West-East transect through the Swiss Plateau. Apart from the winter of 1816/17_today (difference between Western and Eastern Switzerland = 0.7°C) and fall of 1817_today (-0.5°C), no distinctive gradient can be observed for any of the other seasons. There is a minor difference in winter of 1815/16_today and in fall (-0.2°C) and spring (-0.3°C) of the 1816_today scenario. There is no significant gradient in the other seasons of 1817_today. Average seasonal anomalies in minimum temperatures for the central Swiss Plateau are in general more similar to anomalies in Western than in Eastern Switzerland

4.2.2.2 Maximum temperature

Similar to anomalies in minimum temperature, a correlation between altitude above sea level and maximum temperature anomalies can be found, although with opposite signs. There is a positive correlation in spring of 1816_today (correlation coefficient of 0.66) and summer (0.66 and 0.44) and fall (0.35 and 0.8) of both simulated scenarios, implying smaller negative anomalies with altitude. A negative correlation is detected for winter 1816/17_today (-0.6) and for spring of 1817_today (-0.1). This relation can also be seen from the corresponding plot (figure 4.2.9), though less clearly than for minimum temperature.

Spring 1816_today

There is a decrease in maximum temperature of 2.5°C in the Swiss Plateau, which is 0.5°C more than in the Alps and on their southern side. Anomalies of maximum temperature range from -1.9°C to -2.9°C in the Swiss Plateau, from -1.6°C to -2.7°C in southern Switzerland and from -1.4°C to -3°C in the Alps. Especially March and May exhibit a strong cooling, whereas the drop in temperature is less strong in April. Maximum temperatures in May exceeded the ref_2000 mean by 3.3°C in the Swiss Plateau, which is significantly more compared to the Alps (-2.2°C) and southern Switzerland (-2°C).

Summer 1816_today

Consistent with observations and expectations, anomalies in temperature are largest for maximum temperatures in summer 1816_today and especially in June and July. The average

anomaly in summer maximum temperatures is -3.8°C for the Swiss Plateau and -3.6°C for the Alps and their south side with a maximum of -4.2°C for all three regions. The lower bounds of the range are -3.3°C (Swiss Plateau), -3°C (Southern Switzerland) and -2.5°C (Alps). In June, monthly anomalies of even -5.5°C are simulated for the Alps and their south side (-5.1°C for the Swiss Plateau) with mean anomalies of approximately -4.5°C . Anomalies in July were somewhat lower (-3.9°C for all regions) but still clearly higher than in August (-2.6°C on average). Also the spatial variance is noticeably higher in June for the three regions.

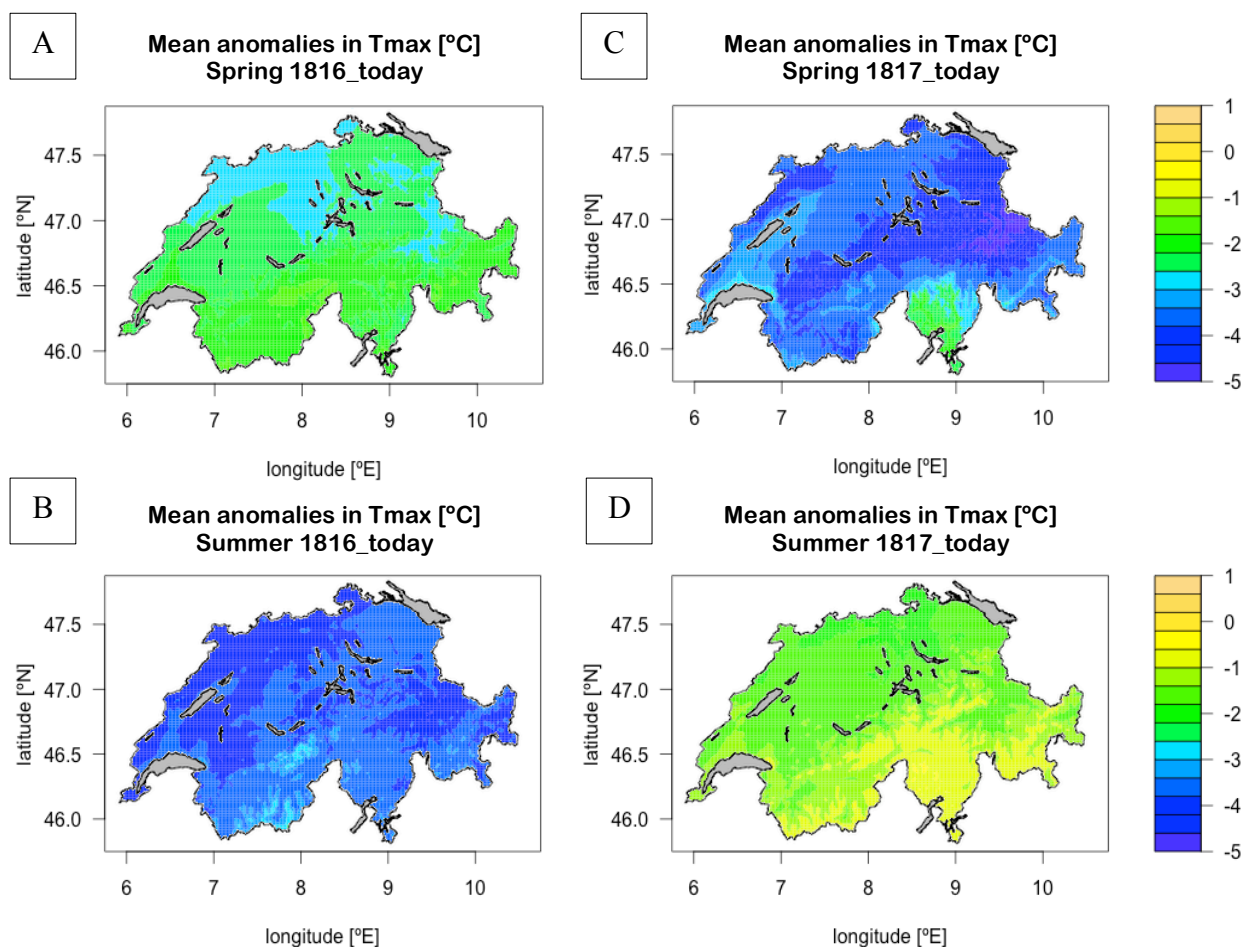


Figure 4.2.9: Average seasonal anomalies in daily maximum temperatures [in $^{\circ}\text{C}$] between the simulated years 1816/17_today and the ref_2000 average. The upper plots show the seasonal means of temperature anomalies for spring 1816_today (A) and 1817_today (C), the lower plots the anomalies in summer 1816_today (B) and 1817_today (D), respectively.

Spring 1817_today

The simulation for spring of 1817_today again shows strong anomalies in maximum temperatures, especially for northern Switzerland (-3.6°C , southern Switzerland -2.7°C and in Ticino only -2.4°C). April is even the month for which simulations compute the largest monthly anomalies of the two scenarios 1816/17_today for northern Switzerland (-5.6°C), meanwhile the average anomaly on the south side of the Alps does not exceed -3°C . On the contrary,

anomalies in southern Switzerland show a distinctly larger variance (range from -6.2°C to -0.6°C) in April than it is observed in any other month for any of the three regions.

Summer 1817_today

Anomalies in maximum temperature are still significantly negative for all grid cells in each region, although of considerably smaller magnitude (-1.7°C in the Swiss Plateau, -1.1°C in the Alps and -0.9°C in southern Switzerland). The spatial variance is also smaller, ranging from -1°C to -2.1°C in the Swiss Plateau, from -0.5°C to -1.7°C in southern Switzerland and from -0.4°C to -1.9 in the Alps.

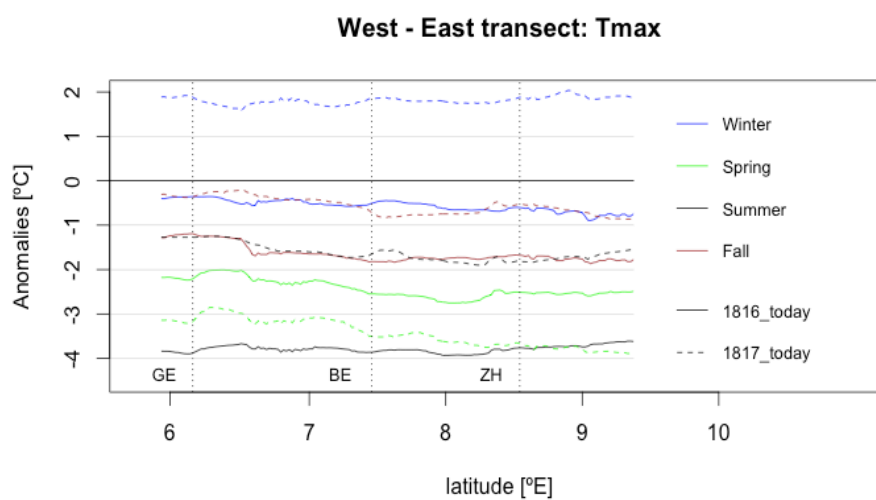


Figure 4.2.10: West-East transect through the Swiss plateau. Bold lines represent mean seasonal anomalies in maximum temperature [$^{\circ}\text{C}$] from theref_2000 average for 1816_today and dotted lines for 1817_today. Blue lines show anomalies for winter, green for spring, black for summer and brown lines for fall.

Transection

The West-East gradient is slightly stronger pronounced in maximum than in minimum temperatures (figure 4.2.10). Contrary to minimum temperature, average anomalies in maximum temperatures for central Swiss Plateau are more similar to Eastern Switzerland. The central Swiss Plateau and Eastern Switzerland experienced on average 0.3°C more cooling in winter, spring and fall of 1816_today. The most distinctive west-east gradient appears in summer of 1817_today (-0.7°C). For summer of the 1816_today scenario, anomalies in maximum temperatures show a even slightly positive gradient ($+0.1^{\circ}\text{C}$).

4.2.2.3 Precipitation

A significant correlation between average seasonal anomaly in precipitation and altitude is only given for summer of 1816_today (correlation coefficient of 0.5) and 1817_today (0.4).

However, largest anomalies appear for 5 of 7 seasons in the central or eastern Alps (spring and summer 1816/17_today and fall 1816_today), which is also apparent from *figure 4.2.11*.

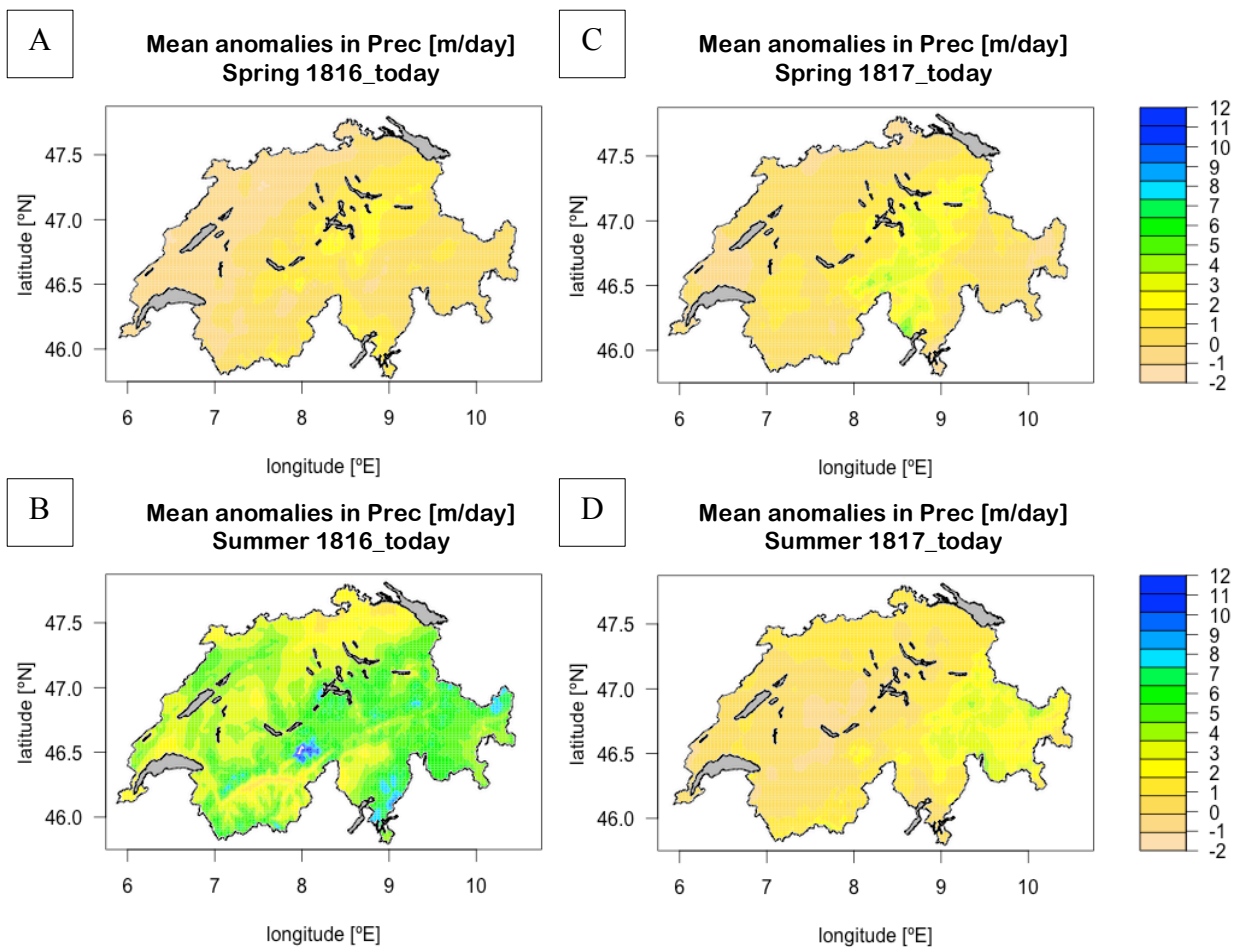


Figure 4.2.11: Average seasonal anomalies in precipitation sums [in mm/day] between the simulated years 1816/17_today and the ref_2000 average. The upper plots show the seasonal means of precipitation anomalies for spring 1816_today (A) and 1817_today (C), the lower plots the anomalies in summer 1816_today (B) and 1817_today (D), respectively.

Spring 1816_today

Precipitation does not show distinctive anomalies for neither of the three regions. The simulation computes a little dryer climate for the Swiss Plateau, though the deviation from the average spring rainfall of ref_2000 (-0.1mm) is not significant. The Alps (+0.6mm) and southern Switzerland (+0.7mm) experience daily precipitation sums somewhat above average. Spatial variance in anomalies is rather small for all three regions (0.3 for the Swiss Plateau and the Alps, 0.5 for southern Switzerland).

Summer 1816_today

Notably large rainfall anomalies are simulated for summer of 1816_today with daily precipitation sums on average 2.9mm over the mean in the Swiss Plateau and approximately

5mm in the Alps and on their south side, both with large spatial variance (1.4 and 3.0 respectively) and range (from 1.5mm to 13.1mm rainfall surplus in southern Switzerland and from 2.0 to 6.9 in the Alps). Spatial variance in the Swiss Plateau is remarkably lower (only 0.6). This pattern is even stronger pronounced for the monthly anomalies of June and July, which are the two months with the largest precipitation surplus. For June, simulations output on average +3.2mm precipitation per day for the Swiss Plateau, +6.1mm for the Alps and +7.3mm for southern Switzerland, whereby spatial variance especially in the Alps (17.9) is very large. Average precipitation surplus in July are higher for the Swiss Plateau (4.2mm) and the Alps (6.7mm) but lower for southern Switzerland (5.8mm). The highest surplus is simulated for the Gotthard region, which can also be seen in *figure 4.2.11*, plot B.

Spring 1817_today

Average anomalies in daily precipitation sums are of minor magnitude for the Swiss Plateau (+0.3mm) and southern Switzerland (+0.4mm). Anomalies in the Alps are somewhat higher (+1mm) with a maximum over the Central Alps, which is also apparent from *figure 4.2.11* (plot C). The spatial variance (1.1 for southern Switzerland and the Alps, 0.4 for the Swiss Plateau) is also smaller than in summer but larger than in spring of 1816_today.

Summer 1817_today

Simulations show a higher precipitation surplus than in spring of 1816/17_today, yet considerably lower compared to summer of 1816_today. Largest anomalies are again simulated for the Alps (+1.5mm) with the maximum shifted eastwards towards the Grison Alps.

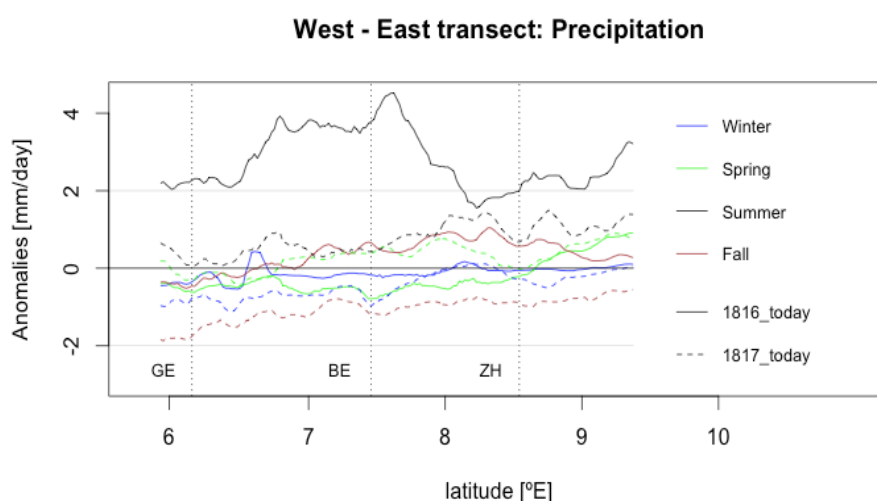


Figure 4.2.12: West-East transect through the Swiss plateau. Bold lines represent mean seasonal anomalies in precipitation [mm] from the ref_2000 average for 1816_today and dotted lines for 1817_today. Blue lines show anomalies for winter, green for spring, black for summer and brown lines for fall.

Daily precipitation in the Swiss Plateau and South of the Alps exceed the mean of ref_2000 by 0.8mm on average. Spatial variance is about the same size as in spring of 1817_today.

Transection

There is a positive west-east gradient in precipitation anomalies for each season except of summer and fall of 1816_today (*figure 4.2.12*). It is of size of 0.6mm in winter 1816/17_today and summer and fall of 1817_today in eastern compared to western Switzerland and of 0.7mm in spring of 1817_today. The most distinctive gradient is found for spring of 1816_today with average anomaly in daily precipitation sums in eastern Switzerland exceeding those in central and western Switzerland by 1mm and 1.1mm respectively. The largest average anomaly in fall of 1816_today is simulated for central Switzerland, which is +0.3mm compared to the East and +0.6 compared to the West. For summer of 1816_today, simulations show the largest anomalies in rainfall over the Seeland between the Lake Geneva and Solothurn, where circa 2mm more precipitation falls than in the rest of the Swiss Plateau.

4.2.2.4 Solar irradiance

Solar irradiance has only been simulated for the Swiss Plateau, as the value of each grid cell is constituted by interpolation between station times series (see chapter 2&3). Thus, simulation output of the downscaling is only shown for northern Switzerland. The spatial distribution of seasonal anomalies in solar irradiance is presented in *figure 4.2.13*, the development along the West-East gradient in *figure 4.2.14*. No distinctive anomalies are simulated for winter 1815/16_today and 1816/17_today as well as for fall 1817_today (*figure 4.2.14*). A slightly negative gradient is outputted for fall 1816_today with an average decrease in solar irradiance of 0.9 MJ/m² per day in Western Switzerland and of 1.3 MJ/m² per day in Central and Eastern Switzerland.

The largest anomalies are simulated for summer of 1816_today, though there is no significant West-East gradient to distinguish (circa -5.4 MJ/m² per day for the entire Swiss Plateau). Distinguishable differences in anomalies between western and eastern Switzerland are found for spring 1816/17_today and summer 1817_today. In spring 1816_today (-1.5 MJ/m² in the West compared to -2.7 MJ/m² in the East) and summer 1817_today (-2.8 MJ/m² versus -4.0 MJ/m²), the gradient is of -1.2 MJ/m² per day. A gradient of even -1.3 MJ/m² per day is found for spring 1817_today (-1.7 MJ/m² versus -3.0 MJ/m²). The size of anomalies in central Switzerland clearly tends towards anomalies in eastern Switzerland in all seasons with no significant differences in winter 1815/16_today and 1816/17_today and fall 1817_today.

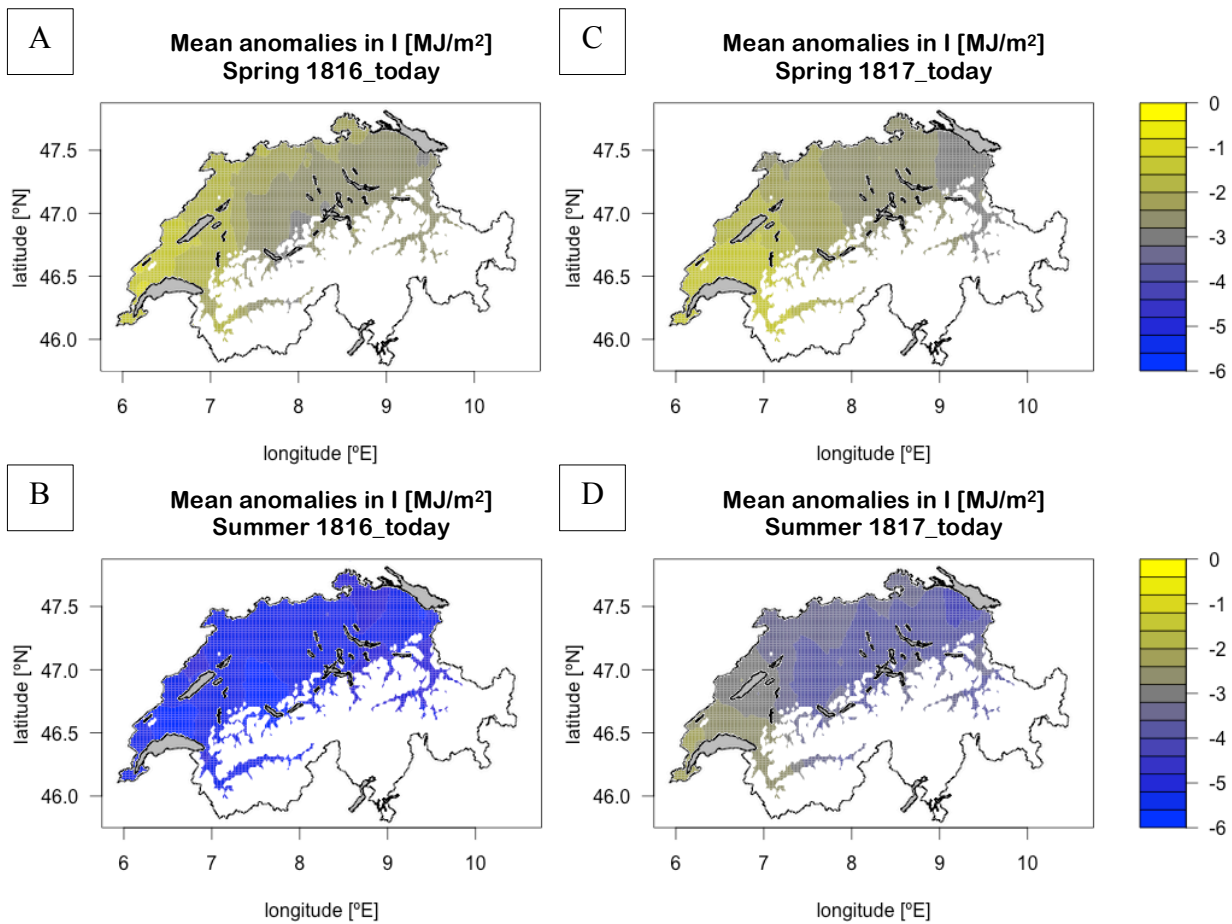


Figure 4.2.14: Average seasonal anomalies in solar irradiance [in MJ/m²] between the simulated years 1816/17_today and the ref_2000 average. The upper plots show the seasonal means of anomalies in solar irradiance for spring 1816_today (A) and 1817_today (C), the lower plots the anomalies in summer 1816_today (B) and 1817_today (D), respectively.

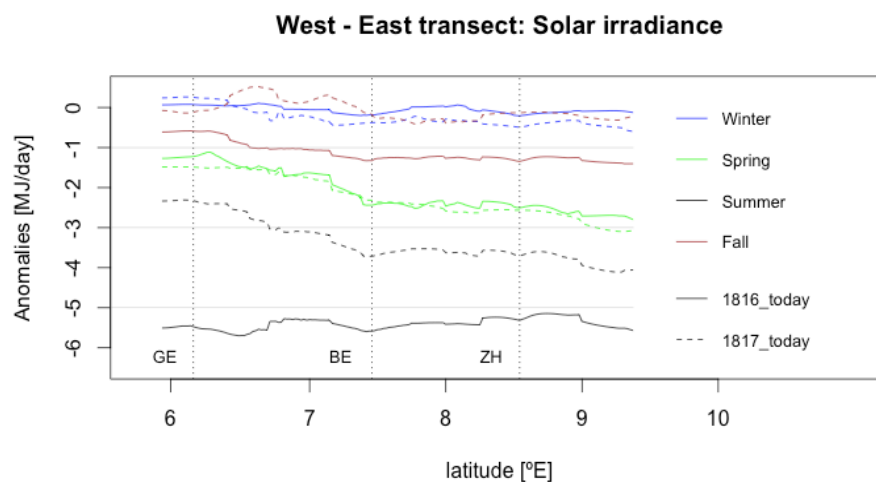


Figure 4.2.13: West-East transect through the Swiss plateau. Bold lines represent mean seasonal anomalies in solar irradiance [MJ/m²] from the ref_2000 average for 1816_today and dotted lines for 1817_today. Blue lines show anomalies for winter, green for spring, black for summer and brown lines for fall.

4.3 Crop modelling

The results of the crop modelling are presented in this section. The crop modelling has been applied to assess potential yield of two spring crops (maize and potato) and one winter crop (barley). Potential yield is the maximum yield (in t/ha dry matter) that might be achieved under the respective climate scenario, assuming an optimal management strategy with respect to irrigation and time of sowing and harvest. Simulation has been solely conducted for the north side of the Alps (regions 1-3 & 6, including the Valais) and only for grid cells with altitude <1500 mamsl, as arable crops are not usually cultivated above this elevation threshold.

For each crop, yields have been assessed for the simulated climate scenario 1816/17_today and for an average year of ref_2000. Potential yields of potato and barley have additionally been generated for the climate scenarios 1816, ref_hist and T_reference, all considering different maximum and minimum temperatures. The T_reference scenario takes the climate of 1816_today but with average daily temperatures of ref_2000 in order to assess the impact of temperature on yields: $T_{reference} = \{T_{min}, T_{max}: \text{ref_2000 average}; \text{Prec, I: 1816_today}\}$

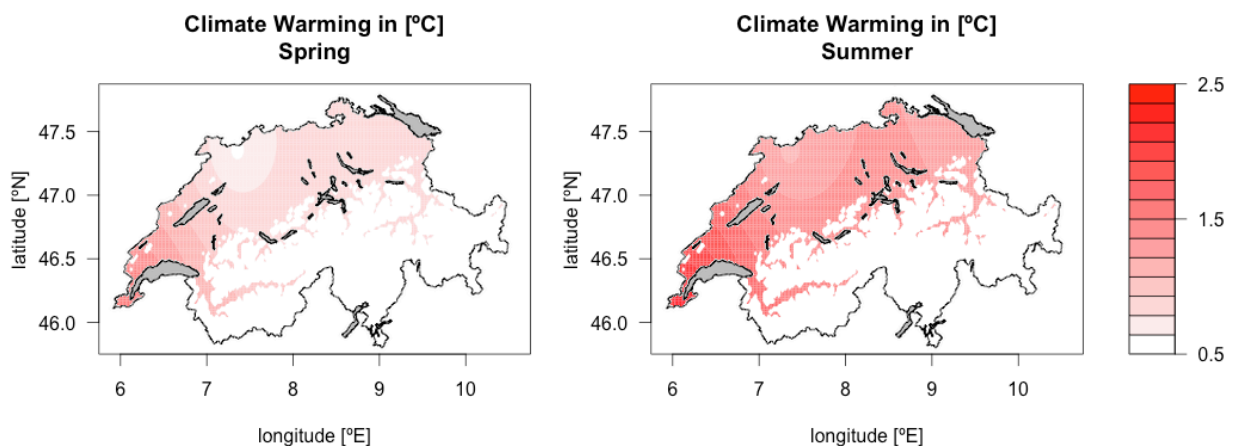


Figure 4.3.1: Average seasonal climate warming component [in °C] of daily average temperature for spring (left panel) and summer (right panel). It is calculated as the average difference in daily mean temperature between ref_2000 and ref_hist.

In order to model crop yields for 1816 and for the ref_hist average, a climate warming component is subtracted from the maximum and minimum temperatures of the respective scenarios for today. Thus, crop yields for 1816 are simulated on the identical temperature anomalies as crop yields of the 1816_today scenario. This climate warming component is generated for each grid cell, as is the difference between the average daily maximum and minimum temperature of ref_2000 and ref_hist. The seasonal average climate warming computed for spring

(left panel) and summer (right panel) is presented in *figure 4.3.1*. For precipitation and solar irradiance, the values of the 1816_today scenario and the ref_2000 average are used.

In the following, the output of the crop modelling is separately presented for each crop. The first figures show the spatial distribution of percentage changes in potential crop yields for 1816_today compared to the ref_2000 average. The development of yields (in t/ha) along the West-East gradient is shown in a second figure for all climate scenarios that have been computed for the crop under consideration. The reference scenarios are represented by black, the 1816 scenarios (1816 and 1816_today) by red lines, dotted for 1816 and ref_hist (for barley and potato) and bold for the scenarios today (1816_today and ref_2000). Assessed yields for 1817_today are shown in blue and the ones for the T_reference scenario in green. Note that the scaling differs for each crop in order to highlight the development along the gradient.

For simulation of potential biomass accumulation, intercepted radiation is the most decisive factor after the crop has entered growth phase (equation 9). Thus, spatial distributions of absolute anomalies (in MJ/m²) in total annual intercepted radiation iR with respect to the ref_2000 average for 1816_today (left plot) and 1817_today (right plot) are presented in a last figure.

4.3.1 Barley

Barley may be sown either as winter or as summer crop. For this study, only winter barley is used in order to have a comparison between spring and winter crops. It is usually sown from late September to early October in Switzerland. Common harvest dates are between mid-July and early August [Dierauer, 2010]. Crop simulation starts in early October in ref_2000 and harvest is scheduled for early July.

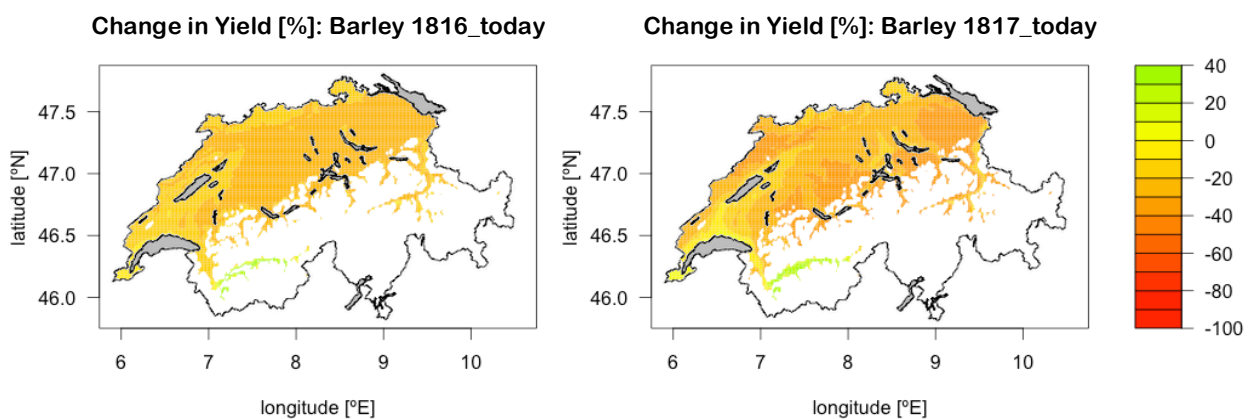


Figure 4.3.2: Percentage change in yield of barley between the ref_2000 average and 1816_today (left panel) and 1817_today (right panel) respectively.

1816/17 today and ref_2000

Average percentage changes in yield are shown in *figure 4.3.2* and listed in *table 4.3-1*. Highest yields are achieved in the pre-Alps and the Jura (region 6) in all three scenarios. Model outputs on average 9.5 t/ha for ref_2000. For 1816_today, average yields of 7.7 t/ha are assessed corresponding to a loss of 1.8 t/ha or 18%. The change is slightly greater assessed for 1817_today with a decrease of 19.6% (-1.9 t/ha). The lowest yields are estimated for the Valais with 7.4 t/ha for the ref_2000. However, this is the only region for which the model outputs a gain in potential yields for 1816_today (+0.1 t/ha) and 1817_today (+0.5 t/ha), though the change in the 1816_today scenario is not significant (p-value of 0.5). The highest increase in crop productivity is simulated for the Rhone valley, which appears clearly in *figure 4.3.2*.

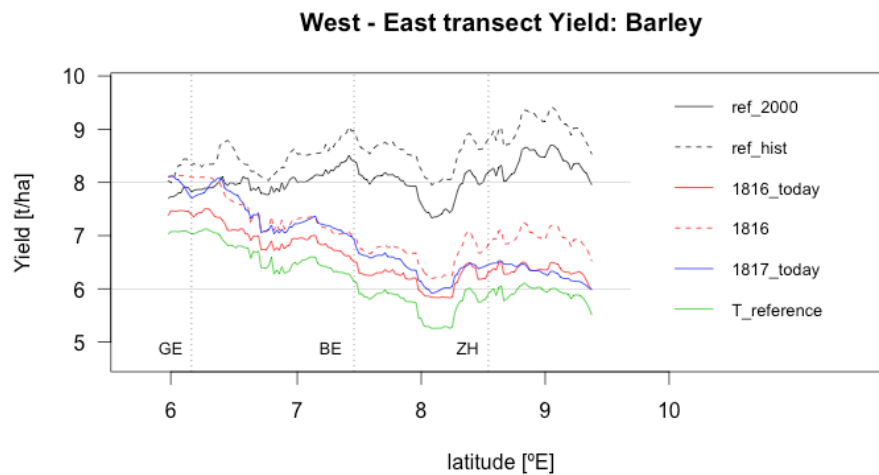


Figure 4.3.3: Development of potential crop yields of barley along the West-East transect for the different climate scenarios. Black lines represent the ref_2000 (bold) and ref_1816/17 (dotted) averages and red lines 1816 and 1816_today, respectively. Potential crop yields assessed for 1817 today are shown in blue and for the T reference scenario in

Average potential yield in western Switzerland is assessed to 8.5 t/ha for the ref_2000, 0.5 t/ha higher than in the central and eastern Swiss Plateau. Yield decreases in both scenarios, 1816_today and 1817_today, in all three regions. Highest absolute and relative losses are modelled for east Switzerland (-1.8 t/ha or -22%). Losses for central Swiss Plateau are simulated somewhat lower (-1.7 t/ha, -21.2%). The smallest change occurs in the western Switzerland with an average decrease of 15.7% (-1.3 t/ha). Hence, the slightly positive west-east gradient in the ref_2000 average thereby becomes negative for the 1816_today scenario (*figure 4.3.3*). A similar pattern holds for 1817_today, although the disparity between West and East (0.8 t/ha or 10 percentage points) increases by 0.3 t/ha or circa 60% of the west-east gradient in 1816_today (0.5 t/ha, 6.3 percentage points).

1816 and ref_hist

Potential yield is increased in ref_hist on average by 0.6 t/ha (approximately +7%) compared to ref_2000 for the Swiss Plateau and the Valais and even by 0.9 t/ha (+8.5%) for the pre-Alps and Jura. Absolute changes in potential crop yields 1816 with respect to ref_hist are not assessed significantly different than for 1816_today with respect to ref_2000, yet percentage changes are circa 0.7% smaller. The spatial distribution of percentage anomalies in 1816 appears very similar to the distribution for the 1816_today scenario (*figure 4.3.4*). There are also no disparities in development along the West-East gradient (*figure 4.3.3*).

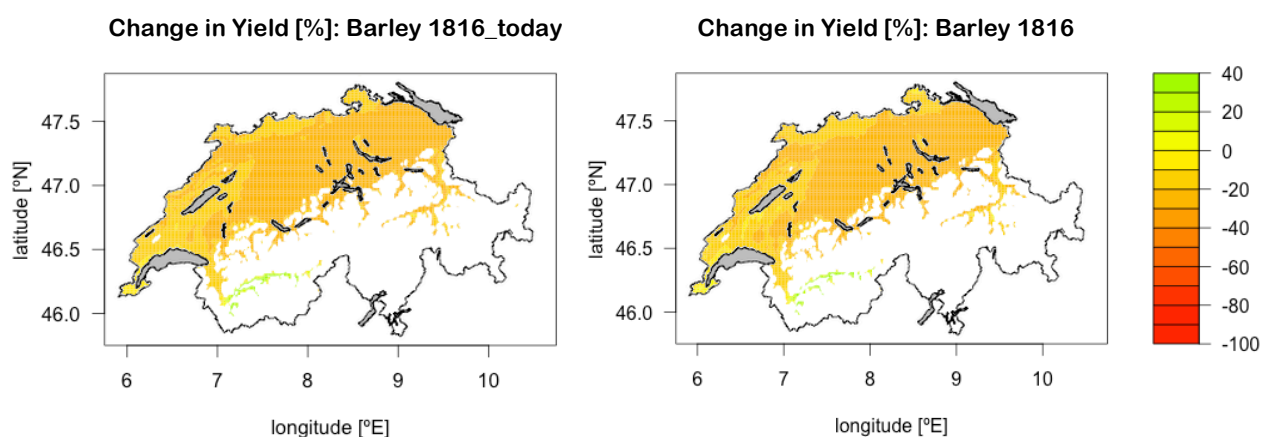


Figure 4.3.4: Percentage change in barley yields in 1816 with respect to the ref_hist average (left panel) and between the ref_2000 average and the 1816_today scenario (right panel).

T_reference

The lowest crop yields in barley are simulated for the T_reference scenario with average losses of 2.3 t/ha assessed for eastern (-28.5%) and central Swiss Plateau (-28%) and 1.7 t/ha for western Switzerland (-20%). Thereby, the West-East gradient amplifies to 1.0 t/ha. Potential crop yields also decrease on average in the pre-Alps (-2.7 t/ha or -27.7%) and the Valais (-0.6 or -8.1%), as shown in *table 4.3-1*.

*Table 4.3-1: Potential crop yields of barley (in t/ha) in the reference scenarios are shown for each region as well as the absolute and percentage change for each climate scenario compared to its respective reference. * =not significant (p -value of students t -test > 0.05).*

Region	ref_	1816_today		1817_today		T_reference		ref_	1816	
	today	t/ha	%	t/ha	%	t/ha	%	hist	t/ha	%
1	8.5	-1.3	-15.7	-1.0	-12	-1.7	-20	9.0	-1.4	-15
2	8.0	-1.7	-21.2	-1.6	-19.7	-2.3	-28	8.6	-1.8	-20.8
3	8.1	-1.8	-22	-1.8	-22	-2.3	-28.5	8.7	-1.8	-20.3
5	7.4	+0.1*	+1.3	+0.5	+6.7	-0.6	-8.1	8.0	+0.2*	+2.5
6	9.5	-1.9	-18.5	-1.9	-19.6	-2.7	-27.7	10.4	-2.1	-18.2

Intercepted radiation

Spatial distribution of absolute anomalies in annual intercepted solar irradiance is presented in *figure 4.3.5* for the climate scenarios 1816_today and 1817_today with respect to the ref_2000 average. The distribution pattern of *iR* coincides well with the pattern of percentage anomalies in potential crop yield, as it has been expected, considering equation 9 for radiation dependent biomass production. The most solar irradiance is intercepted in higher elevations (region 6) for the ref_2000 (850 MJ/m²) and 1816_today (724 MJ/m²) scenarios. In 1817_today, crop planted in the Valais captures slightly more solar irradiance (735 MJ/m²) than crops in region 6 (720 MJ/m²) and also more than in the other two scenarios (+4% compared to the ref_2000 average). An average decrease of 15% (-128 MJ/m²) compared to ref_2000 is assessed for the pre Alps for 1816_today and 1817_today.

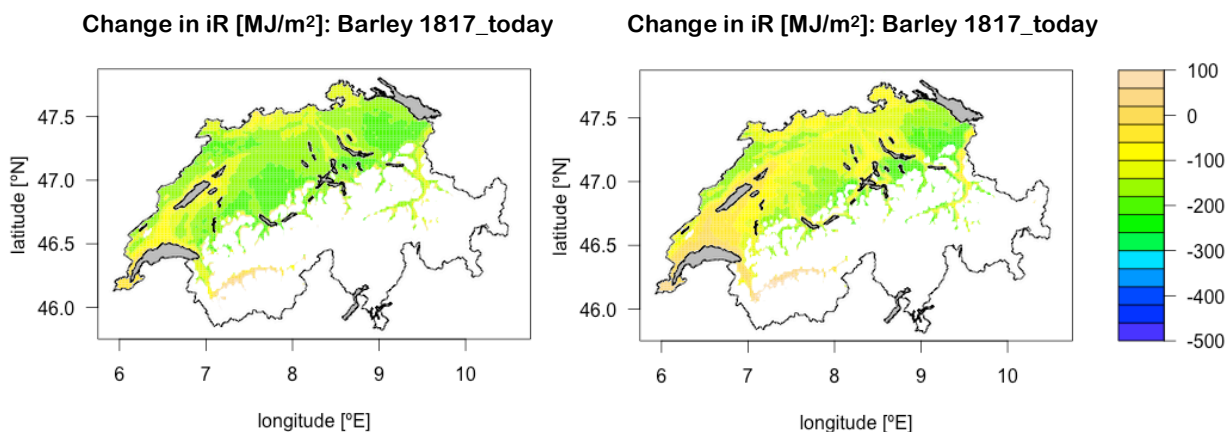


Figure 4.3.5: Absolute anomalies in annual intercepted radiation iR [in MJ/m²] of barley for the scenarios 1816_today (left panel) and 1817_today (right panel) with respect to the re_2000 average.

For the Swiss Plateau, the model assesses the highest *iR* for the western part (744 MJ/m²), hence slightly higher than in the East (710 MJ/m²) and the central part (697 MJ/m²). The comparison of simulated percentage anomalies for 1816_today with respect to the ref_2000 mean shows a pattern similar to percentage anomalies in yield (-15% for region 1, -21% for region 2 and -22% for region 3). In the 1817_today scenario, the West-East gradient in *iR* is of the same size as it has been found for yield, although on a lower percentage level (-8% or -57 MJ/m² in West and -18% or -128 MJ/m² in Eastern Switzerland).

4.3.2 Potato

Potato is a spring crop. In the temperate climate zones it is usually planted between late March and mid-April and the harvest period generally begins in late August and may stretch to early October [FiBl, 2008]. However, the sowing date varies strongly with altitude, as it

mainly depends on temperature. The average growth period simulated for the Swiss Plateau in the ref_2000 starts in late March and ends with harvest dates in early August.

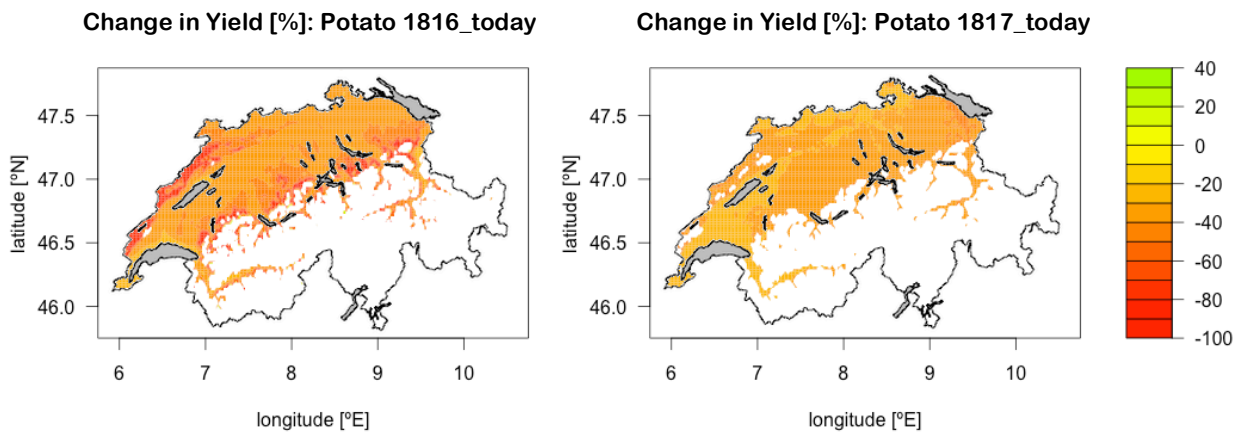


Figure 4.3.6: Percentage change in potato yields between the ref_2000 average and the 1816_today (left panel) and 1817_today (right panel) scenarios respectively.

1816/17_today and ref_2000

The highest potential yields assessed for ref_2000 are found in the Swiss Plateau (between 16 and 16.7 t/ha). Potential yields in the pre-Alps and the Valais are simulated slightly lower (13.2 t/ha and 15.6 t/ha respectively).

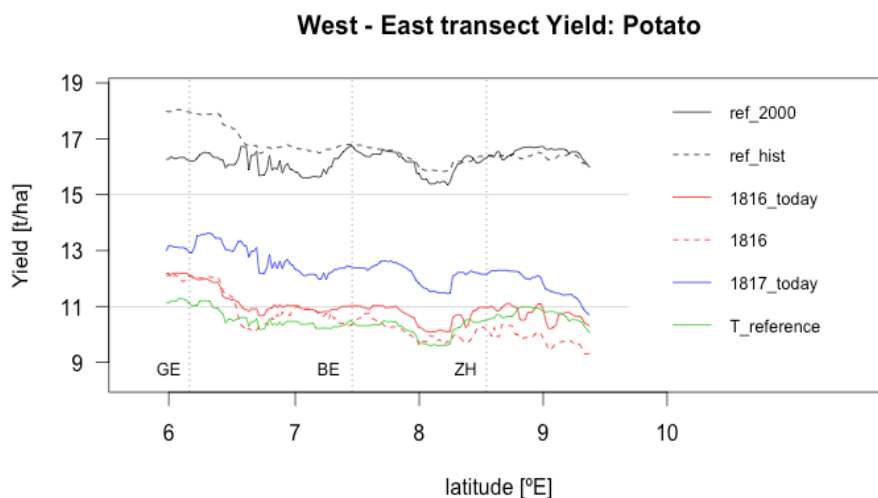


Figure 4.3.7: Development of potential crop yields of potato along the West-East transect for the different climate scenarios. Black lines represent the ref_2000 (bold) and ref_hist (dotted) averages and red lines 1816 and 1816_today, respectively. Potential crop yields assessed for 1817_today are shown in blue and for the T_reference scenario in green.

The model predicts negative anomalies in all five regions for both scenarios, 1816_today and 1817_today (figure 4.3.6). The most drastic losses occur in region 6, where potential crop yields decreased on average by more than 50% (-7 t/ha) in 1816_today and by 31% (-2.5 t/ha)

in 1817_today compared to the ref_2000 mean (see *table 4.3-2*). Negative anomalies assessed for western (-35.1%) and central Swiss Plateau (-36%) in 1816_today do not significantly differ (both -5.8 t/ha with p-value of a welsh two sample t-test of 0.95). For eastern Switzerland, negative anomalies are assessed slightly lower (-5.6 t/ha or -34.5%). Thus, no distinctive West-East gradient can be found (*figure 4.3.7*). However, there is a gradient in potential yield change of 1 t/ha in 1817_today, where losses in eastern Switzerland (-4.5 t/ha) clearly exceed losses in the central (-4.1 t/ha) and western Swiss Plateau (-3.5 t/ha). For the Valais, the simulation outputs losses of -5.9 t/ha (-38%) for 1816_today and -2.7 t/ha (-22%) for 1817_today.

1816 and ref_hist

Potential yields computed for ref_hist in the Valais (15 t/ha) and the pre-Alps (11.1 t/ha) are slightly lower than in the respective region for ref_2000, where there is no significant difference found for the eastern and central Swiss Plateau. Yields in western Switzerland are assessed somewhat higher (+0.3 t/ha), hence a weak West-East gradient already exists in ref_hist that is also persistent in 1816 (*figure 4.3.7*). However, percentage anomalies in potential yield (circa -40% or -6.5 t/ha) do not differ significantly between the three regions. Yield losses computed for the Swiss Plateau in 1816 are on average 0.8 t/ha higher compared with losses assessed for the 1816_today scenario. The percentage anomalies in potato yields 1816 are on average 5% higher than the ones estimated for the 1816_today scenario (*figure 4.3.8* and *table 4.3-2*).

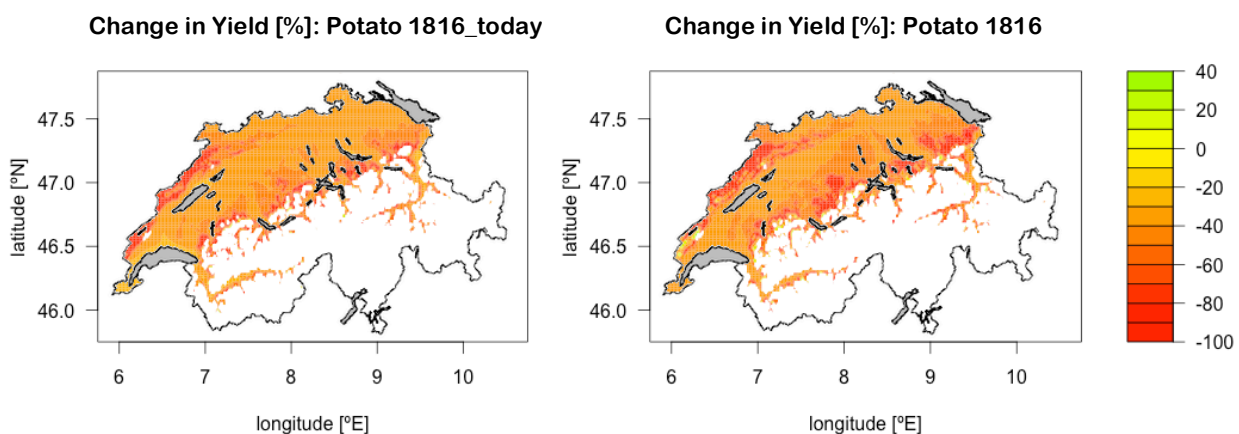


Figure 4.3.8: Percentage change in potato yields in 1816 with respect to the ref_hist average (left panel) and between the ref_2000 average and the 1816_today scenario (right panel).

T reference

No significant differences in potential yield change compared to changes in the 1816_today scenario are found for the three regions of the Swiss Plateau (*table 4.3-2*). But there is a notable difference in region 6, where potential yield is assessed to decrease by 35% or 4.7 t/ha,

which is 2.3 less than it has been simulated for 1816_today. Losses assessed for the Valais are also slightly lower (-5.4 t/ha compared to -6 t/ha).

Table 4.3-2 Potential crop yields of potato (in t/ha) in the reference scenarios are shown for each region as well as the absolute and percentage change for each climate scenario compared to its respective reference.

Region	ref_	1816_today		1817_today		T_reference		ref_	1816	
	today	t/ha	%	t/ha	%	t/ha	%	hist	t/ha	%
1	16.4	-5.8	-35	-3.5	-22.2	-5.8	-35	16.7	-6.6	-40
2	16.0	-5.8	-36	-4.1	-25.4	-5.9	-37	16.0	-6.4	-40.4
3	16.2	-5.6	-34.5	-4.5	-28.2	-5.6	-34.7	16.2	-6.4	-40
5	15.6	-6.0	-38	-2.7	-22	-5.4	-34.3	15.0	-6.5	-41.3
6	13.2	-7.0	-50.7	-2.5	-31	-4.7	-35	11.1	-6.2	-52.5

Intercepted radiation

Figure 4.3.9 shows the absolute change in iR for potato. For ref_2000, simulations compute average intercepted radiation being comparable to that of barley with 660 to 690 MJ/m² for the Swiss Plateau, 760 MJ/m² for the Valais and 890 MJ/m² for region 6. However, absolute as well as percentage anomalies in captured solar irradiance of the 1816_today scenario for the Swiss Plateau (-170 MJ/m² or -25% in the West and -182 MJ/m² or -27% in the Central and East) and the Valais (-94 MJ/m² or -12%) are higher compared to anomalies assessed for barley.

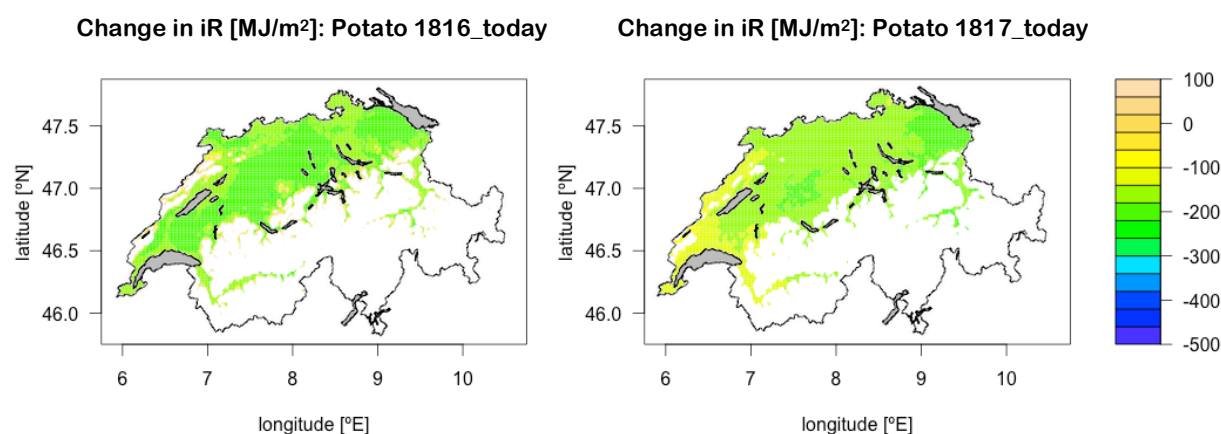


Figure 4.3.9: Absolute anomalies in annual intercepted radiation iR [in MJ/m²] of potato for the scenarios 1816_today (left panel) and 1817_today (right panel) with respect to the re_2000 average.

Slightly positive anomalies are computed for region 6, which contradicts the strong percentage and absolute decrease in potential yield (see above). This is because in higher altitudes, limitation due to temperature becomes more decisive. Differences in a temperature stress index (0-1 with no limitation at value 0) between the ref_2000 mean and the 1816_today sce-

nario show an increase with changing altitude (on average +0.5 in the higher Jura and pre-Alps and +0.2 in the Swiss Plateau).

The situation in the pre-Alps is computed clearly differently for the 1817_today scenario with a assessed decrease of approximately 320 MJ/m² (-36%). Negative anomalies in intercepted radiation are also assessed for the Valais (-177 MJ/m² or -23.5%) and the Swiss Plateau. Similar to the distribution pattern in potential yield, significant differences between anomalies in western and eastern Switzerland can only be found for 1817_today. Intercepted radiation is simulated to decrease by 145 MJ/m² (-21%) in the western, by 165 MJ/m² (-25%) in the central and 180 MJ/m² (-27%) in the eastern Swiss Plateau.

4.3.3 Maize

Maize is also a spring crop with a high volatility towards temperature fluctuations. Thus, sowing in Switzerland usually does not take place before mid-April to early May to avoid damage due to late frost [Dierauer, 2010]. However, a too late sowing date entails a decrease in potential yields, since less solar irradiance can be intercepted. Harvest may start between mid-September and early October. For ref_2000, the average sowing date in the Swiss Plateau is set at early April and the average harvest date at early October.

1816/17_today and ref_2000

The simulations show a high spatial variability in potential yields compared to variance in barley and potato for all three scenarios but most distinctly for 1816_today. Highest potential yields are assessed for the Swiss Plateau in ref_2000 (on average 18 t/ha) with no significant interregional differences. Average potential yields of 14 t/ha are simulated for the Valais and of 6.5 t/ha for the pre-Alps and the Jura (table 4.3-3). The model assesses for all three regions

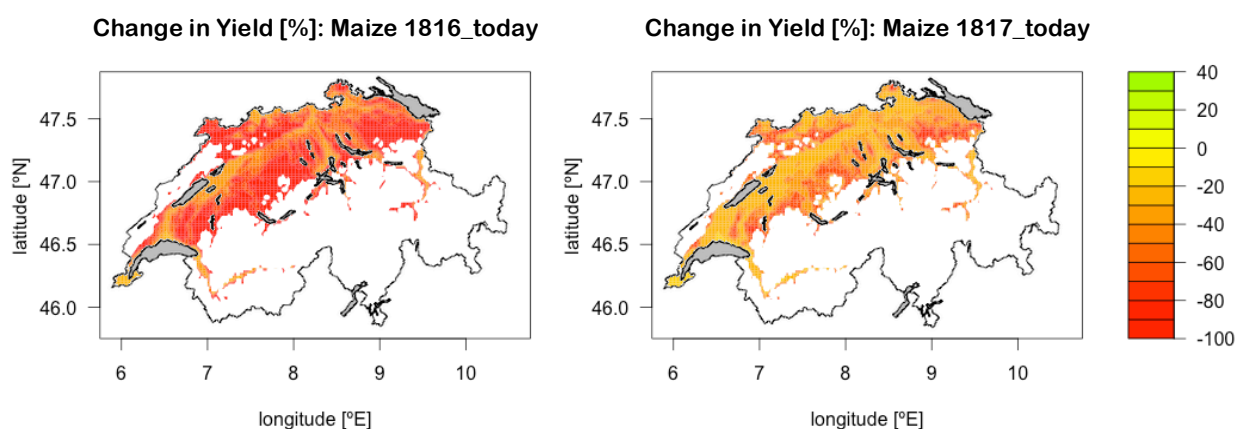


Figure 4.3.10: Percentage change in yield of potato between the 2000-2009 period and 1816 today (left panel) and 1817 today (right panel) respectively.

the most severe losses in yield among the three crops considered in this study. In western Switzerland, potential crop yields decrease on average by 10.5 t/ha (-60%) in 1816_today compared to the ref_2000 average, which is slightly less than in the central (-12 t/ha or -68.5%) and the eastern (-11.7 t/ha or -65.7%) Swiss Plateau (*figure 4.3.10*). However, spatial variability is notably higher in the central and eastern parts with a standard deviation in losses of 5.1 t/ha compared to the West with a standard deviation of only 4 t/ha. This difference in variability leads to a partially overestimated West-East gradient as illustrated in *figure 4.3.11*. The strongest percentage decrease is estimated on average for region 6 (-86%). This, however, the smallest loss measured in absolute values (-5.2 t/ha), as potential yields are estimated already rather low for ref_2000. Losses of up to -7.5 t/ha (-58%) are estimated for the Valais. In both regions, the spatial variability is even higher than in the Swiss Plateau with a standard deviation of 6.5 t/ha in the pre-Alps and Jura and 5.5 t/ha in the Valais.

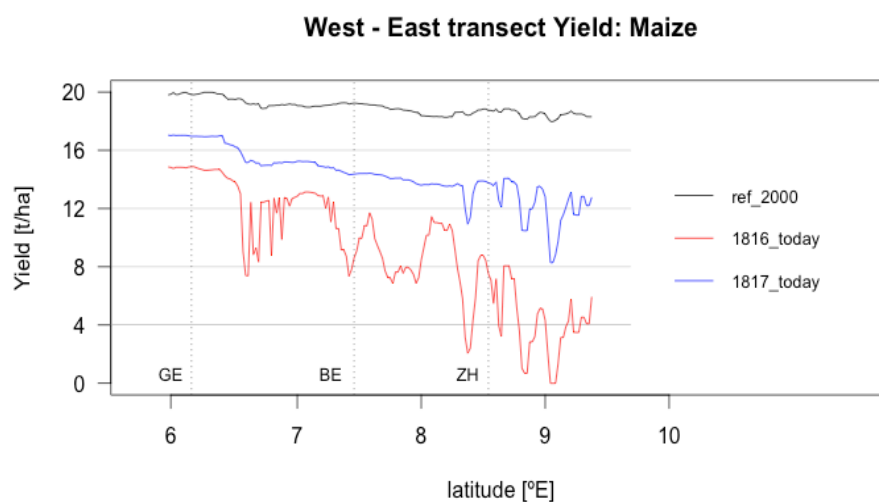


Figure 4.3.11: Development of potential crop yields of maize along the West-East transect for the different climate scenarios. The black line represents ref_2000 average and red line 1816_today. Potential crop yields assessed for 1817_today are shown in blue.

Losses estimated for the 1817_today scenario are clearly smaller. However, the West-East gradient in potential yield is stronger pronounced than in 1816_today, even though it seems different in *figure 4.3.11* due to the high intraregional variance. For the western Swiss Plateau the model assesses a decrease of 32.8% (-5.2 t/ha), which is about 1.1 t/ha less than in the

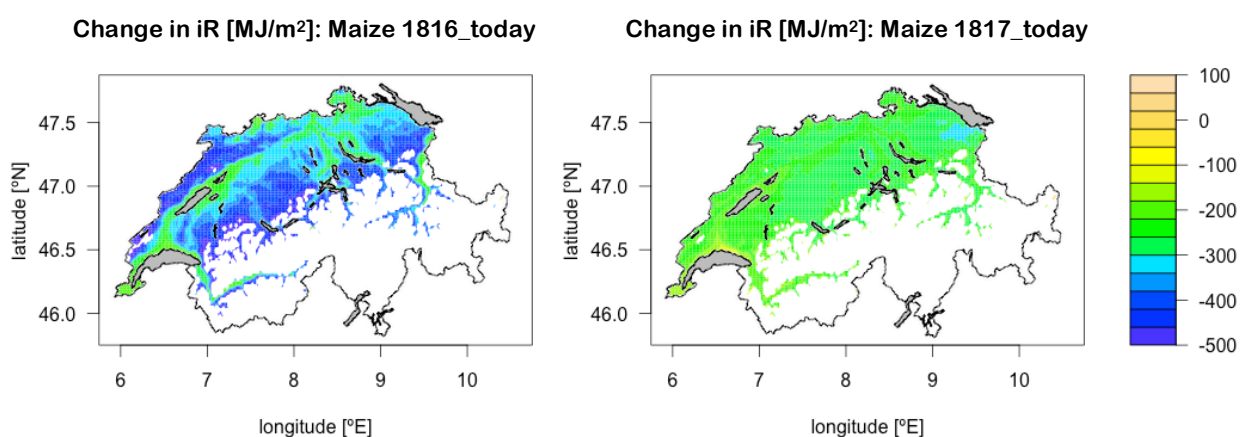
Region	ref_2000	1816_today		1817_today	
	t/ha	t/ha	%	t/ha	%
1	18.1	-10.6	-60	-5.2	-32.8
2	18.0	-12.0	-68.5	-6.2	-38.1
3	18.1	-11.7	-65.7	-6.4	-39.1
5	14.1	-7.5	-58	-4.3	-32.8
6	6.4	-5.2	-85.8	-3.5	-46.0

Table 4.3-3: Average potential crop yields of Maize (in t/ha) in ref_2000 are shown for each region as well as the absolute and percentage change assessed for 1816 today and 1817 today.

central (-38%) and eastern (-39%) part. For the region 6, average losses are estimated to 3.5 t/ha (-46%) and in the Valais to 4.3 t/ha (-33%).

Intercepted radiation

The spatial distribution of anomalies in iR is presented in *figure 4.3.12*. Average annual intercepted radiation in *ref_2000* is approximately the same in the Swiss Plateau and the Valais (somewhat more than 1000 MJ/m^2) and circa 150 MJ/m^2 lower in region 6. Similar to the pattern in yield, the strongest decrease in iR is assessed for the Alps and Jura for both, the 1816_today (-400 MJ/m^2 or -46%) and the 1817_today (-233 MJ/m^2 or -27%) scenario.



*Figure 4.3.12: Absolute anomalies in annual intercepted radiation iR [in MJ/m^2] of maize for the scenarios 1816_today (left panel) and 1817_today (right panel) with respect to the *ref_2000* average.*

There is only little difference between the regions of the Swiss Plateau with a decrease of 28% in the western, 31.5% in the central and 30.5% in the eastern part (circa -310 MJ/m^2) in 1816_today. A weak but significant West-East gradient is found for the 1817_today scenario, in which iR is estimated to decrease by 21% (-220 MJ/m^2) in western and 26% (-270 MJ/m^2) in eastern Switzerland. For the Valais, a decrease of 32% (-326 MJ/m^2) is computed for 1816_today and of 20% (-200 MJ/m^2) for 1817_today.

4.3.4 Soil moisture

CropSyst does include limitation in biomass accumulation due to water scarcity as described in chapter 3.2 (equation 12). However, it does not account for crop damages caused by an oversupply of water, and considered the large amount of rainfall especially in summer 1816, this limitation factor should be taken into account. The main problem caused by excessive soil-water is the inadequate aeration of the plant's root system due to oxygen deficiency [Carter, 1986; Sojka 1986]. If waterlogged conditions prevail over a long period, roots get

damaged and the potential yields decrease. *Figure 4.3.13* shows the average anomalies in water depth (in mm/m soil) assessed by CropSyst for 1816_today and 1817_today compared to the ref_2000 average for the Swiss Plateau. The pore volume is estimated to 43.5% or 435mm/m soil.

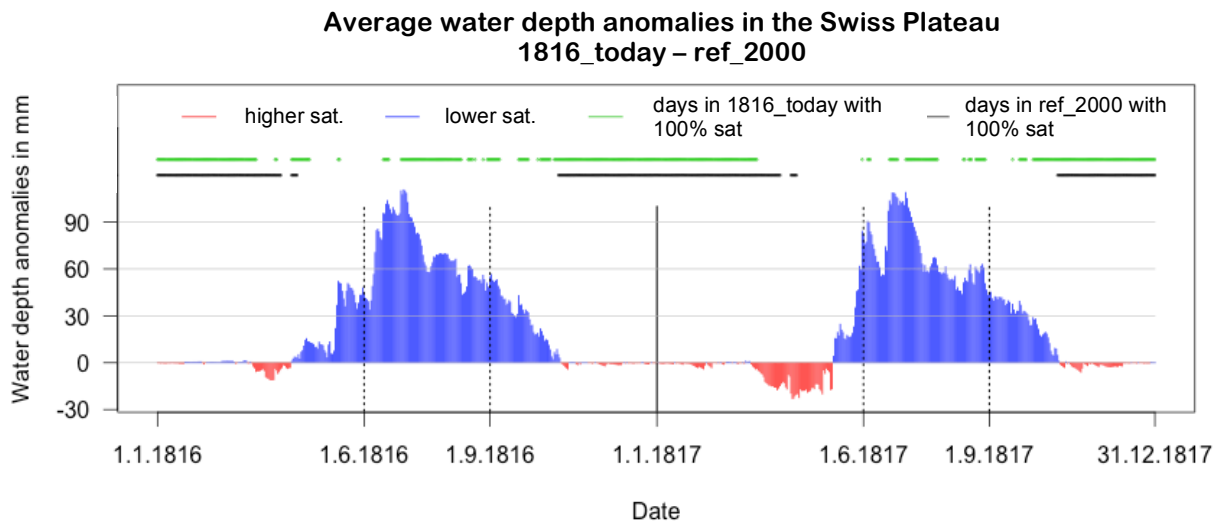


Figure 4.3.13: Average anomalies in water depth (in mm/m soil) between 1816/17_today and ref_2000 for the Swiss Plateau. Days with higher water content are shown in blue, days with lower water content in red. The green dots represent days with saturated soil conditions in 1816/17_today and the black dots the same for the ref_2000 average.

Both simulated years show notably higher water content especially over the summer months with an average increase of the water depth by 63mm (1816_today) and 61.2mm (1817_today) respectively. The day-to-day variance looks quite similar for both years. This also appears on a daily water stress index (WSI) calculated by CropSyst. For 1816/17_today, the WSI is zero for each day, hence there is no limitation in biomass accumulation due to water scarcity. However, there is a large variability in the spatial distribution of daily water contents, especially for 1816_today, which makes it difficult to draw any conclusions from the anomalies in water depths regarding interregional differences.

A more convincing approach is to compare days on which water content equals the pore volume (saturated condition). The number of such days increases significantly in the 1816_today scenario compared to ref_2000, but not in 1817_today (*figure 4.3.14*). In ref_2000, the soil is almost continuously saturated from mid-October to mid-April, followed by a dryer period with not-saturated conditions from mid spring to early fall (black dots in *figure 4.3.13*). In 1816/17_today, days with saturated conditions are less homogeneously distributed, with saturated conditions appearing frequently during the dryer second period (green dots). However,

the number of days with 100% saturation in 1817_today (*figure 4.3.14*, blue) is close to the number in ref_2000 (black), with a significant gradient from western parts of the Swiss Plateau towards central and eastern parts assessed for both climate scenarios. For 1816_today (red), the model estimates distinctively more days with saturated conditions, compared to the other two scenarios, although with a less pronounced gradient along the West-East transection.

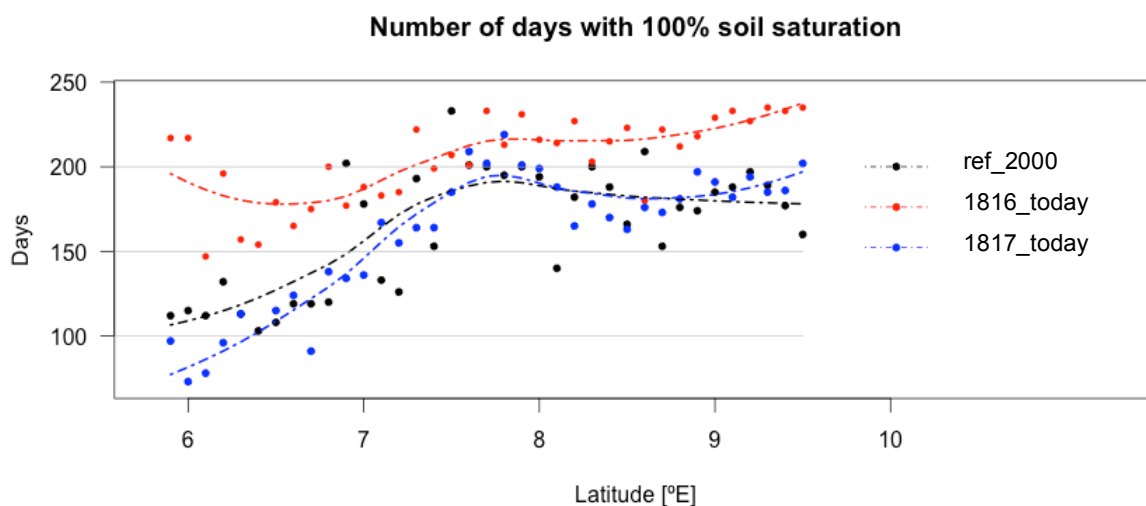


Figure 4.3.14: West-East transection for the number of days at which soil saturation reaches 100%. The ref_2000 average is represented in black, 1816_today in red and 1817_today in blue. The lines show the respective spline fits.

Stress Day Index

A further approach to estimate losses in potential yield due to excessive water supply is given by Kanwar et al. for corn cultivated in summer (e.g. maize) [Kanwar et al., 1998]. They assess relative yield RY (relative to the maximum achievable yield in a land block) based on a linear relationship with a Stress Day Index (SDI):

$$(13) \quad \text{Relative yield } RY = a - b * SDI$$

In this approximation, a and b are model specific parameters of a best-fitted linear equation with observed yields. The SDI is based on a concept designed by Ravelo et al. (1982) among others:

$$(14) \quad \text{Stress Day Index } SDI = \sum_j CS_j SD_j$$

The SDI is calculated as the sum of the product of a crop susceptibility factor CS and a stress day factor SD for stage j over all phenology stages. Hardjoamidjojo et al. (1982) suggest using an excessive soil water parameter (SEW_{30}) for the stress day factor that has been originally developed by Sieben (1964). This parameter is the annual sum of water content (in mm)

above the 30cm water table level. To account for effects by other factors such as soil type, temperature, fertility etc., Evan and Skaggs (1982) suggested applying a normalized crop susceptibility factor NCS_j instead of CS_j . The values for CS_j and NCS_j used in this study are shown in table 4.3-4.

Table 4.3-4: CS and NCS for corn for excessive soil water conditions for the different phenology stages. Values are taken from Kanwar et al., 1998, source: Evan and Skaggs (1982)

Growth stage	Days after planting	Mean CS	Normalized CS
Establishment	18 - 35	0.28	0.16
Early Vegetative	36 - 55	0.32	0.18
Late Vegetative	56 - 75	0.65	0.38
Flowering	76 - 99	0.36	0.21
Yield Formation	100 - harvest	0.1	0.06

Figure 4.3.15 shows the development of the SDI along the West-East transection for ref_2000 (black) and the two scenarios 1816_today (red) and 1817_today (blue). Generally, the curves show the same behaviour like the curves for the days with saturated conditions: a less pronounced gradient for the 1816_today scenario and a similar development along the West-East transection for 1817_today and ref_2000. However, the SDI calculated for 1817_today is ± 40 points higher on average than the SDI of ref_2000. This is, as the number of days with a high saturation level but not saturated conditions are significantly higher in 1817_today than in 1816_today.

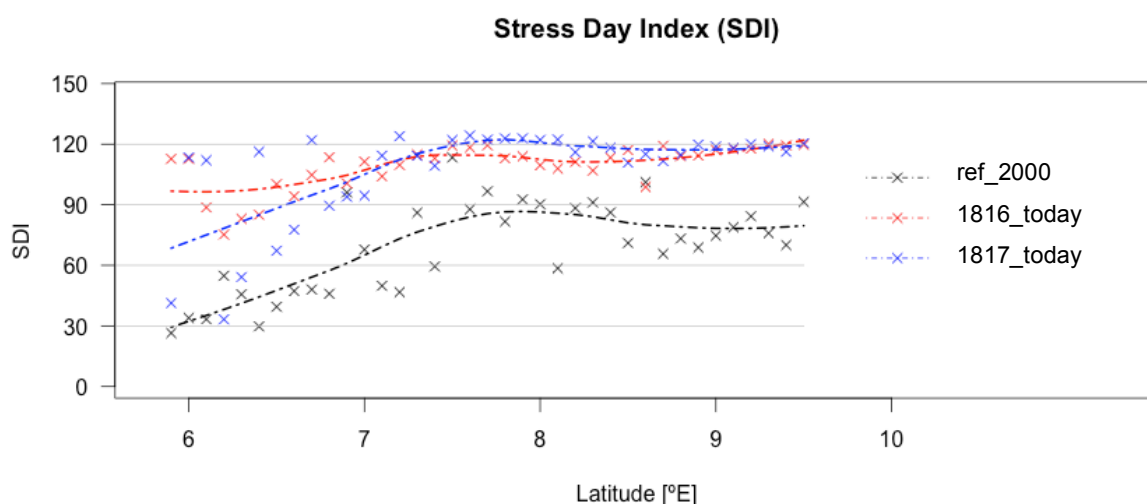


Figure 4.3.15: Development of the SDI along the West-East transection. Black represents the SDI for ref_2000, red for 1816_today and blue for 1817_today. The dotted lines show the respective spline fits.

As CropSyst does not account for stress due to an excess soil water supply, the RY cannot be derived from modelled crop yields. Hence, a and b are not accessible. However, Kanwar et al. conducted the regression for a year (1986) with above-average rainfall. The calculation gives the values 0.9 for a and 0.0036 for b , respectively. Thus, we derived an approximation of RY by inserting these numbers in equation **13** with the SDI of ref_2000 and 1816/17_today, respectively. Comparing the resulting RY for ref_2000 and 1816_today shows no significant West-East gradient with relative yield losses in Western Switzerland (ca. -24%) being larger than for the central (ca. -12.5%) but similar to losses in the eastern (ca. -23.5%) Swiss Plateau. The comparison with 1817_today, however, shows a weak pronounced West-East gradient with relative yield losses assessed lower for the West (ca. -18%) than for the central (ca. -19%) and eastern (ca. -24%) Swiss Plateau.

4.3.5 Phenology

This last section of the results gives a short overview over shifts of phenology stages within the growing season. Starting dates for an average climate in the Swiss Plateau are summarised in *table 4.3-5* for each stage distinguished according to the the crop modelling. Note, however, that these dates only serve as a reference as there is large spatial variability within the grids.

Table 4.3-5: Start dates of the phenology stages distinguished in the crop model. Dates are listed for each crop separately for the three climate scenarios of today.

Phenology stage	Barley			Potato			Maize		
	ref_2000	1816_today	1817_today	ref_2000	1816_today	1817_today	ref_2000	1816_today	1817_today
Sowing	15-10	15-10	15-10	22-03	22-03	22-03	20-04	20-04	20-04
Emergence	27-10	01-11	07-11	19-04	29-04	04-05	07-05	12-05	17-05
Flowering	12-06	15-06	18-06	10-06	23-06	22-06	21-06	08-08	01-08
Grain or tuber filling	23-06	28-06	30-06	25-07	13-07	07-07	15-08	12-09	28-08
Harvest	31-07	06-08	08-08	06-08	27-08	19-08	01-10	01-10	01-10

Apparently, there is no change in sowing dates in the 1816/17_today scenario compared to the ref_2000 average. However, there are significant shifts concerning the starting dates as well as the period length of the different stages within the growing season. The grain-filling period of maize is shortened by 13 and 27 days in the 1817_today and 1816_today scenario, respectively and flowering is initiated 42 and 48 days later. The flowering period is also significantly reduced for potato. However, contrary to maize, tuber-filling is extended by a factor of 3 to 4, which leads to postponed harvest dates. The most distinctive change in phenology of barley is the postponed emergence date. This leads to a shift in the starting dates of the consecutive stages but not to significant changes in length.

5 Discussion

The results are discussed and analysed in this chapter, divided into three sections. The first part focuses on the climate simulation, whereby main findings are compared to the state of research. In the second part, the outcome of the weather simulation and the resampling process is evaluated. Results of the crop modelling are discussed in a third part.

5.1 Climate simulation

The results of the climate simulation show a significantly colder and damper climate for the scenario 1816/17_today compared to the ref_2000 average. Extreme events, however, do not occur more often than in ref_2000. This is generally in line with the state of research, characterising the summer 1816 rather by extreme climate conditions than by extreme weather events [Auchmann et al., 2012]. The results of the climate simulation also show a notably too cold climate for summer 1817_today, although less significant. The same applies for spring of the 1817_today scenario, for which temperature anomalies are simulated similar to summer of 1816_today (*figure 4.2.7 and 4.2.9*). Precipitation increases less significantly in spring of 1817_today and the decrease in solar irradiance is comparable with the decrease in spring of the 1816_today scenario. Anomalies in all four climate variables are estimated decisively smaller for fall 1816_today and 1817_today as well as for winter 15/16_today and 16/17_today. Overall, the cold seasons summer 1816_today and spring 1817_today and the high rainfall frequency in summer 1816_today mostly mark the climate in Switzerland in the period after the Tambora eruption as well as for the scenarios 1816/17_today.

The analysis of temperature time series for Geneva by Auchmann et al. (2012) shows smaller anomalies in minimum than in maximum temperature. This agrees with the temperature simulations for the Swiss Plateau. A higher cloud cover has an isolation effect over night, mitigating the negative anomalies in minimum temperature. At daytime, clouds reflect more sunlight, which amplifies the decrease in maximum temperature (chapter 1.1.1). Cloud coverage tends to decrease with altitude, which explains the increase of anomalies in minimum temperature in connection with altitude, gradually converging with anomalies in maximum temperature (chapter 4.2.2 and 4.2.3, *figure 4.2.7 and 4.2.9*). However, there is no significant gradient in minimum or maximum temperature along the West-East transect through the Swiss Plateau

(figure 4.2.8 and 4.2.10), even though results do show a gradient in solar radiance (figure 4.2.14) and precipitation (figure 4.2.12). Hence, possible differences in crop yields between East and West Switzerland might rather be explained by disparities in those two climate variables than by disparities in temperature. A quantitative comparison of simulated solar irradiance with the actual situation in 1816/17 is not possible, as only qualitative records of cloudiness exist for this time period (chapter 2.1.1).

Average precipitation sums in summer and spring of 1816_today are estimated similar for the south and the north side of the Alps. This contradicts to some extent the findings of Bodenmann et al. (2011) and Luterbacher et al. (2004), which show significantly less rainfall for southern Switzerland. Some of this dissimilarity, however, might be explained by large spatial variability of precipitation in southern Switzerland and higher mean precipitation intensity. Significantly less days with precipitation $> 0.1\text{mm}$ are simulated for the lowland of Ticino (chapter 4.2.3). Considering the negative correlation between precipitation and solar irradiance, this suggests generally more cloudless days and a summer perceived as less harsh.

5.2 Method evaluation

The method applied in this study relies on highly simplified assumptions ignoring to a great extent interdependencies with large-scale weather conditions. The weather type classification intends to account for this inadequacy. However, a Monte Carlo simulation ($n=10'000$) applied to measure what fraction of variability in the sampling can solely be explained by changing weather types, gives a rather poor outcome. On average, only 20% of variability can be assigned, except for summer 1816 (33%) and fall 1816/17 (circa 50%). This is also apparent from the seasonal frequency distributions of weather types, which show rather small differences between 1816/17_today and ref_2000 apart from summer of 1816_today (chapter 4.1, figures 4.1.1-3 & 4.1.5). The central issue is that the classification is attained by interpolated values. The outcome of the Monte Carlo approach computed for a classification, that is solely based on summer 1816 data of Geneva (46%, figure 4.1.4), is similar to the result in Auchmann et al. (2012). Thus, a certain fraction of correlation with the weather situation gets lost due to the interpolation, and a station-specific classification would certainly conserve more information. However, this would require a larger pool of analogues and hence a longer period for ref_today, as the possible constellations of weather situations escalate (see chapter 3.1.2). There is further evidence in the distribution of weather types to suggest a bias between ref_hist and the ref_today with regard to wind directions. The classifications show more nor-

therly winds in *ref_hist* and more easterly winds in *ref_today* under all pressure situations. This applies for the classification of interpolated and those of stationary values. It might either indicate a change in wind classification schemes, which, however, is rather unlikely, as the bias is observed at Geneva and Hohenpeissenberg. Or it stands for a shift in large-scale weather situations between the two time periods. However, further research is required to answer this issue, which would exceed the scope of this thesis and is not further discussed in here.

The comparison of z-scores of *1816/17_today* and *1816/17* shows a similar day-to-day variance in anomalies of temperature and precipitation (chapter 4.2.1.1 and 4.2.1.2, *figure 4.2.1* and 4.2.5). Although day-to-day variance in absolute temperature shows significantly large dissimilarities, seasonal and monthly average temperatures correspond well. As the development of crops is less vulnerable to short-term than to long-term weather anomalies, the simulated climate is appropriate to estimate changes in crop yields representative of the situation in 1816/17. Nevertheless, the method would be improved by integrating precipitation data for 1816/17 from more than one station and quantitative data of solar irradiance. Time series of precipitation exist for Hohenpeissenberg for the period 1800-1820, though with large data gaps and no records for 1816 at all. Considering these data restrictions, the analysis of z-scores and absolute values suggests the day resampling within weather types to be an appropriate approach for statistical climate reconstruction.

Comparing anomalies in temperature simulated for *1816/17_today* and observed in 1816/17, the influence of climate warming has to be considered. Temperature simulated for *1816/17_today* decreases on average 0.2-1.0°C more relative to the *ref_2000* average than actual temperature in 1816 decreased relative to the *ref_hist* average (chapter 4.2.1.1, *figures 4.2.2-4*). The average annual climate warming computed as the difference between *ref_2000* and *ref_hist* is circa +0.9 in Eastern and +1.3 in Western Switzerland, most pronounced in summer (*figure 4.3.1*). In view of this fact, the difference in anomalies seems reasonable. Nevertheless, an inclusion of a large-scale climate model would be necessary to appropriately capture how climate warming affects weather anomalies caused by volcanic eruptions. To our knowledge, presently no model accounting for this relationship and only little literature exist. On balance and in consideration of the climate warming component, temperature and precipitation in 1816/17 seem to be represented well in terms of absolute anomalies by the

1816/17_today scenario. As mentioned above, no statement can be made regarding solar irradiance, as no appropriate data basis for this comparison exists.

5.3 Crop modelling

The outcome of the crop modelling shows a significant decrease in potential crop yields for the 1816/17_today scenario for almost every grid cell of the MeteoSwiss raster. However, there is large variability in percentage and absolute anomalies as well as in the spatial distribution of the anomalies between each crop. This is particularly due to the differing vulnerability towards weather anomalies and different growing seasons. For the Swiss Plateau, CropSyst assesses yield losses to approximately 18% of barley, 33% of potato and 63% of maize for the summer in the year after the reoccurrence of the Tambora eruption (1816_today). The decrease is estimated to be even stronger above 700mamsl, in absolute and relative measures. Thus, it would not be profitable to grow potato or maize in those altitudes at all, which would mainly affect potato growers as maize is already barely cultivated above 700mamsl nowadays.

Barley cultivation seems to be less affected by the cold summer of 1816. On the other hand, the model estimates losses for the 1817_today scenario similar to losses estimated for 1816_today, whereas a less strong decrease in potential yield is assessed for maize (-36%) and potato (-25%) compared to the year before. This is possibly due to the harsh spring 1817, which had a stronger effect on winter than on spring crops.

The following two sections focus on the relation between changing climate conditions and decreasing crop yields. Crop yields may either be affected directly by changing weather conditions, which is discussed in the subsequent part, or they are affected indirectly through a shift in phenology caused by changing temperatures. This connection is analysed in a second part.

5.3.1 Direct impacts: Weather conditions

Potential yields of maize and potato on the Swiss Plateau assessed for the 1816_today scenario show a highly positive correlation with minimum and maximum temperature during growing season ($\text{coef}_{\text{maize}} = 0.8$, $\text{coef}_{\text{potato}} = 0.7$). The correlation with solar irradiance is also positive, but of less significance and lower for maize (0.3) than for potato (0.5). Note that this correlation is not to compare to the correlation with intercepted radiation, as iR is not only a

function of radiation, but of GAI as well (equation 11). Hence, iR is also highly dependent on temperature, which is the main factor defining the start of the different phenology stages. A negative coefficient is found for the correlation with precipitation (circa -0.55 for both spring crops). However, a large fraction of this correlation might be explained with lower radiation associated with higher precipitation sums. This relationship gets even stronger for rainfall events of lower intensity, but a longer precipitation period.

Interestingly, some correlation coefficients significantly change for ref_2000. Average potential potato yields assessed for the reference scenario show a clearly weaker correlation between monthly precipitation sums, with a coefficient fluctuating around zero. An even inverse relationship with a coefficient of -0.3 is found for temperature. A similar pattern is found for potential yields of barley, strongly negative correlated with monthly temperatures in ref_2000 (on average -0.8) and much weaker in the 1816_today scenario (-0.4 to -0.2). This might indicate that temperatures in the Swiss Plateau nowadays are already above T_{opt} for those two crops, which has also been discussed in literature [Reddy and Hodges, 2000; Kooman, 1995; Al-Kathib et al., 1999; Lobell et al., 2012].

These correlation coefficients are based on highly simplified calculations. Nevertheless, they give a rough idea of how the change in climate conditions directly affects estimates of potential crop yields. It suggests, that the loss in yields in lower altitudes is particularly caused by the decrease in incoming solar irradiance and lesser by lower temperatures or higher precipitation. However, a cooling climate may affect crop yields by inducing a shift in phenology. This relation is discussed in the next section. Above 700mamsl, temperature limitation and thus the decreasing daily minimum temperature in 1816/17 becomes the more decisive factor.

It further has to be considered that CropSyst does not account for damages caused by an excessive soil water supply. The analysis of water depth output suggests, that soils were saturated over a longer period in summer 1816 (chapter 4.3.4, figures 4.3.13 and 4.3.14). Such water-logged conditions result in poor root development, facilitate putrefaction and increases the hazard of damages through microorganisms like bacteria or fungi [Haverkort, 1985]. Although the number of days with saturated soil for 1817_today is estimated similar to the number in ref_2000, the SDI implies a stress factor due to excessive soil water comparable to the situation in 1816 (figure 4.3.15). Thus, actual losses in crop yields are likely to be even higher in 1816/17 and for the 1816/17_today scenarios than estimated by CropSyst. Precipitation

sums increasing from West to East aggravate soil aeration along the transection, which is likely to amplify the West-East gradient in crop yields. A numerical illustration supports this hypothesis for the 1817_today scenario, but not so for 1816_today.

5.3.2 Indirect impacts: Phenology

Each stage during the growing season is initiated by a certain threshold of accumulated thermal time and absolute temperature (see chapter 3.2.3). Low temperatures in spring prompt the model to postpone the sowing date of spring crops, which further causes a shift of the subsequent phenology stages, throughout which the radiation surplus in June is not fully captured. However, this might have a positive effect on crop yields: The late sowing date also postpones the photoperiod. If this is attended with a change in radiation distribution, the late sowing date might have a beneficial effect on intercepted radiation. This phenomenon explains at least partly the lower potential yields of barley and potato estimated for the T_reference scenario compared to 1816_today despite the higher temperature (chapter 4.3.1, *figure 4.3.3* and chapter 4.3.2, *figure 4.3.7*). It further supports the hypothesis that the climate in Switzerland today is already too warm for some cultivars. In general, shifts in phenology stages explain some of the variance between the scenarios. Spatial variability within one scenario, however, is rather determined by direct weather effects.

The grain-filling period of maize is modelled significantly shorter for 1816/17_today, which can at least partly explain the severe losses of maize yield in those scenarios. On the other hand, the vegetative stage between emergence date and flowering is extended by several weeks, coinciding with the period that shows the highest precipitation surplus for 1816_today. Considering the high vulnerability towards excess water supply in the vegetative stage (see *table 4.3-4*), the postponed flowering might aggravate maize yields even further. The grain-filling stage of barley is simulated similar to ref_2000, and the tuber-filling of potato is even extended (chapter 4.3.5, *table 4.3-5*). Thus, the decrease in yields of those two crops is rather caused by the lower intercepted solar irradiance than by different stage lengths. Although the harvest date of potato postponed to end of August. Considering the highly saturated conditions in July and August (*figure 4.3.13*), this enhances the hazard of damages caused by water-logged conditions.

5.3.3 Comparison with crop data from 1816/17

Results of the crop modelling cannot be directly compared with actual development of crop yields in 1816/17, as, to our knowledge, no spatially recorded documentation of crop yields in Switzerland exists for the early 19th century. Hence, only an indirect comparison based on second order indices can be performed. The most important indices to measure crop yields in that time are the revenues attained by tithing market crop prices [Krämer, 2015; Pfister 1984].

Tithing was not only an important source of revenue for the ecclesiastical and secular magistracy, but also a meaningful index of crop productivity and wealth. Thus, detailed statistics over tithe revenues had been collected by regional authorities and supra-regionally summarized [Pfister, 1984]. However, no crop-specific statistics exist. Times series of tithe for Bern presented by Pfister (1984) show a significant downward stroke for the years 1816/17, indicating a significant decrease in crop yield. Although an even more constricting decrease is recorded for 1780.

In Krämer 2015, the development of market prices and a consumer price index is presented based on values collected from various sources (see *figure 1.1.3*). As described in chapter 1.1, they all show a strong increase in the period after the Tambora eruption (1816-1818). The disparity between eastern and western Switzerland in this increase of prices is mostly explained by differences in crisis management and trade relations and not by diverse crop yields [Krämer, 2015].

However, the results of the crop modelling indicate towards a West-East gradient in crop yields (*figure 4.3.3, 4.3.7 and 4.3.11*), mainly caused by disparities in the distribution of solar irradiance (*figure 4.2.14*). This gradient persists in simulations for both years, 1816_today and 1817_today. Interestingly, it is even stronger pronounced in the 1817_today scenario for barley and potato, although possibly for different reasons. The significantly stronger West-East gradient in solar irradiance in summer of 1817_today than in summer of 1816_today (*figure 4.2.14*) may result in lower *iR* in the eastern parts of the Swiss Plateau. The gradient in barley yields might further be caused by disparities in spring temperature (*figure 4.2.10*) causing a shorter tuber-filling stage in eastern parts compared to western parts. This relation can indeed be found for several grids located in the East. However, a more detailed analysis of changes in phenology would require further research and is not part of this study. Also the SDI and the

number of days with water saturated soils show a slight gradient for both years, again somewhat stronger pronounced in 1817 (*figure 4.3.14 and 4.3.15*).

These findings coincide with disparities of crop prices in 1817 between western and eastern Switzerland (*figure 1.1.3*), with a price peak between late spring and early summer observed for cities in German-speaking Switzerland but not for cities in the Romandy. Speculations with crop already have been taking place for many centuries and might also have an influence on the crop price development in the time after Tambora as discussed in Krämer 2015. Combined with low running stock caused by the bad harvest in 1816, the poor expectations regarding crop yield due to the cold spring 1817 may have encouraged people even more to hold back the remaining crop in storage. This might have supported the sharp price peak in central and eastern parts of the Swiss Plateau.

The gradient in yields predicted by the crop modelling is supposedly too weak to explain all of the disparity between eastern and western Switzerland observed in the years 1816/17, although it suggests that dissimilarities in crop yields amplified differences within the Swiss Plateau. However, more detailed crop data or time series of solar irradiance for the 1800-1820 period would be necessary to verify the findings of the crop modelling.

To state it collectively, results of this study predict a drastic insection in crop yields for the climate scenario 1816/17_today. The decrease in potential yields of barley and potato are estimated to be even higher for a reoccurrence of the Tambora eruption today than in 1816/17. However, the results do not allow a conclusive cognition to what extent spatial differences in yield losses lead to dissimilar market prices and shortages in food supply. For further research, the crop model output may serve as input data for a price model. Based on this, it might be investigated how the economy responses to such a decrease in yield of the 1816/17_today scenarios and markets potentially reacted back in 1816/17.

6 Conclusion

This thesis focused on impacts of the Tambora eruption 1815 on Switzerland. The main objective was to simulate climate conditions resulting from a reoccurrence of the Tambora eruption today and to model consequential effects on crop yields. Climate conditions have been derived applying a weather type classification and a subsequent resampling process. Potential crop yields were then estimated for the Swiss Plateau on the basis of the simulated climate scenarios.

Station data of the 1800-1820 period recorded at three weather stations was used to quantify anomalies in daily minimum and maximum temperature and precipitation for 1816/17. Each day within a historical reference period (ref_hist), consisting of all years unaffected by volcanic eruptions in the 1800-1820 period, was subsequently allocated to the corresponding weather class. Weather classes were determined by thresholds of pressure, pressure tendency and wind directions. For each day in 1816/17, the closest analogue with respect to z-scores of daily average temperature and precipitation within the 1981-2009 period (ref_today) was selected. The days selected in the resampling process eventually constitute the climate for the two years subsequent to a reoccurrence of the Tambora eruption, representing 1816/17_today. Daily minimum and maximum temperature and precipitation were available for the ch02.lonlat grid of MeteoSwiss and daily solar irradiance as station records. Following this, the values of those four climate variables served as input data into CropSyst in order to estimate potential crop yields of winter barley, potato and maize.

The simulation of climate shows conditions for 1816/17_today similar to conditions deduced from station records for 1816/17. Monthly averages correspond well with observed values, although there is a certain offset in the day-to-day variance. Negative anomalies in minimum and maximum temperature with respect to the 2000-2009 period (ref_2000) are most distinctive in summer of 1816_today and spring of 1817_today. Precipitation increases in all seasons in the 1816/17_today scenarios and most significantly in summer of 1816_today. A similar pattern is found for decreasing solar irradiance with the largest decline in summer of 1816_today. However, a distinct shift in frequency distribution of weather types is found only for summer 1816_today. The analysis of anomalies along a West-East transection through the

Swiss Plateau reveals a positive gradient in precipitation (except for summer 1816_today), indicating a larger precipitation surplus in Eastern Switzerland. Furthermore, there is a negative gradient found for solar irradiance in spring of 1816/17_today and summer of 1817_today with a stronger decrease in Eastern Switzerland. No significant gradient is detected for minimum and maximum temperature. Comparing z-scores of 1816/17 and 1816/17_today suggests that temperature and precipitation anomalies within 1816/17_today simulated as a part of this study may well represent conditions as they have prevailed in 1816/17, taking into account a climate warming component for temperature.

Results of the crop modelling for the Swiss Plateau show significant yield losses in all three considered crops for the scenario of a reoccurrence of Tambora today, with more severe crop failures for 1816_today. Yields of potato and maize decrease stronger compared to average yields in ref_2000 than yields of barley. For higher altitudes, crop failure is estimated close to 100%. Changes in crop yields in 1816 are assessed as similarly strong as changes within the 1816_today scenario. The comparison of potential yields estimated for ref_hist and ref_2000 further suggest that present temperatures are already above the optimum growth temperature for potato and barley. The analysis of yield anomalies along the West-East transection through the Swiss Plateau indicates larger losses in the eastern part. This coincides with a stronger increase of market prices in Eastern Switzerland observed for 1817. Thus, more severe crop failure in the eastern Swiss Plateau might have reinforced dissimilarities in the food situation between western and eastern Switzerland.

Appendix

<i>Station</i>		Altitude (mamsl)	I	p
Aadorf / Tänikon	TAE	539	*	*
Aigle	AIG	381	*	
Altdorf	ALT	438	*	*
Basel / Binningen	BAS	316	*	*
Bern / Zollikofen	BER	552	*	*
Beznau	BEZ	325		*
Buchs / Aarau	BUS	386	*	*
Bullet / La Frétaz	FRE	1205	*	
Chasseral	CHA	1599	*	*
Chur	CHU	556		*
Delémont / Delsberg	DEM	439		*
Fahy	FAH	596	*	*
Genève-Cointrin	GVE	420	*	*
Glarus	GLA	516	*	*
Gösgen	GOE	380	*	
Güttingen	GUT	440	*	*
Hohenpeissenberg*	HPB	977		*
Interlaken	INT	577	*	*
La Chaux-de-Fonds	CDF	1018	*	*
Langnau i. E.	LAG	745		*
Leibstadt	LEI	341	*	
Luzern	LUZ	454	*	
Neuchatel	NEU	485	*	*
Nyon / Changins	CGI	455	*	
Payerne	PAY	490	*	*
Pilatus	PIL	2106		*
Pully	PUY	455	*	*
Schaffhausen	SHA	438	*	*
St. Gallen	STG	775	*	
Vaduz	VAD	457	*	*
Wynau	WYN	422	*	*
Zürich / Kloten	KLO	426	*	*

Table A: List of the 31 SwissMetNet stations used in this thesis, including Hohenpeissenberg (*Deutscher Wetterdienst). The full station names are shown in column one and the abbreviation in column 2. Altitudes (mamsl) are listed in column 3. Column 4 and 5 show whether data of solar irradiance I (4) and pressure p (5) is available (*). The stations G, D and Hpb are highlighted in grey.

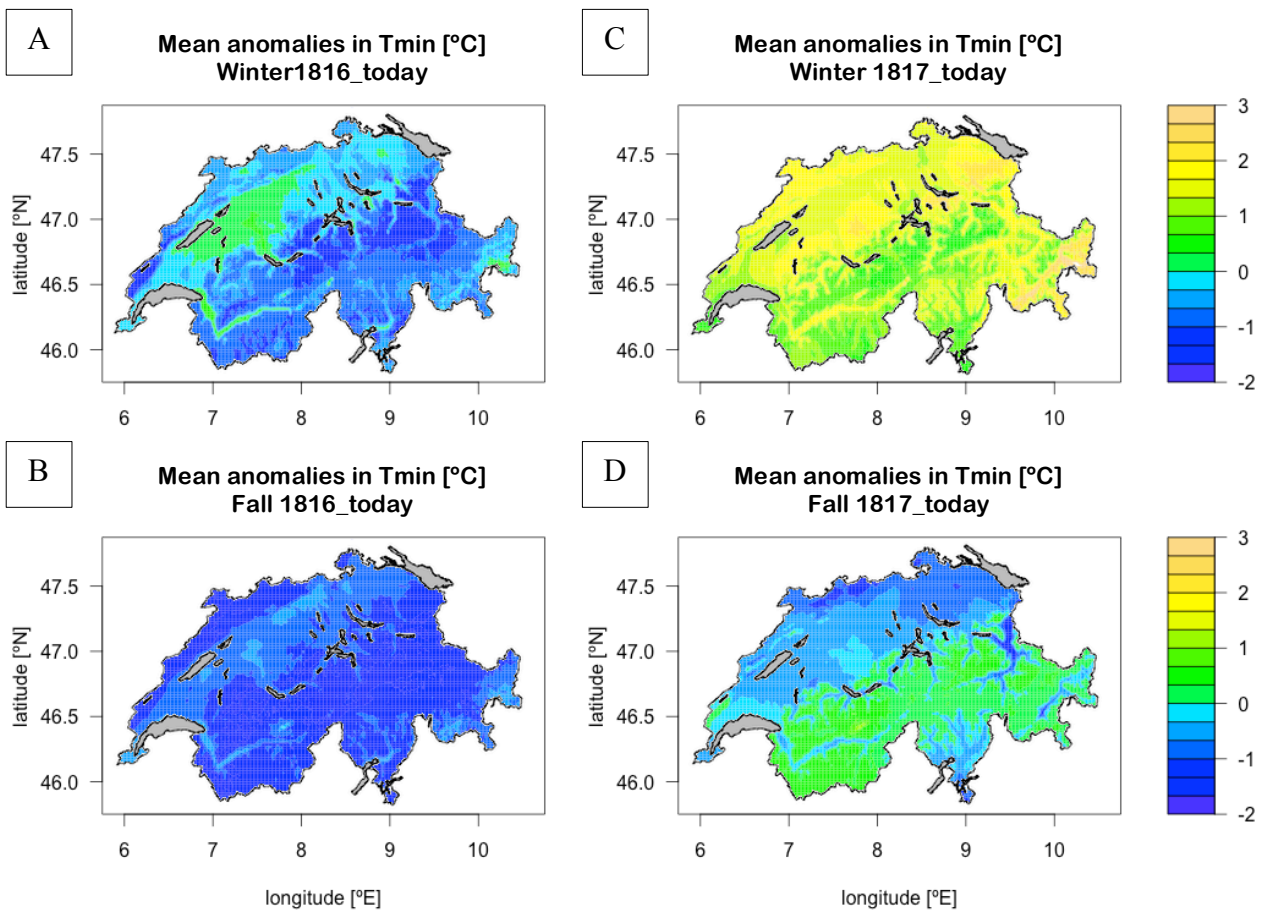


Figure A.1: Average seasonal anomalies in daily minimum temperature [in °C] between the simulated years 1816/17_today and the ref_2000 average. The upper plots show the seasonal means of precipitation anomalies for winter 1816_today (A) and 1817_today (C), the lower plots the anomalies in fall 1816_today (B) and 1817_today (D), respectively.

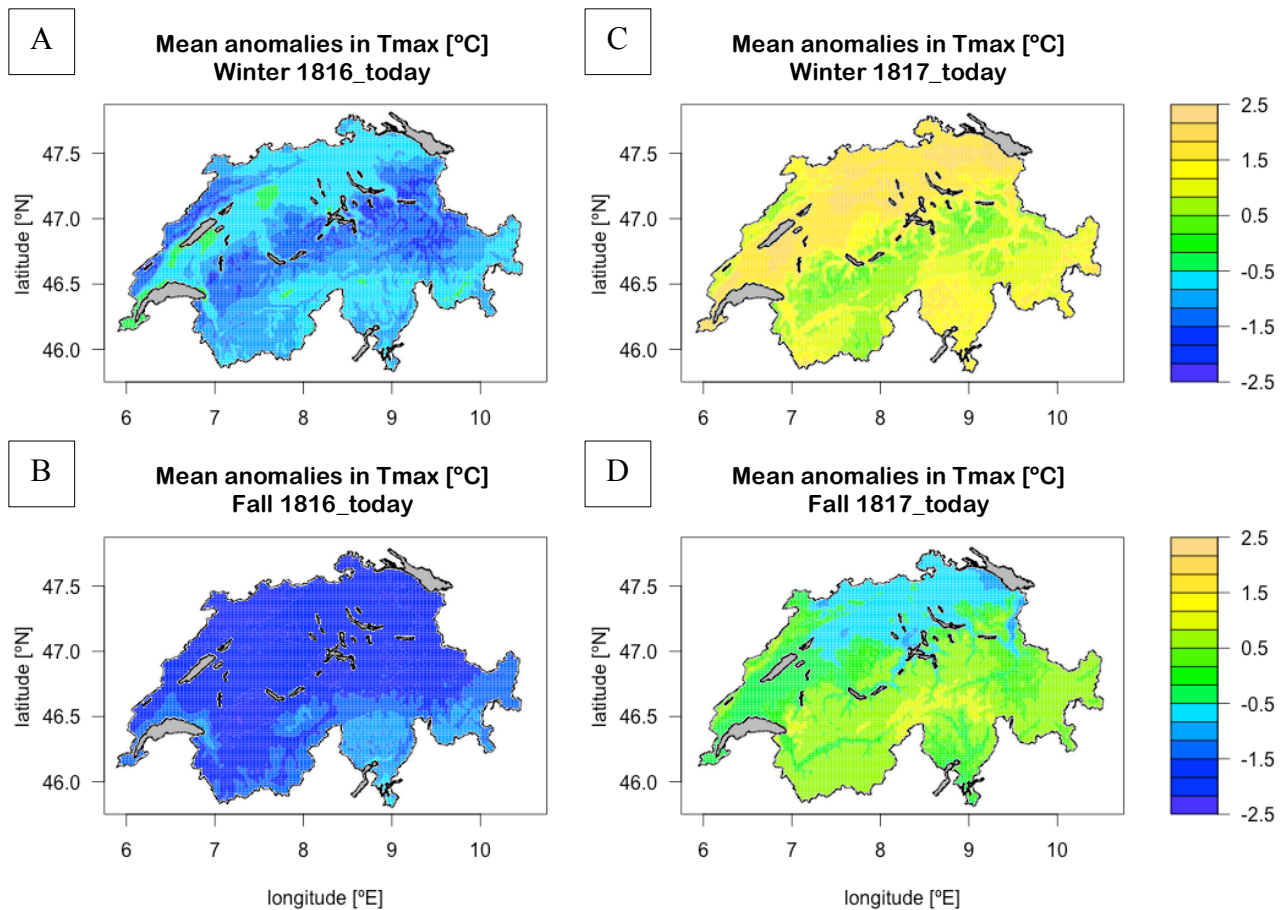


Figure A.2: Average seasonal anomalies in daily maximum temperature [in °C] between the simulated years 1816/17_today and the ref_2000 average. The upper plots show the seasonal means of precipitation anomalies for winter 1816_today (A) and 1817_today (C), the lower plots the anomalies in fall 1816_today (B) and 1817_today (D), respectively.

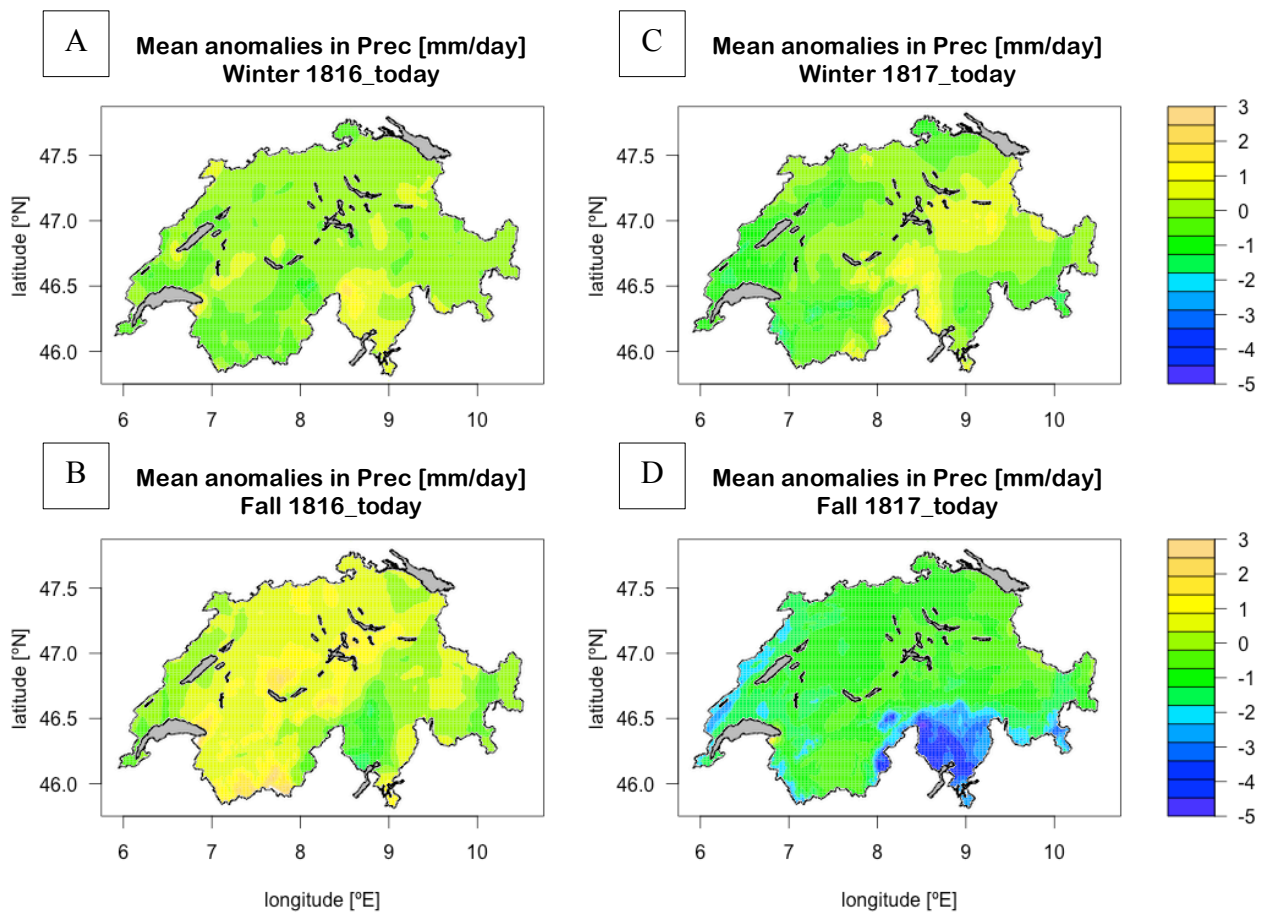


Figure A.3: Average seasonal anomalies in precipitation sums [in mm/day] between the simulated years 1816/17_today and the ref_2000 average. The upper plots show the seasonal means of precipitation anomalies for winter 1816_today (A) and 1817_today (C), the lower plots the anomalies in fall 1816_today (B) and 1817_today (D), respectively.

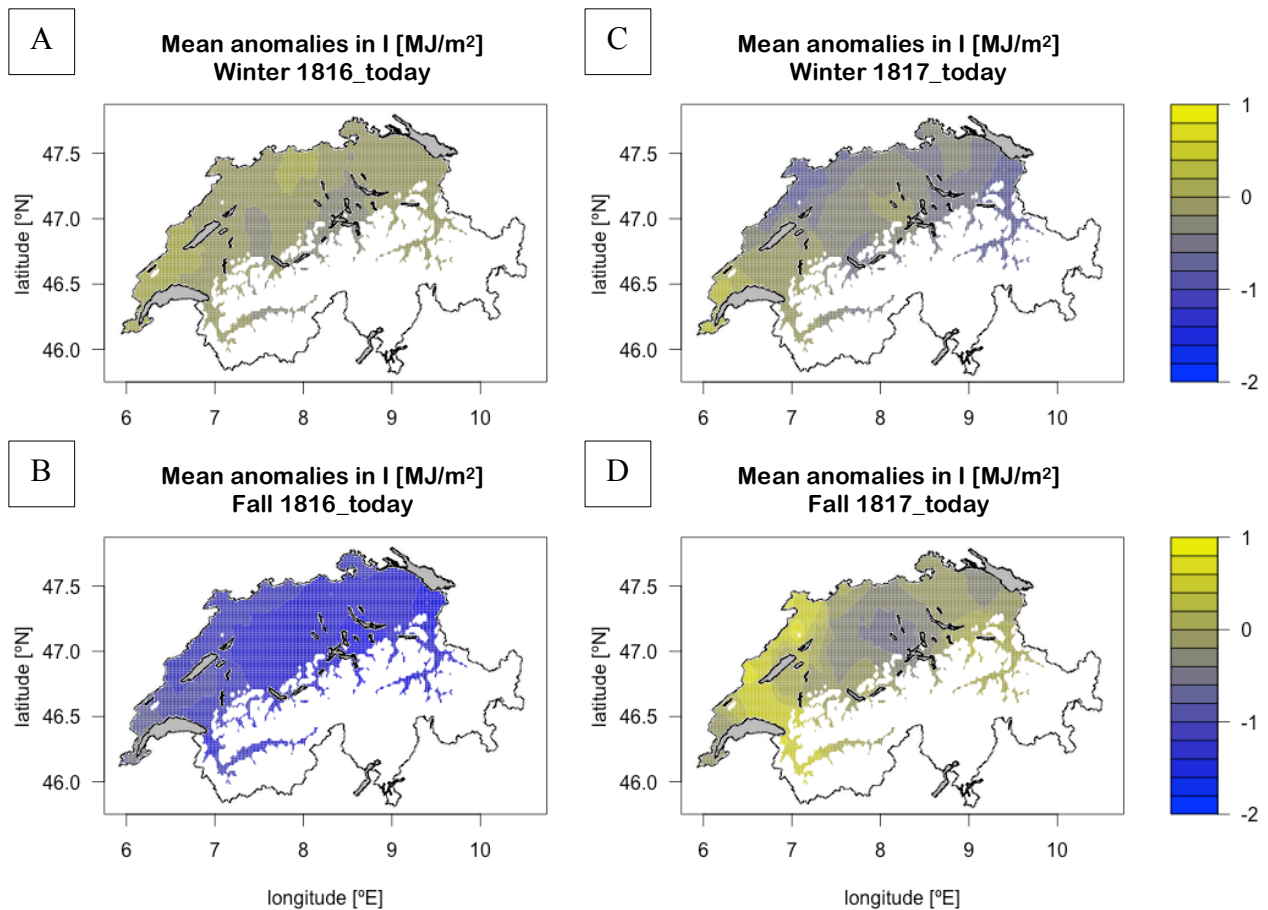


Figure A.4: Average seasonal anomalies in solar irradiance [in MJ/m²] between the simulated years 1816/17_today and the ref_2000 average. The upper plots show the seasonal means of precipitation anomalies for winter 1816_today (A) and 1817_today (C), the lower plots the anomalies in fall 1816_today (B) and 1817_today (D), respectively.

References

- Al-Khatib, K., Boydston, R. (1999): *Weed control with Brassica green manure crops*. Allelopathy Journal, Vol. 2, p. 255-270.
- Aslan, Z., Okcu, D., Kartal, S. (1997): *Harmonic analysis precipitation, pressure and temperature over Turkey*, Il Nuovo CIMENTO, Vol. 20, p. 595-605.
- Auchmann, R., Brönnimann, S., Breda, L., Bühler, M., Spadin, R., Stickler, A. (2012): *Extreme climate, not extreme weather: the summer of 1816 in Geneva, Switzerland*. Climate of the Past, Vol. 8, Nr. 1, p. 325-335.
- Begert, M., Seiz, G., Foppa, N., Schlegel, T., Appenzeller, C., Müller, G. (2007): *Die Überführung der klimatologischen Referenzstationen der Schweiz in das Swiss National Climatological Network (Swiss NBCN)*. Arbeitsberichte der MeteoSchweiz, 215, 43p.
- Bodenmann, T., Brönnimann, S., Hirsch Hadorn, G., Krüger, T., Weissert, H. (2011): *Perceiving, explaining, and observing climatic changes: A historical case study of the "year without a summer" 1816*. Meteorologische Zeitschrift, Vol. 20, Nr. 6, p. 577-587.
- Bo Bossard-Borner, H. (1998): *Im Bann der Revolution. Der Kanton Luzern 1798-1831/50*. Luzerner Historische Veröffentlichungen, Bd. 34, Luzern.
- Brandsma, T., Können, G.P. (2006): *Application of nearest-neighbour resampling for homogenizing temperature records on a daily to sub-daily level*. International Journal of Climatology, Vol. 26, p. 75-89.
- Briffa, K., Jones, P. D., Schweingruber, F., and Osborn, T. (1998): *Influence of volcanic eruptions on Northern Hemisphere Summer temperature over the Past 600 Years*. Nature, Vol. 393, p. 450-455.
- Carter, C. (1986): *Oxidation reduction due to a high water table*. In: Saavalainen, J., Vakkilainen, P. (eds, 1986): *Proceedings of international Seminar on Land Drainage*. Helsinki University of Technology, Helsinki, p. 112-126.

- Chenoweth, M. (2001): *Two major volcanic cooling episodes derived from global marine air temperatures*. Geophysical Research Letters, Vol. 28, p. 2963–2966.
- Cole-Dai, J., Ferris, D., Lanciki, A., Savarino, J., Baroni, M., Thiemens, M.H. (2009): *Cold decade (AD 1810–1819) caused by Tambora (1815) and another (1809) stratospheric volcanic eruption*. Geophysical Research Letters, Vol. 36, doi:10.1029/2009GL040882.
- Dierauer, H. (2008): *Merkblatt Biomais, Ausgabe Schweiz*. Forschungsinstitut für biologischen Landbau FiBL (ed.), online available on: www.shop.fibl.org.
- Dierauer, H. (2010): *Merkblatt Biogetreide, Ausgabe Schweiz*. Forschungsinstitut für biologischen Landbau FiBL (ed.), online available on: www.shop.fibl.org.
- Evans, R.O., Skaggs, R.W. (1984): *Crop susceptibility factors for corn and soybeans to controlled flooding*. American Society of Agricultural Engineering (ASAE), Paper No. 84-2567, ASAE, St Joseph.
- FiBL (ed.) (2010): *Merkblatt Biokartoffeln, Ausgabe Schweiz*. Online available on: www.shop.fibl.org.
- Fox, J., Andersen, R. (2005): *Using the R Statistical Computing Environment to Teach Social Statistics Courses*. Department of Sociology, McMaster University.
- Frei, C. (2013): *Interpolation of temperature in a mountainous region using non-linear profiles and non-Euclidean distances*. International Journal of Climatology, Vol. 34, p. 1585-1605.
- Fülleemann, C., M. Begert, M. Croci-Maspoli, and S. Brönnimann (2011): *Digitalisieren und Homogenisieren von historischen Klimadaten des Swiss NBCN – Resultate aus Digi-Hom*. Arbeitsberichte der MeteoSchweiz, Vol. 236, 48 pp.
- Hardjoamidjojo, S., Skaggs, R.W., Schwab, G.O. (1982): *Corn yield response to excessive soil water conditions*. Transaction of the ASAE, Vol. 25, p. 922-927.
- Haverkort, A.J. (1985): *Water Management in Potato Production*. Technical Information Bulletin 15, International Information Centre, Lima (PER).

-
- Hijmans, R.J. (2003): *The Effect of Climate Change on Global Potato Production*. American Journal of Potato Research, Vol. 80, p. 271-280.
- Holzkämper, A., Fossati, D., Hiltbrunner, J., Fuhrer, J. (2015): *Spatial and temporal trends in agro-climatic limitations to production potentials for grain maize and winter wheat in Switzerland*. Regional Environmental Change, Vol. 15, p. 109-122.
- IPCC (2014): *Climate Change 2014: Synthesis Report*. Contribution of Working Groups I, II, III to the Fifth Assessment Report of the Intergovernmental Panel on Climate Change, Pachauri, R.K., Meyer, L.A. (ed.), IPCC, Geneva.
- Justino, F., Setzer, A., Bracegirdle, T.J., Mendes, D., Grimm, A., Dechiche, G., Schaefer, C.E. (2010): *Harmonic analysis of climatological temperature over Antarctica: present day and greenhouse warming perspectives*. International Journal of Climatology, Vol. 31, p. 514-530.
- Kanwar, R.S., Baker, J.L., Mulchtar, S. (1998): *Excessive Soil Water Effects at Various Stages of Development on the Growth and Yield of Corn*. Digital repository of the Iowa State University, Iowa.
- Kiniry, J.R., Jones, C.A., O'Toole, J.C., Blanchet, R., Cabelguenne, M., Spanel, D.A. (1989): *Radiation-use efficiency in biomass accumulation prior to grain filling for five grain crop species*. Field Crop Research, Vol. 20, p. 51-64.
- Kington, J. (1992): *Weather patterns over Europe in 1816, in: The year without a summer?: world climate in 1816*. Edited by: Harrington, C. R., Canadian Museum of Nature, Ottawa, p. 358-371.
- Klein, T., Holzkämper, A., Calanca, P., Fuhrer, J. (2013): *Adaption options under climate change for multifunctional agriculture: a simulation study for western Switzerland*. Regional Environmental Change, Vol. 14, p. 167-184.
- Klein, T., Calanca, P., Holzkämper, A., Lehmann, N., Roesch, A., Fuhrer, J. (2012): *Using farm accountancy data to calibrate a crop model for climate impact studies*. Agricultural Systems, Vol. 111, p. 23-33.

- Kooman, P.L. (1995): *Yielding ability of potato crops as influenced by temperature and daylength*. PhD thesis, Wageningen Agricultural University, Wageningen (NED).
- Krämer, D. (2015): “*Menschen grassten nun mit dem Vieh*”. *Die letzte grosse Hungerkrise der Schweiz 1816/17*. In: Pfister, C. / Rohr, C. (Hsg.): *Wirtschafts-, Sozial- und Umweltgeschichte (WSU)*, Bd. 4, Schwabe-Verlag.
- Lessing, H.-E. (2003): *Automobilität – Karl Dreis und die unglaublichen Anfänge*. MAXIME Verlag, Leipzig.
- Lobell, D., Field, C. (2007): *Global scale climate-crop yield relationships and the impacts of recent warming*. Public Health Resources, Paper 152.
- Lobell, D.B., Gourdji, S.M. (2012): *The Influence of Climate Change on Global Crop Productivity*. *Plant Physiology*, Vol. 160, p. 1686-1697.
- Luterbacher, J., Dietrich, D., Xoplaki, E., Grosjean, M., Wanner, H. (2004): *European seasonal and annual temperature variability, trends and extremes since 1500 A.D.* *Science*, Vol. 303, p. 1499-1503.
- McGee, K.A., Doukas, M.P., Kessler, R. and Gerlach, T. (1997): *Impacts of volcanic gases on climate, the environment, and people*, U.S. Geological Survey Open-File Report 97-262.
- Michaud, G. (1976): *La disette de 1816 – 1817 dans le canton de Vaud*. Lizentiatsarbeit, Lausanne 1976.
- Monteith, J.L. (1977): *Climate a crop efficiency of crop production in Britain*. *Philosophical Transactions of the Royal Society of London, Series B*, Vol. 281, p. 277-329.
- Neff, E.L. (1977): *How much rain does a rain gage gage?* *Journal of Hydrology*, Vol. 35, p. 213-220.
- Pfister, C. (1984): *Das Klima der Schweiz von 1525–1860 und seine Bedeutung in der Geschichte von Bevölkerung und Landwirtschaft*. Bd. 2, Bern.
- Pfister, C. (1998): *Sterbekrisen 1750–1918*. In: Pfister, C. / Egli, H.R. (ed.): *Historisch-statistischer Atlas des Kantons Bern, 1750–1995. Umwelt, Bevölkerung, Wirtschaft, Politik*. Bern, 1998.

- Pfister, C. (1999): *Wetternachhersage: 500 Jahre Klimavariationen und Naturkatastrophen (1496–1995)*. Paul Haupt, Bern.
- Puma, M.J., Bose, S., Young Chon, S., Cook, B. (2015): *Assessing the evolving fragility of the global food system*. Environmental Research Letters, Vol. 10, 024007.
- Rampino, M.R., Self, S. (1984): *Sulphur-rich volcanic eruptions and stratospheric aerosols*. Nature, Vol. 30, p. 677-679.
- Ravelo, C.J., Reddell, D.L., Hiler, E.A., Skaggs, R.W. (1982): *Incorporation of crop needs into drainage system design*. Transactions of the ASAE, Vol. 25, p. 623-629.
- Reddy, K.R., Hodges, H.F. (ed.): *Climate Change and Global Crop Productivity*. CAB International (2000), Wallingford (UK).
- Reith, R. (2011): *Umweltgeschichte der Frühen Neuzeit*. Enzyklopädie Deutscher Geschichte, Bd. 89, München (GER).
- Robock, A. (2000): *Volcanic eruptions and climate*. Reviews of Geophysics, Vol. 38, p. 191–219.
- Sevrük, B. (1985): *Systematische Niederschlagsmessfehler in der Schweiz*. In: *Der Niederschlag in der Schweiz*. Beiträge zur Geologie der Schweiz - Hydrologie, Vol. 31, p. 65-75.
- Schürmann, M (1974): *Bevölkerung, Wirtschaft und Gesellschaft in Appenzell Innerrhoden im 18. und im frühen 19. Jahrhundert*. Appenzell, 1974.
- Shindell, D., Schmidt, G., Mann, M., and Faluvegi, G. (2004): *Dynamic winter climate response to large tropical volcanic eruptions since 1600*. Journal of Geophysical Research - Atmospheres, Vol. 109.
- Sieben, W. H. (1962): *Het verban tussen ontwatering en opbrengst bi j de jonge zavelgronden in de Noordoostpolder*. Van Zee tot Land, 40, The Netherlands, cited by Wesseling, 1974.

- Skeen, E. K. (1981): *The Year without a Summer: A Historical View*. Journal of the Early Republic, Vol. 1, p. 51–67.
- Stothers, R.B. (1984): *The great Tambora eruption in 1815 and its aftermath*. Science, Vol. 224, p. 1191-1198.
- Sojka, R. E. (1986): *Soil oxygen effects on two determinate soybean isolines*. Soil Science, Vol. 140, p. 333-343.
- Stendel, M., Mogensen, I., Christensen, J. (2005): *Influence of various forcings on global climate in historical times using a coupled atmosphere-ocean general circulation model*. Climate Dynamics, Vol. 26, p. 1-15.
- Stöckle, C., Donatelli, M., Nelson, R. (2003): *CropSyst, a cropping systems simulation model*. European Journal of Agronomy, Vol. 18, p. 289-307.
- Stöckle, M., Nelson, R. (2013): *Cropping Systems Simulation Model User's Manual*. Online available as PDF on: <https://nishat2013.files.wordpress.com/2013/11/cropping-system-manual-book.pdf>.
- Stöckli, R. (2013): *Documentation of MeteoSwiss Grid-Data Products*. Online available on: http://www.ifu.ethz.ch/hydrologie/research/research_data.
- Tanner, C.B., Sinclair, T.R. (1983): *Efficient water use in crop production: research or re-research?* In: Taylor, H.M., Jordan, W.R., Sinclair, T.R. (Eds.), *Limitations to efficient water use in crop production*. American Society of Agronomy.
- Winkler, P. (2009): *Revision and necessary correction of the long-term temperature series of Hohenpeissenberg, 1781-2006*. Theoretical Applications in Climatology, Vol. 98, p. 259-268.
- Yang, D.Q., E. Elomaa, A. Tuominen, A. Aaltonen, B. Goodison, T. Gunther, V. Golubev, B. Sevruck, H. Madsen and J. Milkovic (1999): *Wind-induced precipitation undercatch of the Hellmann gauges*. Nordic Hydrology, Vol. 30, p. 57-80.

Declaration

under Art. 28 Para. 2 RSL 05

Last, first name: Flückiger, Simon

Matriculation number: 08-111-155

Programme: M.Sc. in Climate Science

Bachelor

Master

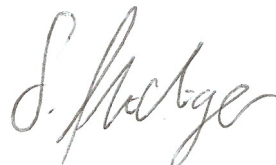
Dissertation

Thesis title: Tambora 1815: impacts of a volcanic eruption on climate and crop yields in Switzerland

Thesis supervisor: Prof. Dr. Stefan Brönnimann and Prof. Dr. Jürg Fuhrer

I hereby declare that this submission is my own work and that, to the best of my knowledge and belief, it contains no material previously published or written by another person, except where due acknowledgement has been made in the text. In accordance with academic rules and ethical conduct, I have fully cited and referenced all material and results that are not original to this work. I am well aware of the fact that, on the basis of Article 36 Paragraph 1 Letter o of the University Law of 5 September 1996, the Senate is entitled to deny the title awarded on the basis of this work if proven otherwise. I grant inspection of my thesis.

Bern, 30th November, 2015



Signature